Method and system for the automatic recognition of lesions in a set of breast magnetic resonance images

POLITECNICO DI TORINO

DOCTORATE SCHOOL

Ph. D. In Informatics and Systems – XXV cycle

Doctor of Philosophy Thesis

Glove Exoskeleton for Extra-Vehicular Activities

Analysis of Requirements and Prototype Design

(Part One)

Favetto Alain

Advisor:
Prof. Giuseppe Carlo Calafiore

Coordinator:
Prof. Pietro Laface

This page is intentionally left blank

Dedicato a mio Padre...
Al tuo modo ruvido di trasmettere le emozioni.
Al tuo senso del dovere ed al tuo altruismo.
Ai tuoi modi di fare che da piccolo non capivo e oggi sono parte del mio essere.
A tutti i pensieri e le parole che vorrei averti detto e che sono rimasti solo nella mia testa.
A te che mi hai sempre trattato come un adulto.
A te che te ne sei andato prima che adulto lo potessi diventare davvero.

This page is intentionally left blank

INDEX

CHAPTER 1:

"You are… on a cliff. Crawling, slithering, gripping, reaching… the whole cliff is falling and you are on it... it is difficult to discount the feeling that you are moving away, detached. In the midst of all this, you carry out your work calmly, methodically. You snap a picture or two, and below notice the Straits of Gibraltar…"

Linenger; May 24, 1997

EXTRA VEHICULAR ACTIVITIES

Imagine opening a door and, through a small step, crossing the threshold, starting to hover weightlessly above the widest oceans and highest mountains, so high to believe that only opening a little more the hand you would be able to seize the entire globe between your fingers. This is probably one of the most significant, extreme and ecstatic experience conducted in space; it takes place when a human being leaves the metal shell of his vehicle and starts floating around it, wrapped in a hyper technological balloon called spacesuit. These operations are called Extra Vehicular Activities [1].

Extra Vehicular Activity (EVA) is any operation done by an astronaut, or a cosmonaut, outside a spacecraft and beyond the Earth's atmosphere. Extra Vehicular Activities require some of the most complex skills, sophisticated technologies and human abilities of all missions undertaken in space. Usually the term refers to a spacewalk made outside a structure orbiting around the Earth (e.g. the Space Shuttle or the International Space Station), but has also referred to the lunar surface exploration, commonly known as moonwalk [2]. EVAs could be tethered or un-tethered. During the tethered EVA the astronaut is directly linked to the spacecraft through an umbilical cable; that cable provides oxygen, electrical power and allows him to return to the vehicle without propulsion. In the un-tethered EVA an oxygen and power supply, and a propulsion system, are needed. This type of mission is relatively recent, in fact it has been performed only three times in 1984 using the Manned Maneuvering Unit (MMU [3]) and once in 1994 during the flight test of the Simplified Aid for EVA Rescue (SAFER [4]). The U.S. Space Agency (National Aeronautics and Space Administration, NASA) and the Russian Space Agency (Rosaviakosmos, RKA) define EVA in two differently ways. Russian cosmonauts perform EVA any time they are in vacuum wearing a space suit; U.S. astronauts, vice-versa must have at least their heads outside the vehicle in order to perform an EVA [2]. These different definitions are due to the different design philosophies of the spacecrafts of the two Space Agency; on the one hand Russian spacecrafts have always had a specialized airlock through which the cosmonaut could exit, leaving the other areas

pressurized. On the other hand the first U.S. spaceships (Gemini and Apollo) had to depressurize the entire habitable volume during EVA.

Brief EVAs History

NASA mission planners mint the term Extra Vehicular Activity in the early Sixties for the Apollo Program designed to land men on the Moon [5]. During the missions the astronauts would leave the spaceship in order to collect samples and reproduce scientific experiments in the new environment. To achieve the objectives aimed by the Apollo Program, NASA realized the Gemini Program in order to train astronauts and develop the ability of working outside the spacecraft.

However, in that historical period Soviet Union was fiercely competitive and strongly interested in holding the early lead it had gained in manned spaceflight. The single-pilot capsule Vostok was quickly modified and converted into a three-person vessel named Voskhod in order to compete with Gemini and Apollo [6]. In this way, after winning the race for the first satellite and the first man in space, the Soviet Union surprised the entire world on March 18, 1965 with the first EVA in low Earth orbit, performed by Alexei Leonov, abroad the spacecraft Voskhod 2. The cosmonaut ventured in the vacuum of space for twelve minutes. When Leonov landed he declared that the entire operation was easily accomplished but that was not totally true. During the mission the space suit ballooned from its internal pressure against the vacuum of space, becoming so stiff to impede Leonov to reach the shutter of his chest mounted camera, but this fact wasn't the biggest issue [2]. At the end of the spacewalk, the suit stiffening caused a more serious problem: when Leonov had to re-enter the capsule through the airlock, he incorrectly entered head-first and got stuck. He had therefore to manually reduce the internal pressure of his spacesuit risking the Decompression Sickness (DCS); this operation added other twelve minutes to his time in vacuum, overheating him by from the exertion. The details of the mission felt in the public domain only after the end of the Cold War [2].

Just three months later, on June 3, Edward H. White, on board the spacecraft Gemini 4, became the first U.S. astronaut to accomplish an EVA mission, floating tethered to his capsule for twenty-two minutes. White was the first man to be able to control his movements in space with a device called Hand Held Maneuvering Unit (HHMU [3]). Again the mission went through troubles: a defect in the capsule's hatch

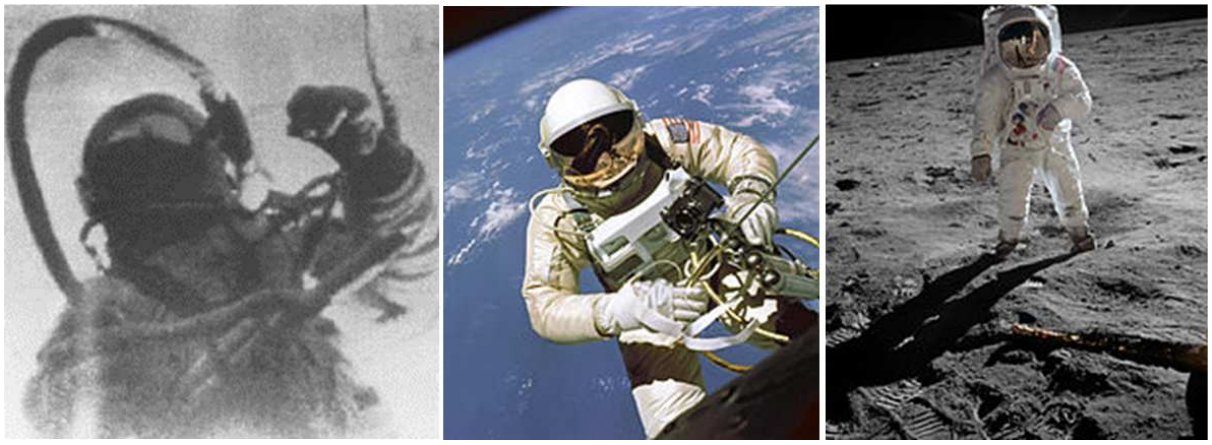

Figure 1: Three main milestones in the EVA history: Leonov during the first spacewalk March 18, 1965 (left), Ed White during the first U.S. spacewalk June 3, 1965 (center) and Buzz Aldrin during the first moon landing mission July 21, 1969 (right).

latching mechanism caused some difficulties, which delayed the EVA and put the crew at risk of not getting back alive to Earth. Enraptured with the spacewalking experience, White remained in space beyond the planned time and, when he was ordered to re-enter by NASA's Mission Control Center, he declared that *"this is the saddest moment of my life"* [7].
On July 20, 1969, after six hours and half Eagle landed, the U.S. astronaut Neil Armstrong descended the small ladder of the Lunar Module (LM) and stepped onto the surface of the Moon saying his famous words *"this is one small step for man, one giant leap for mankind"*. Armstrong's crewmate Buzz Aldrin followed him after a while. Moonwalks were only performed by six Apollo crews in history, in the 1972. During the next five decades hundreds of EVA missions were accomplished, becoming even more sophisticated in terms of equipment and tasks. The longest EVA was eight hours and fifty-six minutes, performed by Susan J. Helms and James S. Voss on March 11, 2001.
All these missions had not only accomplished significant work in space, which was impossible to be done through any other means (e.g. robots), but also yielded a huge knowledge, skills and experience among the astronauts and cosmonauts corps about how to perform meaningful work beyond confines of Earth's atmosphere. It can be declared that modern crewed space program can be divided in two categories: those that already need EVAs and those that will need EVAs in the future. During the Shuttle Program, NASA started dividing Extra Vehicular Activities into five different categories: satellite repair and rescue mission, Hubble Space Telescope (HST) repair and upgrade, International Space Station (ISS) construction, Shuttle and Space Station repair and maintenance and, finally, the developmental EVA, which were planned to test new EVA techniques, performances and characteristics of new EVA tools and to study the expected EVA environment for ISS [8].

The EVA Spacesuit

The spacesuit is an extremely complex garment device, composed by several elements that have to accomplish a high number of tasks, which can be summarized in a single big objective: allowing the astronaut to survive during his mission in the harsh environment of the outer space. The suit subsystems have to provide breathable atmosphere, pressurization, mobility, temperature control, communication, protection from radiation, handle robotic tool and so on [9]. Spacesuits are often worn inside the spacecraft as safety precautions in case of loss of cabin pressure and are mandatory for every kind of EVA mission. Due to the extreme environment the suit must perform a series of functions that are fundamentals for the astronaut's survivability or simply useful for a better and more comfortable work. The main issue related to the space environment is the Decompression Sickness (DCS). *"Decompression sickness takes place when the inert gas (generally nitrogen) that normally is dissolved in body tissues at one pressure forms a gas phase ("bubbles") at a lower ambient pressure, when the tissues become supersaturated with nitrogen"* [10]. In other words DCS occurs when the human body passes from an environment with a certain pressure to another with a lower pressure: e.g. between the cabin and the space suit or inside the cabin during an emergency situation caused by a leakage of atmosphere.
The Earth's atmosphere is composed by seventy-eight percent of nitrogen which is useless for the human being survivability, therefore there is no need to carry it into the space suit. Because of this the internal pressure of the space suit can be smaller and compound mainly by the more useful oxygen. A lower internal pressure is essential to guarantee dexterity and mobility, reducing the stiffness related to every movement, but at the same time it increases the risks related to DCS. To minimize DCS, astronauts have to breathe pure oxygen for a certain amount of time prior to depressurization in order to wash out the nitrogen from the body tissues; this procedure is called pre-breathe [11, 12, 13]. Table 1 shows a comparison between the pressure of cabin, the spacesuit atmosphere, the pre-breathe time and the oxygen concentration for the main Historical Space Program. Nowadays the minimization of the pre-

Program	Cabin Pressure, [KPa]	Cabin Oxygen Concentration, [volume %]	EVA Suit Pressure, [KPa]	EVA Pre-breathe time, [min]	EVA Pre-breathe Conditions
Mercury	34.5	100	---	---	---
Gemini / Apollo	34.5	100	25.8	0	---
Skylab	34.5	70	25.8	0	---
Shuttle	70.3	26.5	29.6	40	In suit[a]
	101.3	21	29.6	240[b]	In suit
ISS/US	101.3	21	29.6	120-140	Mask and in suit; doing exercise
				240[b]	In suit
Salyut, Mir, ISS/Russian	101.3	21	40.0[c]	30	In suit

[a] after 36 hours at 70.3 KPa

[b] under emergency conditions, a minimum of 150 minutes of unbroken Pre-breathe is recommended

[c] can be reduced to 26,5 KPa for a short duration work regime

Table 1: Historical Spacecraft Cabin and Spacesuit Atmospheres.

breathe time is a hot topic related to the future of space missions, especially if the number of EVA hours will be increased. Moreover the space suit has to provide the thermal regulation. On Earth heat can be exchanged between two bodies by convection, radiation and conduction. Vice-versa in space heat cannot be transferred through convection and then the human being's temperature control through sweating doesn't work. Since the space temperature varies greatly and quickly between sunlight and shadow, the spacesuit has to be insulated to the external environment and it is thermally controlled by a device called Liquid Cooling Garment (LCG) [14]. The Liquid Cooling Garment is a close-fitting fabric with flexible tubing of few millimeters of diameters kept in contact to the human skin; a fluid flowing into the pipes helps the heat exchange transporting it towards or away to the human body. Furthermore the spacesuit has to provide breathable atmosphere supplying oxygen and removing carbon dioxide, water vapor and contaminants. These gasses can be exchanged with the spacecraft (in case of tethered EVA) or through a Portable Life Support System (PLSS) [15]. Finally, the spacesuit has to protect the astronaut from all the remaining treats of the space environment like radiations, micrometeoroids and so on.

The spacesuits and the elements related to it are one of the most important and productive research fields related to EVA and space in general; their evolution covers many decades, from the first prototype worn by Yuri Gagarin in the very first manned space mission in 1961, to the hyper technological suits used by ISS and Shuttle astronauts. Allowing the astronaut to accomplish his work only granting survivability isn't any more enough. Tomorrow's spacesuits have to be made in order to improve the astronaut's abilities, allowing him to perform his tasks for longer times, in a better way and with a high level of comfort. During the first decades of the space program, due to the political and economical situation related to the Cold War, most of the information related to the characteristics of space suits remained marked as confidential. Recently, with the declassification of part of this material, a huge amount of information became accessible to everyone interested in it. Knowledge related to the various elements of spacesuits, the constraints, the number of layers, the materials and so on felt in the public domain, becoming available also to the independent research centers.

Brief U.S. Spacesuit History

The Mark IV, originally developed for high altitude fighter aircraft, was the first spacesuit ever produced by the US and was used during the Project Mercury spaceflight. After the preliminary tests performed during the Mercury Project it was found that a value of pressure equal to 24.13 KPa was sufficient for a space suit if the wearer breathes pure oxygen. Before the development of the Mark IV, the U.S. Navy had already tried to realize different types of pressurized suits, but all of them presented big problems in terms of mobility and weight, as a consequence of the internal pressure. The Mark IV designer partially solved the problem related to mobility applying a series of aluminized nylon cords to prevent inner layer from expanding and causing the undesired "ballooning" effect. With its ten kilograms, the Mark IV was the lightest pressure suit ever realized until then and, after few modifications related to the breathing system and the external coating, the original Mark IV was ready to be launched into space. It is important to underline that the Mercury suit was only developed for IVA (Internal-Vehicular Activity) and represented a safety measure in case of leakage or impacts; luckily no Mercury capsule ever lost pressure during a mission, so the suits never needed to be inflated after launch [16]. After Mercury the Mark IV was used for the first steps of the development phases of the Gemini Program. The Gemini Program had different requirements; the bigger capsule and the need to carry out Extra Vehicular Activity caused the old Mercury suit to be quickly phased out on NASA service and replaced with complete new suit: the G3C.

The G3C, worn by the crew of Gemini 3, consisted of six layers of nylon and Nomex, with a retaining web and an external coating of white Nomex fabric. The suit had a full removable pair of boots made of Nomex, a pair of gloves detachable through a special locking ring and a helmet equipped with the communication system. After Gemini 3 the G3C suit was renamed to G4C and upgraded with an additional layer of Mylar for the temperature control. The G4C was developed in two versions: one for the commandant and one for the pilot. The differences between the two suits were related to the different tasks that the crewmembers had to perform. Edward White made the first U.S. spacewalk wearing a G4C. A new version of the suit appeared during Gemini 7 mission; the G5C presented two main new elements compared to the previous one: a Navy-style aviator helmet and a series of additional zip for the complete removal of the suit. During Gemini 7 Jim Lovell was the first astronaut to completely remove his pressure suit during a mission.

When the Gemini program ended the G4C was chosen as starting concept for the new Apollo Program space suit allowing the realization of the A1C, which was an evolved version of the Gemini suit with new energy connections and a protective shell over the helmet visor. During a launch test of the very first Apollo mission a terrible blaze inside cabin killed the crew and, since then, the spacesuit required to be fireproof. NASA decided to phase out the A1C asking for a new spacesuit developed by ILC Dover [17], called A7L. This was the primary spacesuit worn during the Apollo program, the Skylab flight and was the dress of the first man on the moon; Neil Armstrong described his A7L as *"though, reliable and almost cuddy"*. The A7L design was one piece torso-limb composed by five layers, with joints made in rubber for the main articulations, the cable web to prevent the ballooning and special assembly to allow to move easily the shoulder. Metal rings on the neck and the wrists allowed the fast and easy attachment of the gloves and the helmet. The higher mobility granted by the suits permitted to accomplish every task planned on the moon surface. The high complexity of EVA missions planned for the Apollo Program demanded for the first time the addition of some new technological devices still present in today's suits. A self-contained Primary Life Support System for the provision of oxygen and energy was added in order to eliminate the linking pipe between the astronaut and the capsule, allowing free movements on the Moon's surface. The Apollo EVAs missions were much longer than the previous ones and so it was necessary to apply to the spacesuits the very first version of Liquid Cooling Garment (LCG) and Integrated Thermal Micrometeoroid Garment (ITMG). The latter is an external garment applied on the

suit able to protect it from abrasion and shield the astronaut from thermal solar radiation and micrometeoroids; this garment is made of thirteen layers of various materials [18] (one layer of rubber coated nylon, five of aluminized Mylar, four of nonwoven Dacron, two of aluminized Kapton and finally one of Teflon coated Beta filament). The last three lunar missions involved the lunar rover, a car like vehicle to be used on the moon's surface; in order to allow the astronauts to sit and drive the rover two new joints on the waist and neck had been added to the spacesuit. Around six months after the last Apollo mission, NASA launched its very first space station: the Skylab. The suit used during this mission was a simplified version of the Apollo one since the crewmembers were connected to the station all the time and so no un-tethered EVA were required. In 1982 a new spacesuit substituted the Apollo A7L, the Extravehicular Mobility Unit (EMU). EMU is essentially a fully equipped mini spacecraft [19] and is currently one of the two spacesuits used on the International Space Station (the other one is the Russian Orlan). EMU consist of a Hard Upper Torso which includes life support and electrical devices, a soft multilayer Lower Torso Assembly which includes waist bearing and boots and detachable gloves and helmet. This suit contains all the devices already present in the previous spacesuit; it reaches an internal pressure of 30KPa and can support astronauts for eight hours and half of EVA (with thirty minutes of emergency reserve). To perform EVA the Shuttle cabin is depressurized from 101.4KPa to 70.3KPa for one day, after which the astronaut must pre breathe for three quarters of hours. In case of EVA on board of ISS the astronaut has to pre breathe for about four hours [20]. The most extensive information about EMU can be found in Tepper's report [21] and in Hamilton data book [22].

Brief Soviet Union/Russian Spacesuit History

On the other side of the world the Soviet Union was the main US rival for the space race. The very first space Soviet suit for IVA was the SK1 (Skafandr Kosmicheskiy 1), specially realized for Yuri Gagarin's mission in the 1961. The project to execute the first EVA before US required a new spacesuit; in the 1965 Leonov for his spacewalk worn a new model called Berkut (Golden Eagle). The suit presented a double bladder redundancy to protect the astronaut if one of the two got punctured, in this case the second will be automatically inflated [23, 24]; the internal pressure could be set at either 40.5KPa or 27.4KPa. The life support was contained in the backpack and was large enough to provide forty five minutes of activity. Leonov's experience during the first EVA was useful to apply changes and improvements to the Berkut, realizing the Yastreb (Hawk), which was especially developed for the Soyuz docking project and spacewalk and had to be worn on board the vehicle. Therefore its design was thought in order to allow the dressing in orbit before and after EVA [24, 25]. The Yastreb was stiffer than the previous, but a series of pulleys and cables avoided the undesired ballooning effect and helped the cosmonaut during movements. The Krechet94 (Gyrfalcon) was the successor of the Yastreb. Developed for the lunar exploration during the Soviet manned lunar program, Krechet94 was the first semi rigid space suit ever developed; its hard upper torso will be adopted by all the later Russian suits and by the US EMU. The particularity of the Kretchet94 was the methodology of dressing up: this space suit was a rear entry suits, meaning that cosmonauts would enter through a hatch placed in the back, an easier way of wearing compared to the use of zips. The Krechet94 was equipped by the already explained Life Support System (placed into the back) and the Liquid Cooling Garment. The last model of Russian space suit is the Orlan (Sea Eagle), used since the first spacewalks of the Russian space program (the heir of the Soviet space program), it is currently one of the two spacesuits used on the International Space Station (with the U.S. EMU). The Orlan spacesuit has gone through several models, but all of them have similar characteristics: the hard upper torso with the rear entry hatch and the internal pressure of 40.5KPa. The first version of Orlan was developed to be linked to the spacecraft through an umbilical tether, while the others were designed to be self-sustaining. The first spacewalk using an Orlan suit took place in December 1977, when Yuri Romanenko and Georgi Grecko tested the first model Orlan-D

outside the Soviet space station Salyut6 during the mission Soyuz26. Unlike the lunar EVA suit, planned to be used in only one mission, the Orlan-D was designed to remain operational in the space station for two years and for several missions. During the construction of the Soviet space station Mir, which remained operational from 1986 to 2001, a new version of Orlan, improved in terms of control, material and mobility compared to the D model, replaced the previous version, it was called Orlan-DM. When Mir was operative the Orlan-DM was replaced by the Orlan-DMA, made in a new composite fabric with better performances in terms of lightness and toughness. The final version of the Orlan series is the Orlan-M, first used since 1997 in the Mir until the end of the station's operative life and today used on the International Space Station. Orlan-M show modest upgrade with respect the DMA model, the most noticeable were the addition of a second visor on top of the helmet and a bearing in the upper calf area of the legs. In June 2009, the latest computerized version Orlan-MK was tested during a five hours spacewalk on the ISS. The main improvement in the new suit is the replacement of the radio telemetry equipment placed in the PLSS. This device analyses the data from the various elements of the space suit, providing a malfunction warning and drawing a contingency plan.
More detailed information can be found in the Isaac Abramov's book [24, 25].

New Concepts of Spacesuit

Research related to space and spacesuits is a very dynamic field that involves several teams competing with each other to realize tomorrow's astronaut vest. There are now various ideas concerning the new generation spacesuit and, if some of them are direct evolution of different elements of the older versions, there are two particular ideas that overturn the basic concepts on which the spacesuits are built: the Hard-Shell Suit and the Mechanical Counter Pressure.
The Hard-Shell Suit is made in of metal or composite material avoiding the use of fabric for the joints. The joints contain ball bearing and sliding wedge ring segments to allow wide movements with the articulations. This is because the mechanical work needed to change the volume of a constant pressurized system is proportional both to the internal pressure and the variation of volume. If a joint flexing causes a variation of volume, the astronaut has to do extra work every time he has to bend that joint, maintaining the force in order to keep the joint bent. A completely hard joint maintains an internal constant volume all the time, removing completely the negative effect of the counter force. This allows the hard suit to operate a higher pressure which would eliminate the need of pre breathe. The NASA AX5 had the flexibility necessary to guarantee up to 95% of the human movements.
The Mechanical Counter Pressure is a new approach that has been suggested in order to reduce problems related to dexterity of a conventional full pressurized EVA suit. The main idea is to provide oxygen only to the isolated helmet, while on the rest of the body the pressure is provided by a tight, form fitted garment that mechanically compresses the body. In 1968 Paul Webb shows the advantage of a complete elastic MCP suit [19] made up of seven layer of highly elastic material. The suit guaranteed higher mobility and dexterity and required a lower metabolic cost for movements. The good heat dissipation allows reduction of dimensions and complexity due to the fact that a cooling garment is no more needed. Finally, this new concept is safer than current pressurized suits, because punctures cannot cause loss of pressure [26, 27, 28]. Nevertheless this new concept of space suit was never fully developed.

The EVA Glove

Among the various elements of an EVA system the performances guaranteed by EVA Gloves are one of the key factors of the success in performing Extra Vehicular Activity. The human hand abilities like

dexterity, manipulability and perception are unique and define that limb like the most versatile, effective and multipurpose tool that the human being has naturally equipped. This is especially true in case of unknown environment such as EVA environment; in that microgravity environment procedures and tasks are too complex and diverse to be fully defined in advance. Under these conditions hand becomes the primary means of locomotion, restraint and handling. Facilitation of these activities and protection from the harsh environment are the two, often conflicting, objectives of the EVA glove designer. The EVA Glove is an extremely complex structure which must guarantee a series of critical functions in order to insure the accomplishment of the EVA mission; it must provide environmental containment, thermal and radiation protection and high resistance, but it must also be sufficiently flexible to enable the astronaut to move and grasp in an efficient way. Safety and durability are usually the priorities, resulting in a less than ideal flexibility and dexterity properties. Comments received by astronauts and cosmonauts revealed their observations and desires for a better glove, able to stay in place, allow easier gripping without significant further effort and provide a good grace of dexterity and sensorial feedback [16]. Important work has been performed during the years to improve EVA gloves, leading to appreciate results, but more work is needed to deal with the requirements of tomorrow's space missions. ILC Dover is a US company which designs EVA suits and gloves since 1961 and provided the A7L in 1966 for the Apollo mission. This company is still today the biggest provider of this kind of products for NASA [17]. During the years the improvements of EVA gloves were mainly focused on changing materials maintaining the basic concept unchanged. The improvements started from the end of Mercury realizing the Series 1000, the very first U.S. Shuttle EVA glove; this evolution continued until the Phase VI gloves, when the production process completely changed. The new technologies related to the stereo lithography prototyping, laser cutting, laser scanning and 3D modeling opened a new frontier with new potentialities. There is not much information about EVA Gloves until the Series 4000, which were introduced into the Space program in 1985. Series 4000 gloves were originally available in nine standardized sizes, but later some custom sized gloves were produced in some special cases. After the Series 4000, the Phase IV gloves were developed by the refinement of the internal bladder and reduction of dimensions, achieving improvements in fingertip sensibility and global fitting. In order to allow the palm of the pressurized glove to fit with the natural shape of the human hand, a custom formed high strength palm bar and a segmented palm plate were been included. This customization possibility provided more comfort, without limiting flexibility thanks to the special design of the new parts. The wrist of the Phase IV is composed by four ring rolling convolute joints, to provide little variation of the internal volume of the glove during manipulation, granting lower torque and stable motion. However, the Integrated Thermal Micrometeoroid Garment remained basically unchanged from the previous Series 4000 [29]. The following EVA glove was the Series 5000, which differed from the previous mainly in the wrist joint; although this new glove required low torque to move the astronaut's hand, its steel components made it heavier. In this period new technologies like Laser scanning and Stereo Lithography appeared and were partially adopted for the gloves development. These new technological solutions guaranteed big progress in terms of precision and reproducibility and later, during the development of the Phase V, become a constant presence in the design and fabrication process. More accurate scanning was possible; data output and design changing became readily usable by advancing of Computer Aided Design (CAD), that allowed to realize complex shapes and surfaces. Weight was reduced by using titanium and graphite/epoxy composite materials and bearings were replaced with brushing assemblies. Afterwards new requirements in the basic design of the EVA spacesuit required a change in the main concept of EVA gloves leading to the Phase VI which are operating today. Phase VI wrist is made by soft material and the use of lightweight polyester fabric enabled the design of new finger and thumb joints, decreasing the contrary torque and improving mobility and fingertip tactility. The overall TMG protection performances were further increased and

Program	Total EVA Duration, [hours]	Suit Used
Gemini	12:40	G-4C / G-5C
Apollo	165:17	A7L / A7LB
Skylab	82:52	A7LB
Space Shuttle	1894:09	EMU
ISS	835:02	EMU

Table 2: Summary of U.S. Extravehicular Activity Duration Program (1965 to 2009).

new features to allow an easier on orbit replacement, of damaged or worn out TMG, were incorporated. Phase VI gloves incorporate an active internal heating system consisting in a series of resistive elements located at the fingertips; this system originally had a three-volts powered but, thanks to the development of batteries, it was recently substituted by a twelve-volts design [30]. Phase VI gloves were used for the first time in space in 1998 with satisfying results and currently being realized and delivered for fifty seven EVA crewmembers [29].

The Future of EVAs

The new human desire to expand his horizon upon the lands of Moon, Mars and beyond will change the role of Extra Vehicular Activities in space missions. A new vision of EVA is rising, one that embraces spacesuit, rover and robots during the new lands exploration. In the past EVAs covered mainly operational support roles, enabling complex work like repair, maintenance, observation and so on; since the end of Apollo Project EVAs never covered a primary mission role. In this new emerging view EVA acquire primary mission role, becoming a keystone to enable successful mission, to obtain new scientific knowledge and experience [9].

Table 2 and Figure 2 show the behaviour of the total EVA duration in the forty years of human spaceflight history during NASA missions. Since now astronauts reached approximately three thousand hours of EVA time, most of which wearing EMU on the space shuttle or on the ISS. The total duration of each generation increased by more than an order of magnitude compared to the previous one. A new model is rising for exploration missions in the next decades with the *"mountain of EVA"* (Figure 3). NASA plans to increase more than ten times the number of operational hours for the exploration of Moon and Mars. This large increase in EVA hours is relevant for any future mission independently from the particular expedition architecture or goal. There are also projects that aim to extend space experience to everyone who wants to venture in it [7]. According to these planners, in the near future the space will be accessible to anyone with the means and the desire to experience the microgravity and to see the Earth from a new perspective. It will be an unavoidable step of history, caused by the need to *"cross the boundary"* that can be found in the basis of the human nature.

Tomorrow's EVA needs

The new planet exploration Space Program requires a series of improvements on many aspects of EVA, in order to guarantee the human beings involved in it to accomplish the tasks in the best way and with the less possible risks. The possibility of accomplishing EVAs surface operations is the most important and critical point of the future space missions, independently from destinations or details. NASA has already defined the main system capabilities, technology and constraints for the new space suits concept. Beyond the appearance, the new generation suits have detailed specifications in terms of joint torque, joint range, minimum mobility both for IVAs and EVAs. Future research is needed to improve joint performances and ergonomics, also considering the variation of biometrics parameters between

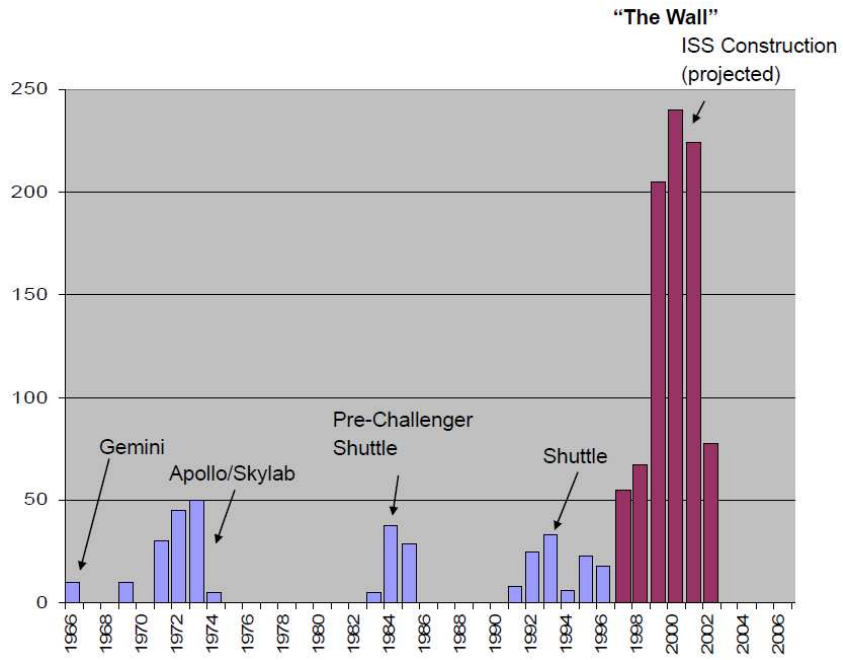

Figure 2: Annual cumulative hours of EVA, showing the "EVA Wall" achieved during ISS construction.

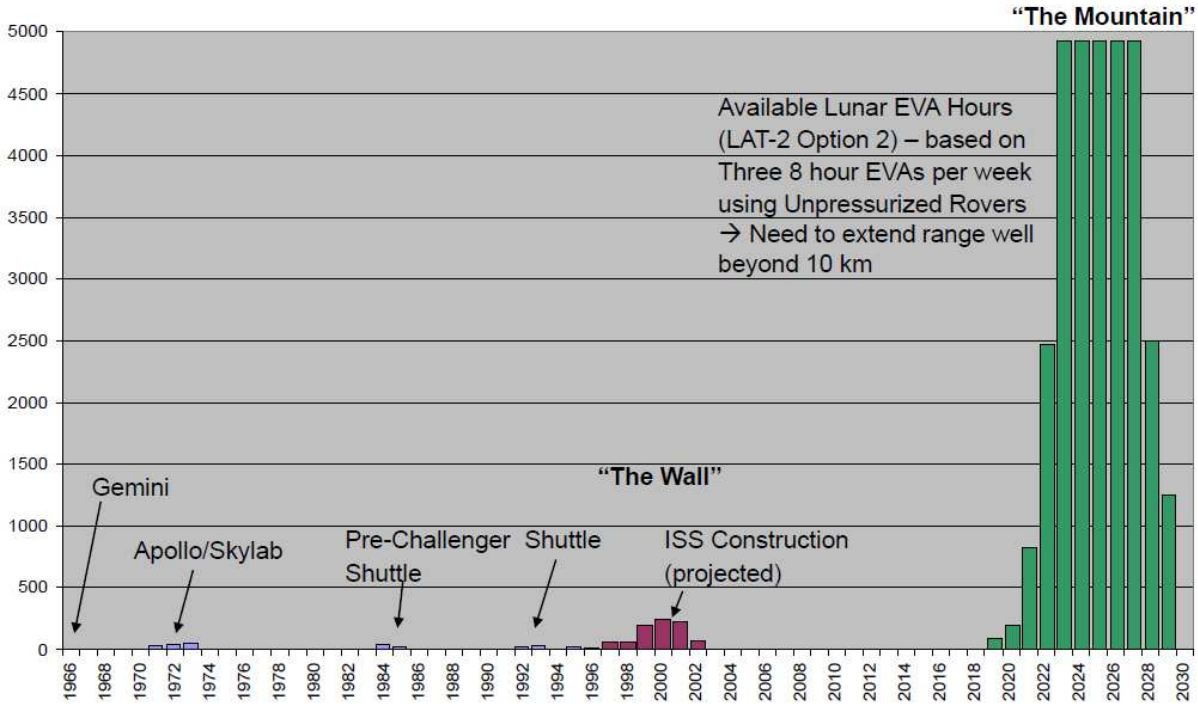

Figure 3: Annual cumulative hours of projected EVA, showing the "mountain of EVA" for Exploration Missions.

different human beings, to prevent injuries and improve safety. Since reduced mobility is the worst issue, all the devices have to be improved in order to work in the best possible way; a new heat rejection, variable pressure regulation, new carbon dioxide remover are only few examples of the huge

amount of improvements required in order to allow the astronaut to work in space like a geologist on hearth. The other big problem related to the EVAs surface operation is protection from environmental hazards. The effects of dusts on the equipment are well known since the Apollo missions [31, 32] and came from abrasion to thermal control problem to false sensor readings and so on. Astronaut Richard Gordon reported: *"the cabin atmosphere was okay. On the way out, it was clean. On the way back, we got lunar dust in the command module. The system actually couldn't handle it; the system never did filter out the dust, and the dust was continuously run through the system and throughout the spacecraft without being removed"* [32]. There is currently a lack of information to well understand how to mitigate harmful effects of continual dust exposure and possible micro meteoroid impacts. The research in dust mitigation will need to distinguish between the different surface environments due to the different effects, structure and nature of the lunar and Martian particles. These are only some examples of the future needs in order to be able to accomplish EVA surface exploration, more information are present in the book *"Recapturing a Future for Space Exploration"* [9].

Tomorrow's EVA Glove needs

EVA Gloves are probably the most critical part of the suit because almost all operations involve the use of the hand. Collecting the results coming from the various post mission interviews there is a consensus about several problems related to the EVA gloves such as reduced dexterity, lack of tactility feedback and higher fatigue. These problems are not the worst; according to a 2005 study on 350 EVA training injuries reported from 2002 since 2004, nearly 50% were finger and hand related traumas. For instance, one of the most common types of lesion reported by astronauts during EVAs is known as fingernail delamination, in which the nail completely detaches from the finger [33]. Moreover growth of bacteria inside the gloves can be a huge problem during EVA missions since activities can last up to eight hours a day, generating a warm and moist environment inside the glove that induces the proliferation of bacteria [34].

The first step to overcome problems related to dexterity and fatigue consists in an accurate evaluation of the glove effect on hand performances. Some work to understand the relation between glove and hand performances has already been done in past; specialized literature has been discovered since 2009 a new and growing interest in this subject in order to develop the constraints and requirements for the design of tomorrow's EVA gloves [35, 36, 37, 38, 39, 40]. A partial solution of these problems was proposed in few papers that suggested a better customization and fitting of the gloves or described special hand training to be done before the missions to prepare the astronaut for the extended duration EVAs [16]. Another high promising way to solve this kind of problems, allowing the creation of a dexterous glove, is represented by the Mechanical Counter Pressure (MCP) technology. In 1983 Clapp designed and tested a MCP glove and compared its performances with the A7L internal pressurized glove [41]. In 2002 Korona et al. developed a hybrid gas elastic glove and compared its performances to the EMU glove [42]. Finally, Tourbier and Tanaka studied the physiological effects of an elastic MSC glove on the human hand [27, 28]. However, the MCP gloves design is still limited by some factors, like the difficult wearability, a non-uniform pressure distribution and an insufficient pressure in correspondence of body concavities; moreover their mobility is still smaller if compared to the bared hand. Overcoming these problems is a fundamental step to be able to realize tomorrow's EVA glove [26]. Fingernail delamination is another issue already under evaluation by researchers; some potential injuries are already prevented with apposite countermeasures and an improved fitting of the glove. However, only a small part has already been solved; new solutions are needed in order to reduce the finger stresses. Since an injured nail requires more or less six months to fully and healthy re-grow, prevention is a key factor to solve this problem. Some researches underlined that nail injuries in the EVA gloves can be prevented with a gas flow around fingertips; some studies related to the improvement of

glove ventilation are already considering that. Regarding the bacteria growth problem, several organic and inorganic anti-microbial treatments have been studied to be applied in space environment by ILC Dover. Some studies showed that apposite coating can partially prevent dangerous microbial proliferation, in particular silver coatings guarantee a good property in terms of comfort and are still under investigation [34, 43]. Recently ILC Dover studied a new revolutionary garment material which could be able to integrate the pressure restraint and the thermal control functions [16].
Improving the space glove is a multidisciplinary, suit-independent task; in the lasts years NASA's Innovative Partnership Program called a series of competition prize contests named *"Astronaut glove Challenge"*, in which non-government researchers can submit their own version of tomorrow's EVA glove [44, 45, 46, 47]. In November 2009, Peter Homer won the first prize of $250000; the main difference between Homer's glove and the Phase VI is the structure of the finger joints. The glove presents a crisscrossed ribbon into an "X" in correspondence to each joint in order to create a hinge-like effect [48, 49].

The Smart EVA Glove Project

The main goal of the Smart EVA Glove project is the development of a tool able of overcoming, or preventing, hand fatigue and of avoiding injuries during space operations. This device would be a significant improvement for the astronauts, allowing them to accomplish their tasks more efficiently, more comfortably and for a longer time, becoming a fundamental addition to the standard EVA's equipment.
The study presented in this thesis is a preliminary approach towards a suitable technological solution able to reduce the fatigue of the astronaut's hand by avoiding interference with its natural movements. The device will has to follow the human hand during its movements, to increase the performances limited by the EVA glove and finally be able to work in the extreme space conditions. In other words the device will has to be a compact and lightweight hand exoskeleton designed to be embedded inside the astronaut's suit in order to partially or fully vanquish the stiffness introduced by the multilayer garment and the internal pressurization.
The development of devices for space applications face always strong limitations regarding the environment in which they operate, therefore the motivation is to study the feasibility of developing a device thin enough to fit inside the EVA glove, strong enough to provide the forces to operate, and robust enough to be reliable for a long period of time.
It is important to underline that, limitations like the harsh environment, the restricted working space and the high complexity of the human hand, increase sharply the complexity of the project requiring sometimes sub-optimal solutions; e.g. the exoskeleton will have a multi-finger design, the coupling of adjacent fingers allows the whole device to be lightened and simplified.

CHAPTER 2:

"Whereas knights of old wore armor of plate, the modern knights of the air wear the invisible but magic armor of confidence in technology"

Mike Spick

STATE OF THE ART

As explained in the previous chapter, the stiffness of the space suits, and in particular of the space gloves, generates many problems during the work of the astronauts in extra vehicular activities such as increasing of the fatigue, reduction of the dexterity, limitation of the overall duration of mission, physical damage on finger and nails and so on. A device similar to a hand exoskeleton has been proposed as a solution in order to overcome all those problems, helping astronauts to perform their job in a better way, for longer time and granting a high level of comfort.

This chapter deals with the analysis of the state of the art of robotic hand-like devices. The study of robotic hands and hand exoskeletons has to be considered as the first step of the design activity of the aimed future device. Moreover a short overview on the possible solutions related to sensors and actuators has been reported.

In the last few years, the number of projects which study the human hand from the robotic point of view has rapidly increased, due to the growing interest in academic and industrial applications. The human hand is a complex mechanism; it has a wide range of motion and a high number of degrees of freedom, allowing an incredibly great variety of movements. In recent years, as robotics has advanced, significant efforts have been devoted to the development of hand-like devices. The two main related application fields are prosthetic-robotic hands and exoskeletons.

On one side, robotic hands are developed with the characteristics complying with those of the human hand, taking advantage of its variety of movements. Moreover, thanks to its versatility, it is possible to avoid the use of a large number of end-effectors when performing tasks that involve interaction with different objects or in unpredictable environment.

On the other side, exoskeletons are designed to fit onto the human hand, aiming at enhancing performance in the carrying out of daily activities or supporting the rehabilitation stage of hand injury recovery.

Exoskeletons

Many examples of hand exoskeletons, both products and prototypes, are available in literature. They are characterized by some common aspects and many unique peculiarities that distinguish each of them. Indeed, despite of very similar functionalities, each hand exoskeleton results to be unique and extremely different from the others, thanks to the characteristics of their mechanism architecture, control system and working principles.

The aim of the following part is to analyse the main aspects involved in the hand exoskeleton design, such as the system kinematics, the actuation system, the transmission and the control strategy, enlighten the differences and the common features. The human hand is a very complex organ of interaction and sensation involved in many different typologies of activities. The extreme dexterity and the high strength-dimensions ratio transformed the human hand, during the years, in the most versatile and multipurpose tool, on the basis of which all the interactions of the today world are designed.

Since the 80's, many researchers worked on the development of hand shaped robotic devices; they aimed to replicate the functions of the human hand, and the studies presented in scientific literature are simply uncountable. The application of this type of devices cover many and different fields, from the industrial dexterous manipulators to the humanoid robots, from tele-manipulators to upper limb prosthesis and orthosis. Orthosis are medical hand exoskeletons, realized in order to support rehabilitation or everyday life activities of people who suffered of injuries or strokes.

A hand exoskeleton is a complex mechatronics system, actively controlled and made to be strictly coupled with the human hand, so that the two systems move together, exchanging forces and torques and interacting with the external world as one single element. The design of this kind of devices shows a certain number of critical issues that have to be faced; for example the control of the exchanged torque and the consistency of the motion of each part with the human hand are both mandatory in order to guarantee the safety of the operator. In practice, the exoskeleton has to apply forces on the fingers in order to oblige them to perform a specific and desired trajectory and improving the natural force they could normally apply. Another goal of some exoskeletons found in literature is to track the movements of the human fingers; the devices made specifically for this task only are also called data gloves [50], usually they don't need any actuator and then cannot fully considered exoskeletons.

The hand exoskeletons could be roughly divided into three main typologies, distinguished according to their goals and targets: rehabilitation, haptic and assistive devices.

Hand exoskeleton made for rehabilitation purposes are devices specifically developed to perform controlled movements in order to recover the functions of damaged or injured hand. Usually the emulation of the correct movement of the finger results to be a key factor, much more important with respect dimensions and high torque generation, in this type of exoskeleton.

Haptic hands are made to emulate the interaction between the human hand and the external world. They show two main functions; first of all they have to track the movements of the hand in order to control or manipulate other objects, then they usually have to provide a sensation feedback, usually force feedback, on the operator's hand. In order to accomplish to the first function the exoskeleton must be able to measure the position of the articulations of the human hand. All the data acquired by the haptic hand, called in this case "master hand", are then used to control the movements of a second device, called "slave". The slave could be both real and software generated in a virtual reality environment [51, 52, 53, 54]. Once the slave interacts with objects belonging to its world, the master has to transmit the contact information to the operator. For example the forces measured by the real slave device, or calculated from the virtual reality environment, are emulated to the operator's human fingers by means of the exoskeleton actuators. This fact generates a realistic human sensation of touch and force sensing.

Finally assistive devices are tools made to compensate specific hand diseases in the patient everyday life, like stroke or tremble. Those pathologies could strongly limit the actions of people during their everyday life, making some activities very difficult or even impossible to be carried out without aid. Assistive devices are usually worn for long time during the days, for that reason constraints related to dimensions, weight and comfort become fundamental aspects in those devices.
Usually the architecture and the elements of the hand exoskeleton are strongly related to the specific application. For example, from the architecture point of view and according to the specific application, different degrees of freedom could be necessary, involving different fingers and articulation. Some applications need the actuation and the control of the motion of each finger [55, 53], some others of only a group of fingers [56, 57, 58]. Similarly, also the number of degrees of freedom of each single finger can change, by coupling the motion of articulations or keeping each articulation free to move independently from the others [59].
Another characteristic that strongly distinguish among the exoskeletons is the choice of the actuators that have to be used. Usually this decision is driven by constraints related to size, weight and power needed. The choice of the correct type of actuator is probably one of the most critical aspects in the whole design of a hand exoskeleton. The size of the actuators is strongly related with the power that they can generate, so usually the requirements of high power and low mass and dimension are fighting together and a compromise in a midpoint must be found. Some exoskeletons are driven by means of pneumatic or hydraulic cylinders [60, 61, 62, 63] whereas many others use classical electrical motors. In this second case the actuators are usually placed far from the joints that have to be actuated and the movement is transmitted by means of wires or tendons [64, 65, 53] or gearboxes [52, 66]. Other exoskeletons use some particular and less common motors, such as piezoelectric ultrasonic motors that, thanks to their limited size, allow the placement directly on the joints [51].
There are currently many different projects underway. Schabowsky et al. [67] introduced a newly developed Hand Exoskeleton Rehabilitation Robot which was designed to provide a full range of motion for all fingers. NASA and General Motors presented a prototype of the Human Grasp Assist device [68]. Worsnopp et al. [69] introduced a finger exoskeleton for hand rehabilitation following strokes, to facilitate movements, especially pinches. Another project is being developed by Ho et al. [70]: their exoskeleton hand is EMG-driven, again for rehabilitation, but working on all the fingers.
All of these projects show a different number of degrees of freedom and different structures but, in general, they are developed with the same objective of mimicking the main characteristics of the human hand. This implies that, a complete understanding of the characteristics of the human hand, involving the anthropometric dimensions, its kinematics, and its dynamics is mandatory. In the forthcoming chapter a comprehensive analysis of all the characteristic and biometric parameters of the human hand has been provided.
In the following part of this chapter some interesting examples of hand exoskeleton found in literature have been analysed, focusing on their main characteristics like actuation strategy, sensors and function strategy. The data gloves are voluntary neglected in the following list because, although as previously said they could be considered exoskeletons, they are not able to provide power on the human hand and so they are not so useful in this specific case. This analysis doesn't aim to cover all the possible exoskeletons available but only the most important or interesting.

Rehabilitation Exoskeleton

University of Tokyo Hand Exoskeleton

The University of Tokyo developed a hand exoskeleton with the goal to perform rehabilitation procedures for patients who are suffering from contracture and strokes [64, 71]. In this device the

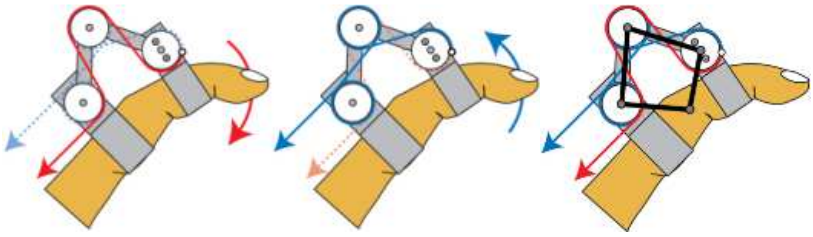

Figure 4: The transmission mechanism of Tokyo University Hand Exoskeleton

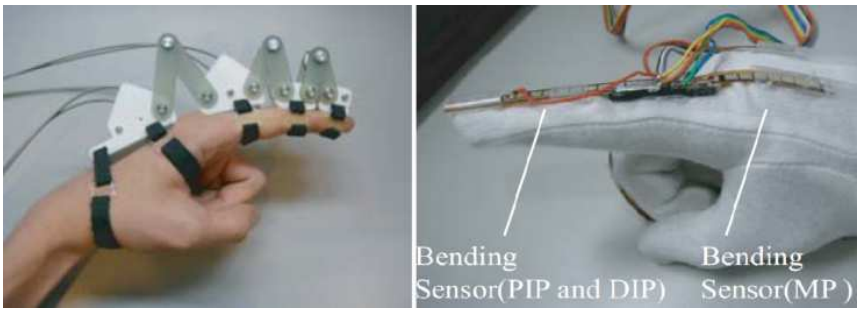

Figure 5: The University of Tokyo hand exoskeleton (left) and its Data Glove (right)

exoskeleton finger actuates the three phalanges of the human finger using only two degrees of freedom. The active movement is provided for the first articulation, while the other two are coupled into one single gait. The movement of each articulation is provided by a four bar linkage, using the finger joint as one of the four vertexes. Moreover, two links of the four bar linkage belong to the exoskeleton and two to the human finger, as shown in Figure 4. Each degree of freedom is actuated by a servomotor placed away from the hand by means of a wire-driven transmission. Figure 4 shows the route of the two wires assigned to the actuation of each articulation, both in extension (the red one) and flexion (the blue one). Each wire ends into a fixed pulley that cannot rotate. The force applied on the wires generates a deformation in the four bar mechanism, causing the approach of two opposite vertexes, and then the rotation of the human articulation.

In general, problems like strokes, or hand paralysis, affect only one hand; for that reason many rehabilitation protocols use the healthy hand in order to guide the injured one to perform tasks. This procedure, in which both the hands perform the same task at the same time, is named “mirror motion”. In this case the hand exoskeleton is coupled with a data glove worn with the healthy hand. The glove gathers the information of the healthy hand, which are used by the exoskeleton to perform the self-motion control on the injured hand. Figure 5 shows the exoskeleton (on the left) and the data glove (on the right). The data glove measures the angles of the phalanges and transmits the information to the exoskeleton that reproduces the same movements. This solution allows a wide range of motion and good control of the finger movements. Moreover, as the motors are placed away from the finger, the weight perceived on the hand results to be strongly reduced. Finally the four bar solution allows the device to be easily attached and adjusted to different finger sizes, keeping at the same time palm and fingertip free and allowing the hand to directly interact with the environment.

Berlin University Hand Exoskeleton

Similarly to the previous one, also the University of Berlin developed its exoskeleton focusing on the help of people who suffered of hand injuries, strokes and paralysis [59, 72, 73]. This hand exoskeleton shows a high number of active degrees of freedom. Each exoskeleton finger actuates all the four

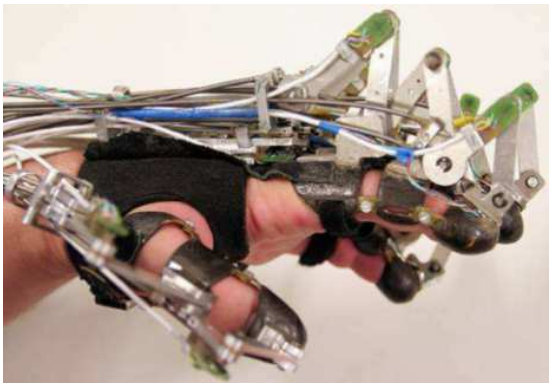

Figure 6: The Berlin University Hand Exoskeleton.

articulations of the human hand independently, granting an overall number of twenty degrees of freedom. This exoskeleton is shown in Figure 6; it uses the same, or very similar, strategy to the previous one, by means of four bar linkages driven through a wire transmission system and actuated by means of electrical motors. This device is equipped with five different types of sensors, two of them dedicated to measure the angular position of each phalanx, other two estimate the force applied on the human finger and the last one measures the current absorbed by the electrical motors. It is interesting to underline the redundancy of the sensor network; both position and force sensors measure the signals directly applied by the motors and those exchanged with the human finger. The position of each phalanx is measured by hall sensors placed in each four bar mechanism, while the position of the shaft of the motors is measured directly with optical encoders. The contact force between the human finger and the exoskeleton is measured with six force sensors, two for each phalanx, and electrodes for EMG placed on the forearm. Finally the torque applied on the shaft is estimated through the current sensors. This redundancy is an important aspect in this specific device. The comparison between different types of sensors, placed in different points of the device, allows mechanical failures or non-correct functioning to be detected, avoiding stresses and problems on the already injured hand.

AFX Hand

The AFX is an exoskeleton designed to support the movements of the index finger and realized in order to help patients after strokes and during their rehabilitation [69]. This device is composed by three degrees of freedom which emulate the flexion-extension movement of the human finger. Figure 7

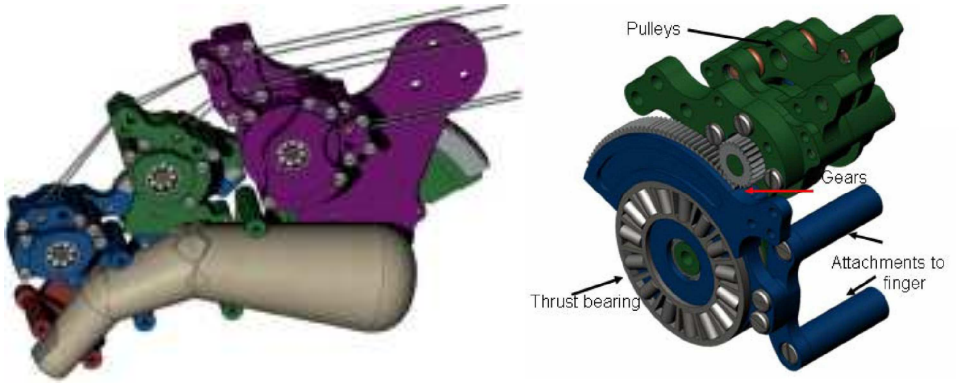

Figure 7: Mechanical structure of the AFX Hand.

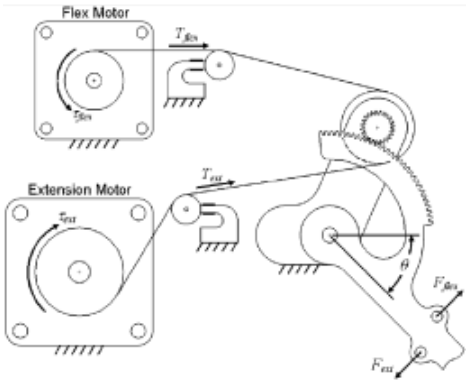

Figure 8: Measurement system of the wire tension.

shows the mechanical structure of this device; the three phalanges are connected together by means of metal segment that can rotate through a set of rollers. Each section of the movement mechanism is composed by a pulley, a small gear and a large gear. Three couples of DC motors represent the actuation system of the three phalanges of the exoskeleton, while the transmission is made with cables. Each couple of actuators is connected to the pulley of the related phalange with the transmission system; the pulley generates the rotation of the smaller gear and then of the larger one. Each large gear is connected to a frame which is directly attached to phalange and rotates around a constant axis that is different from the finger joints one. The exoskeleton and the finger phalanges are not constrained together; their attachment can rotate and shift moving freely. Therefore, although the axes are not coincident, the final motion is automatically adjusted and all the mechanical interferences are avoided during the movement.
Two types of sensors have been equipped on the AFX hand. The first one is an optical encoder attached to every DC motor and used in order to estimate the attitude of the exoskeleton and the joint angles of the finger. The second one is a force sensor, used to measure the tension of the transmission wires. Figure 8 shows the measurement system of the wire tension: a couple of small pulleys are mounted on a cantilever equipped with strain gauges. The internal tension of the wires could then be obtained by computing the difference between the two measured signals coming from the strain gauges.

Pittsburg University Hand Exoskeleton

This device was designed to improve the rehabilitation of natural pinching, controlling the movements of the index finger [60, 74]. This exoskeleton actuates two flexion-extension degrees of freedom of the

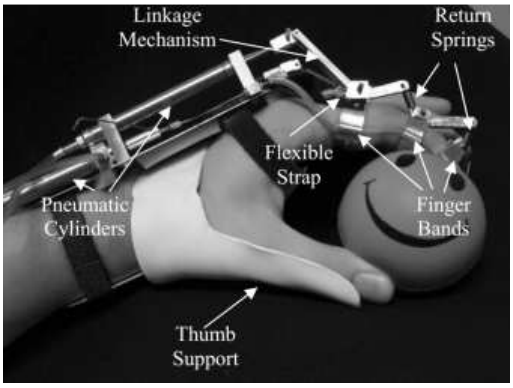

Figure 9: The Pittsburg University Hand Exoskeleton.

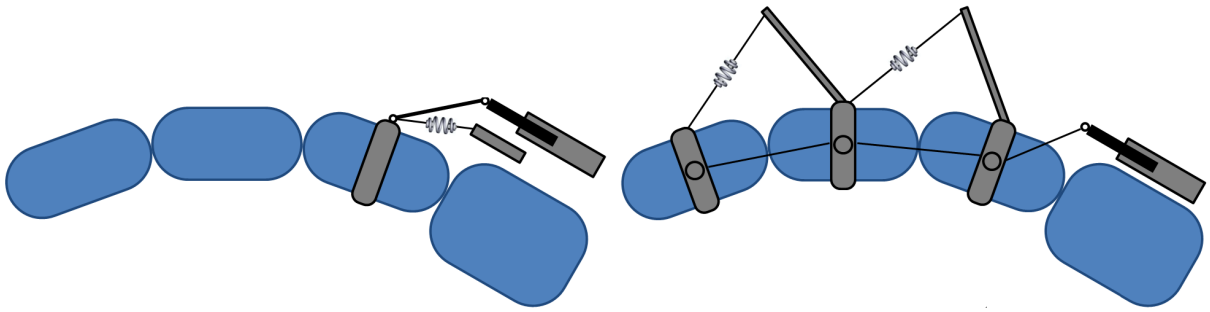

Figure 10: The mechanism for the first phalanx (left) and for the other two (right).

human finger while the third one is passively coupled with the others. The abduction-adduction degree of freedom is kept passive. The actuation is provided by two pneumatic pistons, one for the first phalange and one for the other two. The pinching tasks are performed by moving the index finger against a rigid and fixed thumb as shown in Figure 9. The structure of the exoskeleton consists of an aluminium frame placed on the back of the hand and three aluminium rings placed on each phalanx.
The flexion movement of the two coupled phalanges is performed with a steel cable passing in each aluminium ring, and connected to one piston on the back of the hand. The flexion movement of the first phalange is achieved by a transmission mechanism mounted between the first ring and the base plate. The extension movements are passively produced with springs which connect the adjoining rings. Figure 10 shows the entire mechanism both for the first phalange (on the left) and for the other two (on the right). The control of the exoskeleton movements is performed using EMG signals gathered from the biceps muscle of the patient. Finally, a variable pressure valve is mounted on each piston in order to control the maximum force exerted by the system on the finger phalanges.
This device is mainly focused on repeatedly movement of index finger and is not equipped with any position sensor; this means that it is not possible to control the position of the finger joints during the movements.

HANDEXOS

The HANDEXOS exoskeleton was designed in order to support the rehabilitation procedure after stroke [75]. This exoskeleton uses an under-actuated mechanism that allows the hand to passively adapt to the shape of a generic grasped object. The exoskeleton is composed by five fingers, each of them actuate a

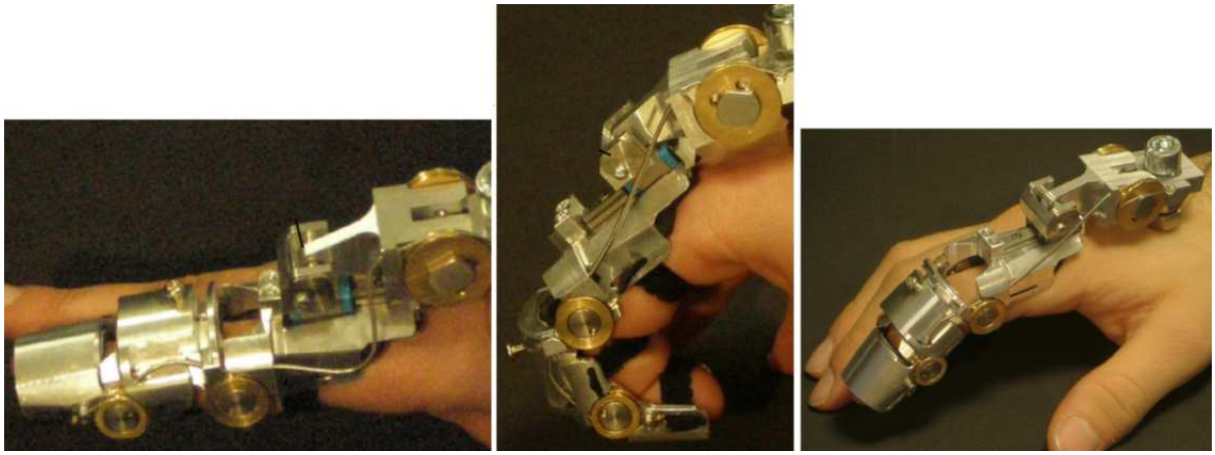

Figure 11: The HANDEXOS Exoskeleton in three different configurations.

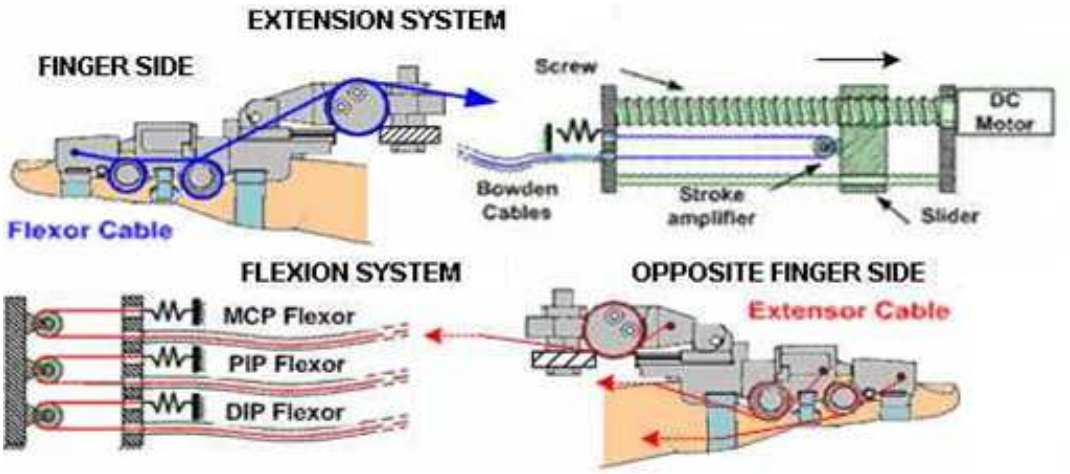

Figure 12: The actuation and transmission system.

single degree of freedom concerning the flexion-extension movement of the tree phalanges. Also in this case the adduction-abduction movement is kept passive. Five DC motors represent the actuation system of the device Figure 11.

Two different strategies have been used in order to place the exoskeleton joints in correspondence with the human finger ones. Regarding the last two articulations of the finger, a couple of pulleys, one for the extension and one for the flexion, have been placed in correspondence of the user's finger joint and on the sides of the HANDEXOS (Figure 12). For the first articulation a different solution is necessary due to the presence of the crotch that impedes the axis of the joint to be reached. In this case two pulleys are placed above the articulation and connected to the first phalanx of the exoskeleton by means of a passive prismatic joint. This joint allows the automatic arrangement of the centre of rotation, avoiding interferences during the movements (Figure 12). As previously said, the actuation system consist of one DC motor for each finger, able to generate the movement of all three articulations with the under-actuated strategy. The extension movement of each finger is generated by a cable running across all the three phalanges that end in correspondence of the last one. The linear DC servomotors that pull the wires are placed extrinsically in order to reduce the dimensions and weight of the device on the hand. The flexion movement of the finger is passively obtained using a series of three cables, one for each phalange, and connected to three linear springs. Those springs generate the torques causing the bending movement of the finger (Figure 12). The main advantage of the under-actuation strategy used in the HANDEXOS is its capability to adapt the movement automatically to the shape of the grasped object.

Sabanci University Hand Exoskeleton

The Sabanci University developed their finger exoskeleton as a rehabilitation device specifically designed for the tendon repair exercises [76]. The structure of this device is connected to all the phalanges of the index finger but the exoskeleton actuates only one single degree of freedom with one DC motor. The control of the flexion-extension movement of the human finger is performed with an under-actuated strategy. Figure 13 shows the exoskeleton and its actuation strategy. Figure 14 shows a schematic representation of the under-actuated structure, provides a detailed description of the motion of the device against an obstacle and its capability to adapt itself to the shape of the grasped object. The kinematic of the exoskeleton can be represented by an equivalent five bar mechanism, coupled with a four bar mechanism, by means of compliant elastic elements.

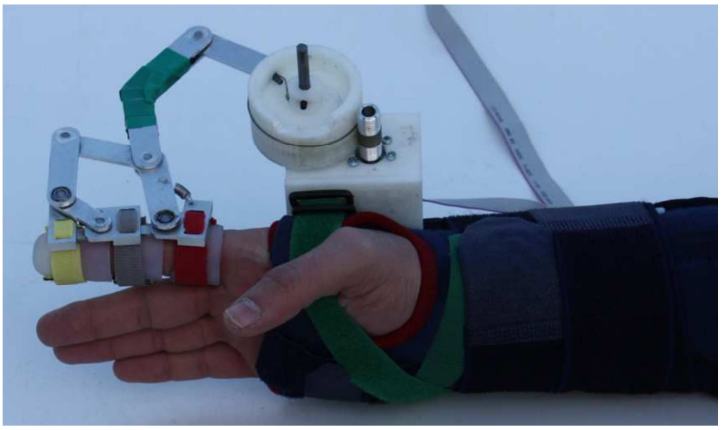

Figure 13: The Sabanci University Hand Exoskeleton.

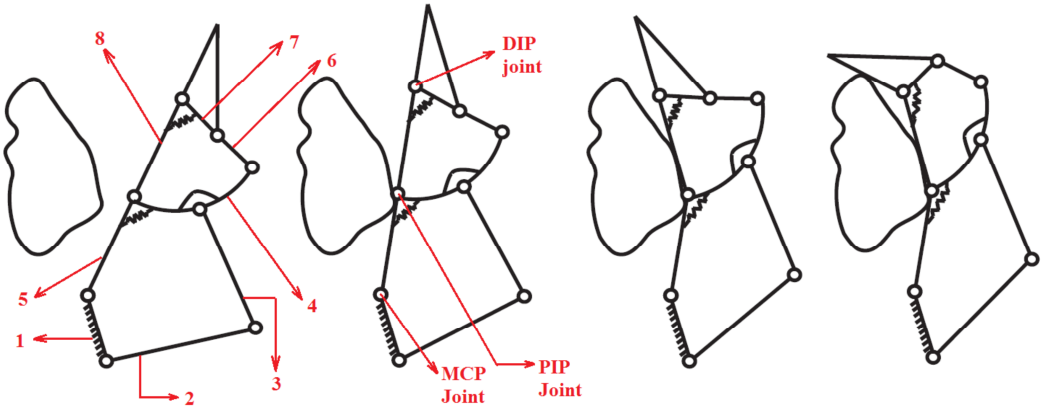

Figure 14: The compliant mechanism.

When the finger is free of contact it behaves like a single rigid body. Vice versa, when the motion of a phalanx is constrained, the torque generated by the motor overcomes the preload of the elastic elements and the other phalanges start to move toward the obstacle in a compliant way. The elastic element maintain the last two phalanges of the finger fully extended until the first one comes in contact with the grasped object or reaches its mechanical limit. Then, the motion of the other phalanges continues until all the three will come in contact with the object or their limits are encountered.
Two different strategies were used in this exoskeleton in ordert to place the rotation axes in correspondance with the human ones. For the last two articulations the device joints are directly placed besides the wearer's ones, while, for the first one, the five bar mechanism has been designed in order to avoid the problem related the finger crotch. The five bar mechanism uses three links coming from the exoskeleton while the last two belong to the human hand.
The device is equipped with two different types of position sensors. Two potentiometers are placed in correspondance of the last two joints, moreover an optical encoder is used to measure the position of the motor axis. Finally three external force sensors are placed between the finger and the exoskeleton. The control system is equipped with EMG sensors to sample the muscles activity and to evaluate the effectivness of the device.

Haptic Exoskeleton

SKK Hand Master

The SKK Hand Exoskeleton is a haptic device [51, 77] composed by two digits: the index finger with four degrees of freedom and the thumb with three degrees of freedom. The transmission of the movements used in this device is realized by means of a series of four-bar linkages placed on the dorsal side of the human finger. The four-bar mechanisms are directly actuated by lightweight ultrasonic motors (USM), as shown in Figure 15.

Two kinds of sensors are equipped on this hand exoskeleton. The first type is an angular position sensor placed inside one of the vertexes of each four bar mechanism and able to gatherer the attitude of each phalanx of the human hand. The second one is a force sensor placed on the four bar mechanism and used to measure the force generated by the device on the operator finger and to control the sensorial feedback.

The aim of the device is to emulate grasping situations, applying forces and torques on the human articulations and providing a sensorial feedback. The data coming from the sensors are used in order to control remote grasping manipulators both in real and virtual environments. The force feedback generated by the motors allows the operator to feel deeper human sensation of touch. Ultrasonic motor shows several advantages with respect classical electrical motors: they are small, lightweight, generate low noise and show a high power to weight ratio. On the contrary some drawbacks such as high hysteresis and high temperature variation could create problems during long term operations.

PECRO Hand Exoskeleton

The PECRO Hand is a two finger exoskeleton realized for haptic interaction in virtual environment and to control end effector during tele-manipulation operations [65, 78]. The two digits replicated on this hand exoskeleton are the index finger and the thumb, both of them with three degrees of freedom, as shown in Figure 16. In the specific case of index finger, two degrees of freedom are related to the flexion-extension, coupling the last two articulations, while the last one is related to the adduction-abduction.

As said many times, be able to mimic the exact position of the centre of rotation of each articulation with the exoskeleton joints is a fundamental aspect to avoid mechanical interferences or damages. This exoskeleton uses a remote centre of motion obtained with a double parallelogram mechanism. This mechanism is able to generate a rigid motion around specific axes, remotely located from the structure,

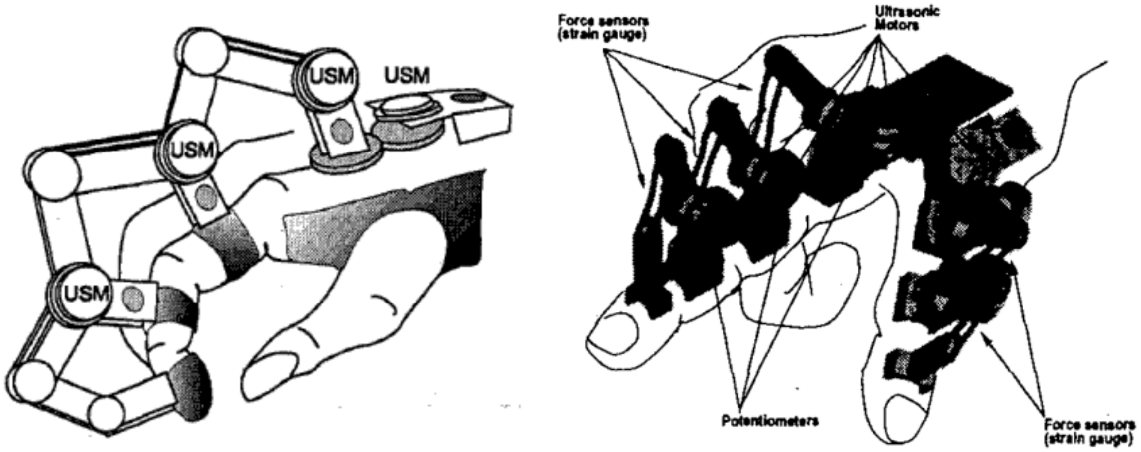

Figure 15: The SKK Hand Master.

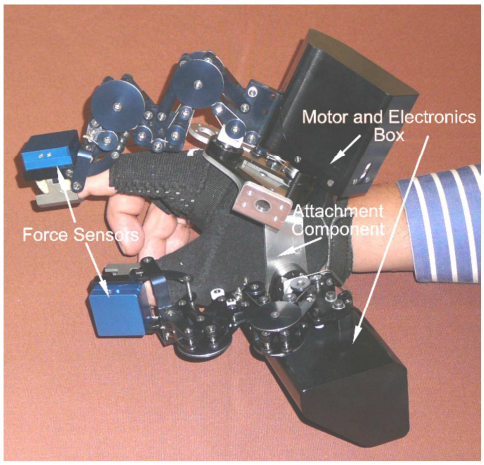

Figure 16: The PECRO Hand Exoskeleton.

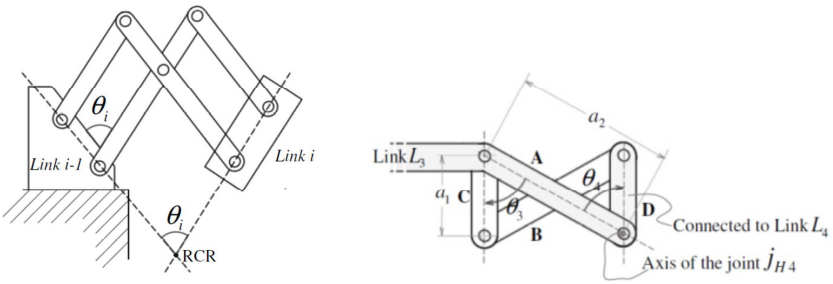

Figure 17: The double parallelogram mechanism (left) and the crossed parallelogram (right).

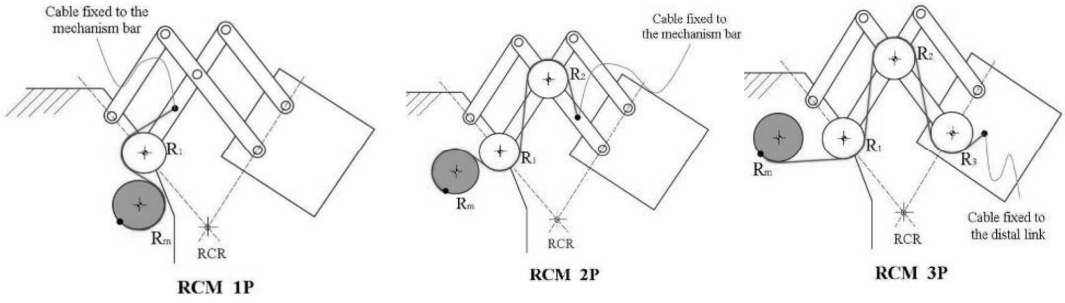

Figure 18: Different wire driven solution with a single pulley (right) and multiple pulleys (middle and right).

without using any link which belongs to the human hand.

The coupling between the last two articulations has been implemented with a crossed parallelogram mechanism. Figure 17 shows the two mechanisms used in this device: the double parallelogram mechanism (on the left) and the crossed parallelogram (on the right).

The actuation system of each finger is composed by three DC motors; the force transmission is done by means of a wire driven mechanism. A very interesting aspect related to this exoskeleton is the method to actuate the double parallelogram using the wire driven mechanism instead of a traditional capstan pulley system. Usually this strategy needs very large pulleys in order to achieve a good speed reduction and then good force amplification. The designers overcome this drawback proposing a more complex system of pulleys. This solution generates mutual rotations of the various links of the double

parallelogram in order to obtain a multiplication effect during each rotation; this effect is obtained adding pulleys along the path of the wires. The cable starts from the motor, follows the path defined by the pulleys and then ends on an attachment point of the link. Figure 18 shows some examples of this solution.
The exoskeleton generates the sensorial feedback by exerting forces on the fingertip of the index finger and on the thumb of the operator. Two kind of force sensors are equipped on this device; first of all a bidirectional strain gauges are placed on the two fingertips allowing to control the tactile sensation that the exoskeleton transmits to the user, then a current sensor is positioned on each motor in order to evaluate the torques generated on the shafts. Finally, the position of each link is measured with encoders, whose data make possible a position control strategy of fingers emulated in the virtual environments.

DLR/HIT Hand

This device is a master hand designed to obtain a bidirectional force feedback and a natural touch sensation [52, 55]. This hand exoskeleton is composed by five fingers and each of them actuates a single degree of freedom. Similarly to the previously described exoskeleton, the movement is performed with a double parallelogram system, as shown in Figure 19. Each finger shows three coupled double parallelogram to realize the flexion-extension movement. Each degree of freedom is actuated by brushless motor that directly applies its power to the first articulation of the finger with a bevel gear connection. The transmission of the power through the finger employs steel wires and slider mechanism designed in order to couple adjoining joint. Finally, fixed ratios are imposed between the three articulations in order to generate the combined movement.
When the controlled slave device is not interacting with the environment, the master hand must not to apply any force on the human hand working passively. The human fingers and the master fingers can then move together without any force exerted. In reality, due to the non-null friction and stiffness of each element of the exoskeleton, a small force is always needed from the operator in order to move the master hand, also in non-contact condition.
Exoskeletons are usually connected to the human hand by means of tapes, stripes, or rings; on the contrary, in this specific case, no physical connection has been placed. An optical sensor and a reflecting plate mounted on a spring have been adopted to determine the contact and non-contact between the device and the operator's finger. This sensor detects the distance between the human finger and the exoskeleton finger while the spring is used to guarantee the contact between the plate and the dorsal side of the fingertip.

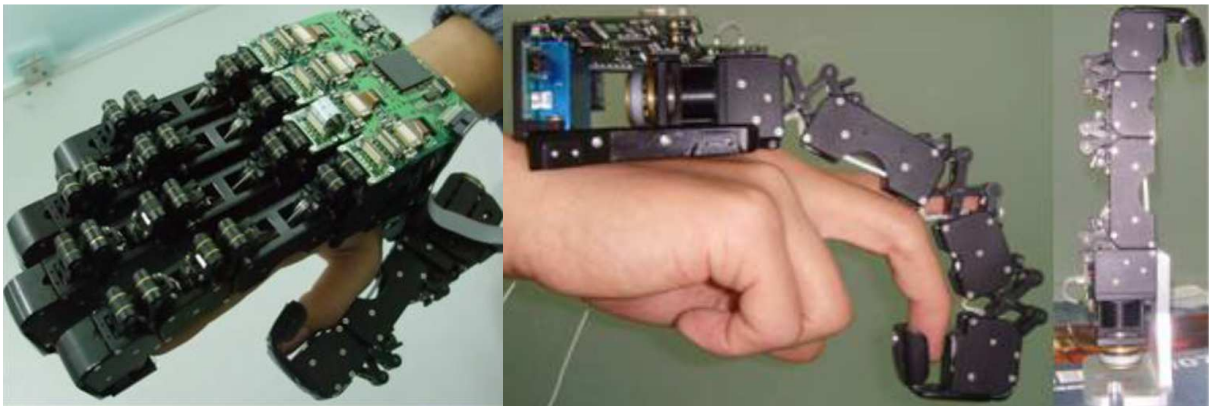

Figure 19: The DLR/HIT Hand Exoskeleton.

When the slave hand does not interact with its environment, the master hand follows the human finger without external contact forces, the designer called this “non-contact mode”. On the contrary, when the slave hand touches an object, the master finger provides a resistive force on the operator finger, this is called “contact mode”.
During the non-contact mode only the position control is employed. When the slave hand interacts with an object, the contact mode starts and the control is changed into force control. At this point the exoskeleton aims to provide on the human finger a force equal to the one perceived by the slave.
The master hand is equipped with two thin force sensors located on the top and bottom of each tip. In addition one strain gauge and one hall sensor are placed on each finger in order to calculate the motor torque and to detect the angular displacement of the joints.

Robotic Center-Ecole de Mines de Paris Hand

This exoskeleton was designed with focus on bidirectional force feedback for virtual reality applications [79, 80]. This hand exoskeleton is composed by two digits, the index finger and the thumb, each of them realized with a single degree of freedom. The three flexion-extension articulations of the human finger are coupled and controlled by a single planar motion using a four link serial kinematic chain as shown in Figure 20.
The designer chose to utilize only one degree of freedom, obtaining under-actuated mechanism, in order to limit the total weight of the device. Each degree of freedom of the exoskeleton is actuated by two motors by mean of a series of pulleys, allowing also complex movements which involve the abduction to be performed. The two fingers of the exoskeleton can be adjusted in order to fit with different hand sizes and, in order to guarantee the correct kinematics, some intermediate pulleys, placed on movables axes, have been added.
The device is equipped with five encoders which measure the angular displacement of the links of the two fingers. The index finger uses two sensors; the first one is placed inside the motor while the second one is placed in the first actuated joint. The thumb is equipped with the last three sensors; one of them is embedded into the motor while the others two are placed on the pulleys in order to measure the abduction-adduction and flexion-extension movements. No force or torque sensors were placed on this device and so it is not possible to control the force feedback generated on the human finger.

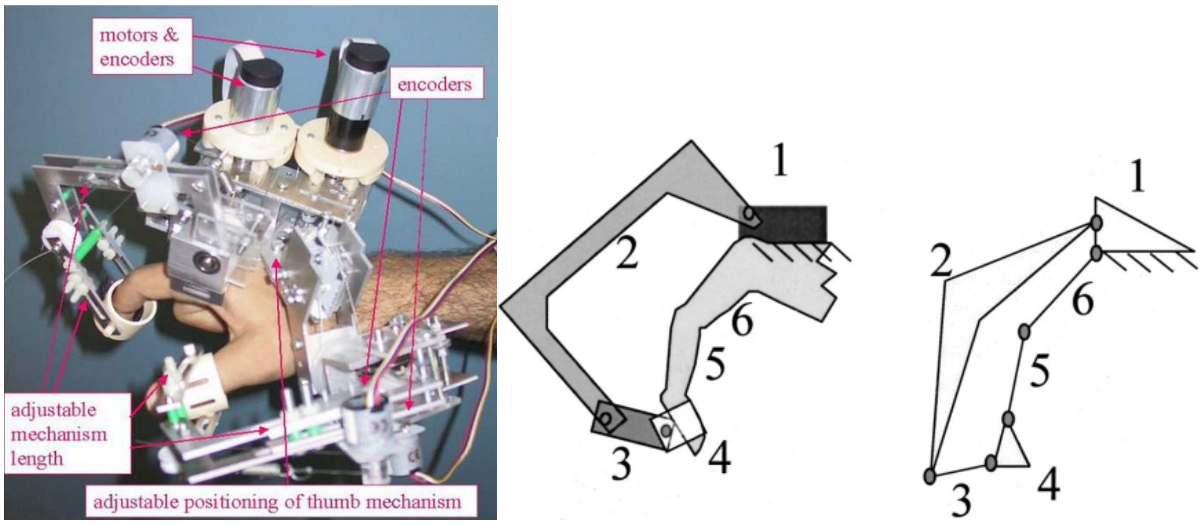

Figure 20: The Paris Hand Exoskeleton.

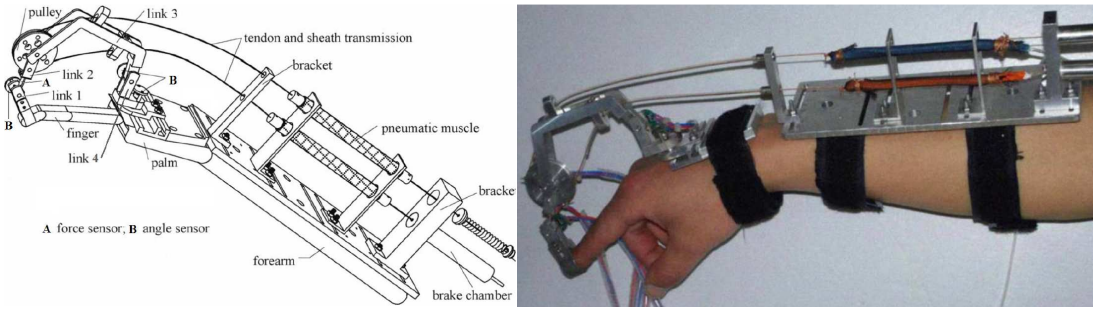

Figure 21: The Nanjing University Hand Exoskeleton.

Nanjing University Hand Exoskeleton

This device has been designed both for haptic applications, with focus on the bidirectional force feedback control, and rehabilitation applications [81].

This hand exoskeleton is composed by only one index finger with one actuated degree of freedom, as shown in Figure 21. The whole flexion-extension movement of the three index finger's phalanges is controlled by mean of a series of four bar mechanisms connected to the human finger in correspondence of the fingertip. The abduction-adduction movement is kept passively in this device.

The actuation system is composed by two pneumatic artificial muscles and a brake system placed on the forearm. The transmission system used to actuate the device is a tendon-drive mechanism. The wire is fixed on one side to one pulley and on the other side to the actuator. The force generated by the actuators is transmitted through the wire to the pulleys causing the rotations.

Two different kinds of sensors are equipped on this device: position and force sensors. A cantilever beam equipped with strain gauges is used as force sensor in order to measure the tendon tension. Moreover, four non-contact magneto-resistive position sensors are placed on the hand exoskeleton. The information related to position and forces of the exoskeleton are used to control the internal pressure of the pneumatic muscles.

Two different control strategies are implemented on this device and are chosen on the basis of the application: rehabilitation or haptic interaction. During rehabilitation tasks, the movements of the finger could be controlled both passively and actively. During the passive control the finger can perform flexion-extension movements without any external force acting on it; this position-based control is fundamental at this stage in order to exercise the articulation mobility. Vice versa the active rehabilitation control allows an active training imposing a controlled force on the human finger coming from the actuation system, implementing a force-based control. For haptic application, the pressure of the pneumatic muscles is tuned in order to reproduce the external sensorial force feedback.

Rutgers Master Hand

This device is a very particular hand exoskeleton designed for dexterous interaction with virtual environments, such as complex grasping and manipulation of virtual objects [61].

This exoskeleton uses a pneumatic circuit in order to actuate its four degrees of freedom, one for each digit excluding the little finger, as shown in Figure 22. The pneumatic circuit is composed by four direct-drive pneumatic cylinders, which connect the palm with the four fingertips. Each actuator is attached to a base frame, placed on the palm of the hand, by means of a universal two degrees of freedom passive joint. The cylindrical shaft of the piston could both rotates and translates inside the cylinder. Finally each fingertip is connected to the shaft by means of a rotational joint. The graphite pistons could move smoothly inside the cylinders, providing force to the human fingertip that can be of several Newton.

Figure 22: The Rutgers Master Hand Exoskeleton.

The device can control the position of the human finger by means of two kinds of position sensors. The first ones are two Hall Sensors, placed at the bottom of each cylinder and able to measure the flexion-extension and the abduction-adduction angles of each actuator. The second type is an infrared sensor placed inside each cylinder in order to measure the relative position between cylinder and piston.
This exoskeleton shows the big advantage to be extremely lightweight and so very comfortable to wear, generating very small additional fatigue in the operator hand. The main disadvantage of this solution is its positioning inside the human hand palm, decreasing the workspace and reducing the grasping possibilities.

Assistive Exoskeleton

University of Tsukuba Hand Exoskeleton

This device is an assistive hand exoskeleton realized to support hand and wrist activities [58, 82]. The device actuates eight degrees of freedom of the human hand. The index finger is controlled by the three active degrees of freedom related to the flexion-extension movement, while the abduction-adduction is kept passive. Others three degrees of freedom actuate the flexion-extension of the combination of the others three fingers, as shown in Figure 23. Finally, the last two degrees of freedom support the movement of the thumb in its flexion-extension. Moreover a five-parallel-link mechanism is used to support six wrist joint motions in three degrees of freedom.
Surface EMG electrodes measure the bioelectric potential in order to estimate the grasping force of the

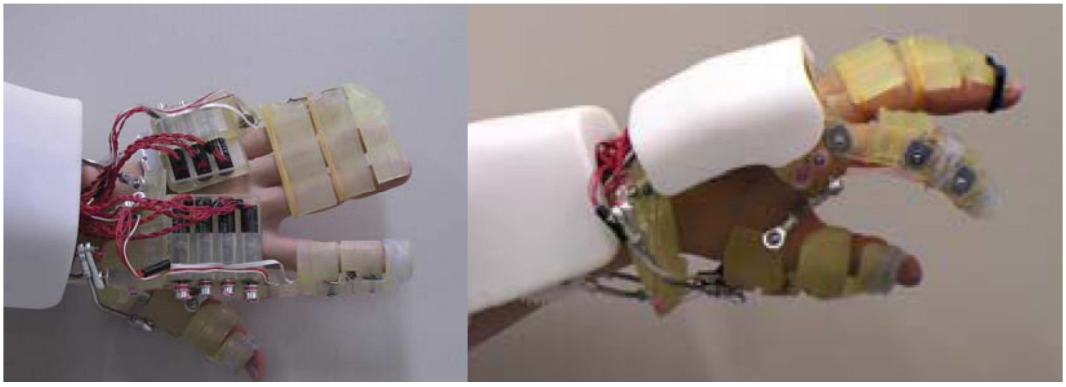

Figure 23: The University of Tsukuba Hand Exoskeleton.

fingers and the torque generated by the wrist joint.
The main mechanical advantage of this device is its placement on the human hand. A lot of hand exoskeletons are designed to be placed on the dorsal side of the fingers, requiring not trivial methods to be attached and to match each centre of rotation. In this hand exoskeleton the entire mechanism is placed on the side of the finger and each joint of the device coincide exactly with the human's finger one. Moreover, since no remote centre of motion is required, the overall complexity of the structure and the friction forces result to be decreased.
The main drawback of this solution is its applicability only for some fingers. It is easy understandable that it is possible to place this device only beside the thumb, the index finger and the little finger. In order to control the middle and the ring finger some special strategies are needed, e.g. constraining or coupling their movements.
The actuation system is composed by eight DC motors placed on the forearm and the force transmission is realized by means of a wire driven mechanism.
The system is equipped with position sensors, while the force is estimated thanks to the measurement of the current flowing into the DC motors. The joints angles of the exoskeleton are measured by rotary potentiometers directly placed over each articulation. Moreover, the position of each motor shaft is measured by rotary encoders. The redundancy related to the position information permits to detect failures and mechanical problems by comparing the two gathered signals. Finally, the knowledge of the motor current enable the system to control the forces applied on the human fingers.
The device controls the movements of the fingers in two different ways called by the designer: "finger-following" and "grasping-force" control. During the finger-following mode the system does not interfere with the finger motion, disabling the power support. The human finger can then moves as wearing nothing. During the grasping-force the device provides to the human finger the desired interaction force. An original aspect of this device is represented by the solution that the designers chose to tune the magnitude of the force. In order to decide the intensity of the applied force, the operator has to wear a cap equipped with accelerometers; the grasping force discretely changes within its range on the base of the direction of the head rotation.

Okayama University Hand Exoskeleton

This assistive hand exoskeleton was designed in order to help people during their everyday life activities [62, 83, 84]. This device actuates the flexion-extension movement of each finger through a single degree of freedom. Moreover the thumb is controlled by two degrees of freedom, one for the overall flexion-extension and one for the abduction-adduction. Each degree of freedom is actuated by means of a single pneumatic artificial muscle, realizing an under-actuated solution without any mechanical coupling

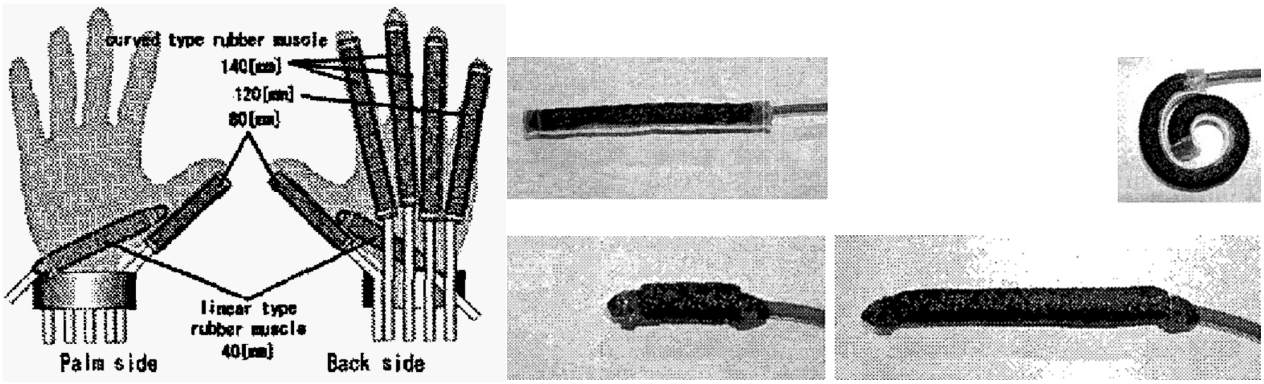

Figure 24: The Okayama University Hand Exoskeleton (left) and the two different pneumatic artificial muscles (right).

between the finger articulations.
The device appears like a soft glove with its actuators placed on the dorsal side of each finger, as shown in Figure 24. Two types of pneumatic artificial muscles have been used in this device. The first one is used for the flexion-extension of the five digits; when is inflated with air this pneumatic actuator automatically bent following a predetermined shape and generating the movement of the finger. The second one is used for the abduction-adduction of the thumb; in this case the pneumatic actuator changes its length linearly. Figure 24 shows the two different kind of pneumatic muscles used. As already said no mechanisms were needed to couple the joint movements; the actuators are directly placed on the glove and the compliance of the human hand guarantees the coupling between the two elements during movements. The curved type artificial muscle consists of a rubber pipe in which the deformation of one side is constrained by means of reinforcements. The linear type, instead, has no reinforcement and so its deformation results to be no constrained, allowing natural extension towards its axial direction. The pressure of each artificial muscle is controlled by pressure sensors placed on one end of the actuators. Moreover, the system is equipped with tactile force sensors placed on the fingertips in order to implement the force control procedure.

Tokyo Institute of Technology Hand Exoskeleton

This hand exoskeleton is designed in order to amplify the forces of the operator during grasping activities [85]. This device actuates ten degrees of freedom of the human hand. The flexion-extension of each finger is controlled by two degrees of freedom, once for the first phalanx and once for the last two. Also the thumb is supported by two degrees of freedom, the first one related to the flexion-extension and the second one related to the abduction-adduction movements. Figure 25 shows the device.
Each degree of freedom is actuated by one artificial pneumatic muscle. Each flexion-extension movement is generated with an under-actuated solution and without any mechanical coupling. The abduction-adduction of the thumb is realized using a flange, connected with one artificial muscle by means of a wire driven mechanism. The correct position of the centre of rotations is guarantee by means of passive prismatic joints that allow adapting displacements; in this way the length of each link is passively adjusted in order to avoid interferences. Each finger of the device is equipped with two pneumatic force sensors located in correspondence of the first and third phalange, between the human finger and the exoskeleton. This pneumatic force sensors are composed by a rubber tube connected to a pressure sensor. It has to be underlined that no electrical components are connected to the device; this means that the glove can work well also in some particular conditions e.g. underwater. The force

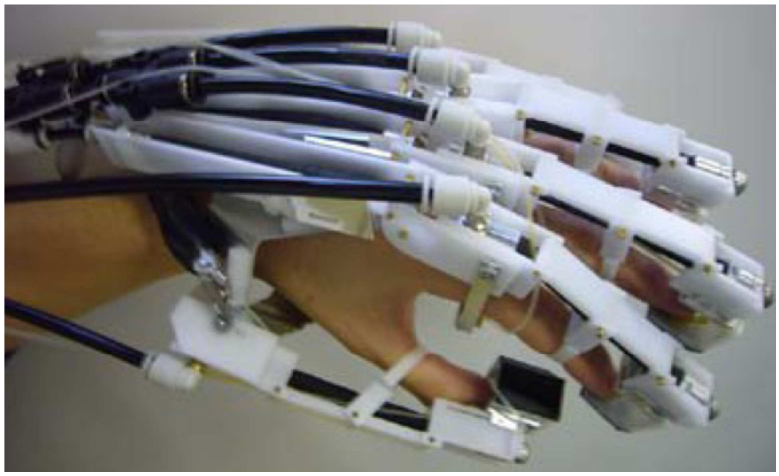

Figure 25: The Tokyo Institute of Technology Hand Exoskeleton.

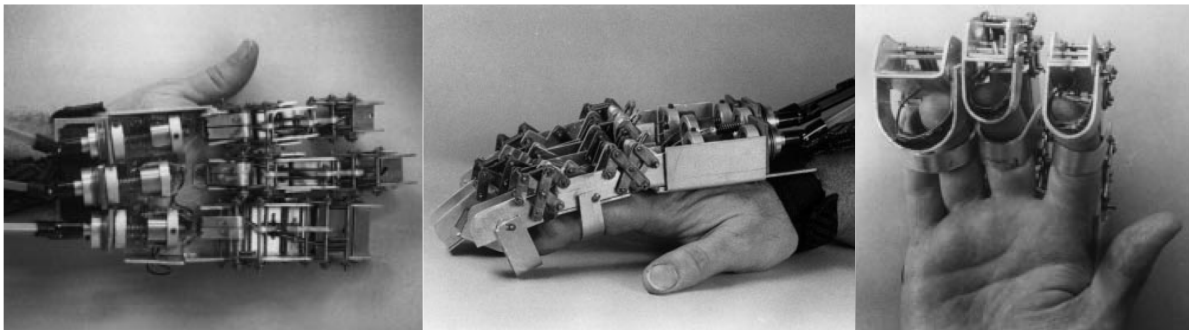

Figure 26: The Vanderbilt University Hand Exoskeleton.

exerted by the human hand is detected and then is sent to the exoskeleton which will provide to amplify it. Finally, the system is equipped with EMG electrodes in order to sample the muscular activity and to evaluate the effectiveness of the power-assist system.

Vanderbilt University Hand

This exoskeleton proposed represents probably the most similar research activity to the project described in this thesis. This device is a hand exoskeleton and is designed to fit over the gloved hand of the astronauts and to limit the stiffness of the pressurized space suits [66]. This three finger assistive device allows independent movements of the index and middle finger, while the ring and the little are constrained together. Each of the three fingers actuates one single degree of freedom, coupling the movement of the first two phalanges and inhibiting the movements of the thirds, as shown in Figure 26.
The exoskeleton is connected to the human finger by means of two rings located on the last two phalanges. The device uses two coupled double parallelograms in order to reproduce the flexion-extension movements.
The actuation system consists into three DC motors and a wire driven mechanism that actuate the fingers only into the flexion direction, while the extension is provided by the stiffness of the spacesuit itself. The exoskeleton is equipped with force sensors placed into one of the rings of each finger, which measure the force exchanged between the human hand and the exoskeleton only in the flexion direction. The movements of this exoskeleton are controlled on the basis of the force measured by the sensors. Two pressure threshold levels have been imposed. If the force measured is lower than the smallest edge the motor starts to provide actuation in order to close the finger, else if the measured force is between the two threshold the motor lock its position stopping any movements, finally, if the measured signal is greater than the biggest edge the space suit stiffness itself will provide the force to open the exoskeleton.

Robotic Hands

The particular goal of the final device exposed in this work imposes strong limitations and constraints that are not typical in the hand exoskeletons development. In particular, the constraints related to dimensions and weigh are not satisfied in the most of the analysed devices. In order to obtain a wider overview and a different point of view on the anthropomorphic robotic hand devices, it has been decided to study also the main robotic hands present in literature.
It is easy to understand that the requirements of robotic hands are strongly different with respect to the hand exoskeleton ones; constraints, needs and goals change, requiring different solutions and strategies. The hand exoskeletons have not to be coupled to the human hand, so the dimensions are not

Figure 27: The Shadow Hand.

strictly constrained to the human ones. Moreover, the possibility to use the fingers and the palm to contain all the gears and mechanisms allows the robotic hands to be more compact. Although all those considerations, the robotic hands could provide some different strategies or ideas to realize the final device, for that reason a short state of the art with the main examples present in literature is reported below.

Shadow Hand

The Shadow is a robotic hand with twenty-four degrees of freedom with position control, shown in Figure 27 [86]. Twenty of the twenty-four degrees of freedom are actuated and equipped with position and force sensors, the other four work passively generating under-actuated movements. Moreover, sensitive touch sensors were placed on each fingertip. Two kinds of actuators are equipped on the shadow hand; electrical motors and pneumatic artificial muscles. The electrical actuation system integrates force and position control while the pneumatic actuations system integrates pressure and position control. The pressure control is realized by mean of 80 valves that measure the pressure of the air flowing through the 40 pneumatic air muscles. The interaction with the environment is deeply gathered by means of the 129 sensors placed on the hand. As well as position sensing for each joint, the hand includes force sensing for each actuator, tactile sensing on fingertips, temperature and motor current and voltage sensing.

Yokoi Hand

Another example of robotic hands is the Zurich/Tokyo Hand, also called Yokoi Hand and shown in Figure 28 [87, 88]. The Yokoi Hand is a prosthetic robotic hand with fifteen degrees of freedom and equipped with different types of sensors. The interesting aspect of this device is represented by its transmission system. The wire-mechanism that actuates the joints aims to emulate the tendon muscle system of the human hand. The fifteen degrees of freedom are driven by thirteen electric servomotors. A bending sensor is positioned in correspondence of each finger articulation in order to measure the attitude of the finger. Finally a series of pressure sensors are placed on each fingertip, on the palm and on the back of the hand in order to measure the interaction with the environment. This hand exoskeleton is partially built from elastic, flexible and deformable materials; the tendons are elastic, the fingertips are deformable and between the fingers is placed a frame made of compliant material. Finally, EMG signals can be used to interface the robotic hand non-invasively to a patient and electrical stimulation can be used as a solution for providing tactile feedback.

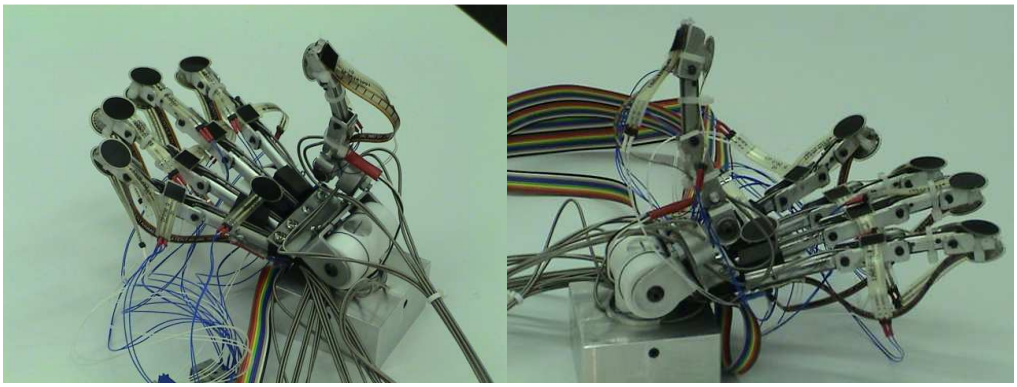

Figure 28: The Yokoi Hand.

RAPHaEL

The RAPHaEL Air Powered Hand is six degrees of freedom robotic hand which is actuated by a novel pneumatic system made with pipe tube actuators connected to a compressor air tank. Figure 29 shows the robotic hand [89]. The three phalanges of each finger are moved by elastic ligaments when the compressed air enters into the actuator triggered by a solenoid. When the air flow is cut off, the finger returns to the straight position thanks to an elastic element placed on its dorsal side. The force, position, and compliance of the finger are controlled by an electronic air pressure regulator through feedback coming from the bending position sensors and force sensors at the tip of each finger. Flex sensors for position and force sensitive resistors for force sensing are used in this Hand.

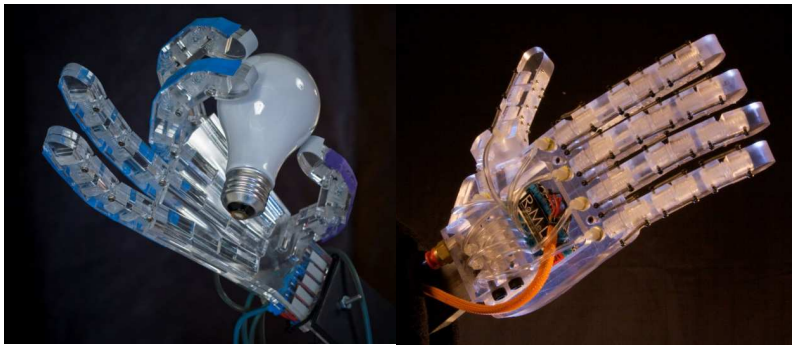

Figure 29: The RAPHaEL Hand.

EH1 Milano Hand

The EH1 Milano Hand is a programmable anthropomorphic human-sized robotic hand, shown in Figure 30 [90]. This devise is realized in order to be able to grasp a variety of objects and to sense them through multiple force and position sensors. Modular actuation units are placed in flanges customized for the application. The cable transmission allows the remote actuation, thus enabling the employment of low payload robotic arms. Each actuator contains a CPU, firmware, sensor acquisition electronics, communication electronics, servo-controllers, and one brushed DC motor. Moreover the hand can be interfaced with computers by means of a simple USB connector.

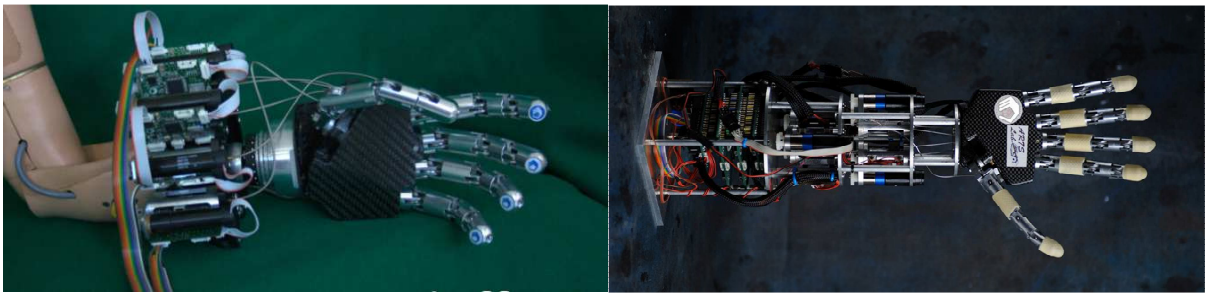

Figure 30: The EH1 Milano Hand.

Sheffield Hand, Touch Bionics i-LIMB Hand, Honda Hand, Eurobot Hand, Robonaut Hand and Utah/MIT Hand, are just some other examples of the developed robotic hands of different research centres in the world. More detail about different hand exoskeletons and robotic hands can be found in [91, 92, 93].

Sensors

Sensors are one of the fundamental elements of each robotic device; control loops and functioning strategies are strongly defined by the choice of the gathered signals, the placement and the number of sensors. The most important signals that have to be gathered in order to control a hand exoskeleton are the position of each articulation and the force exchanged, with the environment or with the human hand. Today there are a lot of sensors, using different principles and technologies, that can be adopted to control the position and the movement of the phalanges or the force exchanged. The previously reported state of art permit to understand that there is not only one correct universal solution; each type of sensor could be suitable, on the base of the project constraints and the actuation system.
Nowadays various kinds of sensors exist in the market, each of them suitable for different applications and specific needs in robotics. Regarding this specific project, due to the many limitations imposed by the space environment, strong constraints related to the choice of the sensors have to be imposed. Some examples of constraints related to the choice of sensors are the size, the working space, the energy consumption and the effects of space environment, in terms of noise, temperature and electromagnetic interference. Some examples of sensors, which have been considered suitable for the final device, are reported below with a very short description.

Electro-goniometer

Electro-goniometer is a kind of position sensor that measure angles using different working principles. It can use potentiometers, strain gauges, light beam or accelerometers to measure the angle between two surfaces. However, potentiometers which must be placed directly on the joint and accelerometers which are based on gravity are not suitable choices for this specific device. The strain gauge type looks like a flexible spring in which the strain gauge mechanism is housed inside a coil and changes its resistance proportionally to the measured angle.

Flexible Stretch Sensor

This type of sensor can be used both as a position or a force sensor. It changes its resistance when bent or stretched. One big advantage of this sensor is its fully customizable dimension. Since it can be both a position and a force sensor, it represents a versatile solution for different applications. Its position on the finger exoskeleton has to be carefully planned in order to be able to use its full potential of measurement.

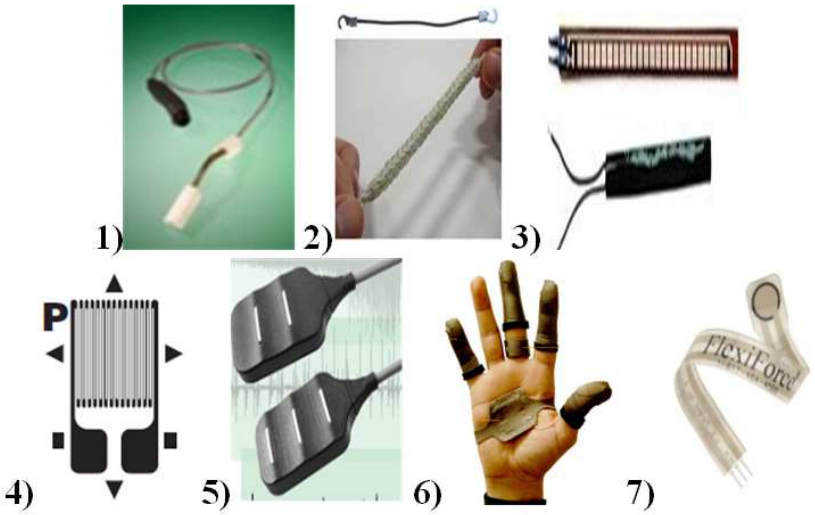

Figure 31: Examples of sensors: 1) Electro-goniometer, 2) Flexible Stretch Sensor, 3) Bend or Flex Sensor, 4) Strain Gauge Sensors, 5) Surface EMG Sensor, 6) Finger Tactile Pressure Sensor, 7) Piezoelectric Sensors

Bend or Flex Sensor

Bend/Flex Sensor is basically a position sensor and its technology is based on resistive carbon elements. When the substrate is bent, the sensor produces a resistance output correlated to the bend radius. The smaller the radius, the higher is the resistance value. It can be created both one- and bi-directional and is available in various resistance ranges on the basis of the material used to realize it. It seems to be a suitable and cheap choice for hand exoskeleton applications.

Strain Gauge Sensors

A Strain Gauge is a sensor whose resistance varies with applied force. It converts force, pressure, tension, weight, into deformation of the substrate changing its resistance. Strain gauges are extremely versatile, realized in thousands of dimensions and shapes. The strain gauge is the fundamental sensing element for many types of sensors, including pressure sensors, load cells, torque sensors, position sensors, etc. It seems to be a suitable and cheap choice for the hand exoskeleton applications.

Surface EMG Sensor

The Surface EMG Sensor measures the electro-physiological signals coming from the brain to the muscles. Those sensors are different from classical EMG because they are placed on the skin and not inside the muscle by means of needles. The measured signals are attributable to the force that the human body wants to apply through the muscles. Another big advantage is that all the muscles that drive the human fingers, with the exception of the thumb, are placed into the forearm; allowing the sensor system to be placed away from the hand. The main disadvantage is that the signals are very complex and deeply interconnected, moreover position and movement artefact requires a very careful post processing of the signals.

Finger Tactile Pressure Sensor

Finger Tactile Pressure Sensor uses capacitive principals to detect the contact and the exchanged forces. Tactile sensors are devices which indicate contact between themselves and some other solid object. This kind of sensors can be touch sensor, which are used just to detect the contact between two objects, or

force sensor, which also indicate the magnitude of the contact force between the two objects. They are usually used for haptic devices and the ranges of forces are not so wide, however some of them could be covered with different material in order to partially customize the range of force measured.

Piezoelectric Sensors

Piezoelectric Force Sensors are devices that change their electrical resistance when a mechanical stress is applied. A deformation occurs in crystal lattice of diaphragm caused by the bending. This deformation generates a change in the band structure of the material that can increase or decrease its resistance. One kind of piezoelectric sensor uses special piezoelectric inks instead solid material, resulting in a very tiny device, adaptable on the surface.

Actuators

The choice of the actuation system is probably the most critical part in the development of robotics devices in general, and hand exoskeleton in particular. In the past years there has been significant progress in the development of actuator technologies. Numerous types of actuators can be found today, both in literature as research activities, and in the market as commercial products.
In this specific project the actuators have to be able to generate enough power to compensate the forces coming from the glove and to move fast enough to grant a good level of dexterity to the human hand. Moreover, due to the space limitations, properties like power to volume and power to weight ratios become very important aspects to be taken into account during the design of the device.

Electromagnetic motors

There are a large number of different kinds of electromagnetic motors, such as synchronous, induction, steppers and dc motors. From an operating point of view there are no big differences between them; the torque is always generated by the interaction of the two magnetic fields of the stator and rotor. The main difference is represented by the way used to generate the magnetic field (coils, permanent magnet or electromagnets). The torque generated by the actuator is strictly related to the distribution of the magnetic field in the gap between stator and rotor and is limited by the maximum magnetic flux density, and then by the maximum current sustainable. As a consequence of thermal limits, the maximum torque value is available only for a limited period of time and it is necessary to decrease the intensity of the torque generated in order to increment the sustainable interval. Moreover the heat generation requires a dissipative system to be designed in order to prevent overheating.
Adding gearboxes to the motor allows the torque generated to be amplified tuning the power output of the motor on the basis of the needs. The problem is that, from a robotic standpoint, gears results in undesirable characteristics of friction backlash and compliance, which complicate the control strategy. Heavy components, low power density and heat dissipation are the main critical aspect of this technology. Despite the disadvantages the electromagnetic motors are the most popular choice in the hand exoskeleton applications thanks to their well-known behaviour.

Hydraulic Actuators

Hydraulic actuation systems trasform the energy stored up by pressurized fluid into mechanical power. In the last years the cooperation between hydraulics and electronics generates electrohydraulic servomechanism with increased sophisticatin and enhanced performances. The hydraulic fluid are usually pressurized with electromagnetic motors and controlled by electrovalves. Electrohydraulic servovalves shows some complex behaviours like complex dinamics, hysteresis and variation of the fluid impedance.

The torque to mass and power to mass ratios of this technology are huge in comparison to electromagnetic actuators; these properties could be increased further augmenting the supply pressure or using servovalves with better performances. On one side the output force, power, stiffness and bandwidth provided by this technology are difficult to be found in any other actuation technologies. On the other side complex non dynamics, lack of backdrivability for force control, leakages and the needs of a fluid supplies are strong disadvantages of hydraulic actuation. If the remote placement of the hydraulic plant could increase the power density of the hand exoskeleton it has to be kept into account that the sistem portability result to be strongly compromised.

Pneumatic Actuators

Pneumatic actuators share many characteristics of their hydraulic counterparts. The difference comes mainly from the different fluid involved into the system: the air. Air is much lower viscous, much more compressible and with worse lubrication properties than hydraulic fluids. Moreover the leakage problem requires more careful design with tighter tolerances. Usually pneumatic actuation involves a piston driven by pressurized gas, similarly to the hydraulic counterpart.
In the last years another typology of pneumatic actuators arose; instead of pistons, inflatable elastic bladder surrounded by crossed un-stretchable mesh becomes famous with the name of artificial pneumatic muscle. Artificial muscles contract as a consequence of a variation of internal gas volume, emulating the behaviour of the human ones. Pneumatic actuators have the advantage of a good force/mass ratio, good velocities and reduced weight. Moreover, the intrinsic compliance due to the gas compressibility can be very useful in certain applications. Despite these advantages, the low actuation stiffness and the low power and velocity with respect to the hydraulic solution could represent problems in some applications.

Piezoelectric Actuators

When external forces are applied on the crystals of piezoelectric material, they generate an electrical charge proportional to the applied mechanical stress. Similarly, when a voltage is applied to a piezoelectric material, it answers with a deformation of its crystal. Strains from piezoelectric materials are usually too small to be directly used in robotic devices and various mechanisms have been designed in order to amplify the capabilities. Linear micro-stepper and ultrasonic motors are some examples of actuators realized with piezoelectric technologies.
Piezoelectric motors translate the vibrations generated by the piezoelectric materials into linear or rotational displacements, using the frictional forces to generate torques or forces. Usually, the ratio between force and velocity generated by this technology, allows the piezoelectric motor to be used directly and without gear reduction. Moreover, the need to use friction forces between the elements in order to generate power, demands a very precise and careful matching. These actuators are typically driven by power signals modulated with various ranges of frequencies; sometimes happen that those frequencies correspond with the audible ones, causing annoying or even hazardous noises.
Two main concepts are based on the piezoelectric actuation: the wave motion or the discrete vibrations. The wave types generally are based on standing or travelling waves generated by differential motion between two plates through frictional coupling and forces. Discrete vibration design relies on the straightforward contraction-expansion of a piezoelectric material in contact with a bar or rod, pushed forward with each vibration. It is possible to combine an expanding piezoelectric element with clamps in order to create an inchworm movement.

Magnetostrictive Actuators

Magnetostrictive materials change dimensions and shape in presence of a magnetic field. This effect, called *magnetostriction*, is caused by magnetic properties of the material, which aligns its internal structure in accordance with the magnetic field, changing then its dimensions. The magnetostrictive materials have been used in past for the construction of actuators for underwater sounds generation or to realize active vibration dumper. Long term prospect for magnetostrictive materials are promising also in robotics thanks to their very high energy density, but today various problems still exist.

Magnetostrictive motors have some similarities with the piezoelectric ones, they require very thigh tolerances and accurate a design, moreover they produce high forces at low speed. Heat dissipation results to be a problem, requiring some heat sinks in proximity to the coils that generates the magnetic field. Current magnetostrictive motors works at drive frequencies in the audible range and so, similarly to the piezoelectric motors, the noise could be a problem.

Shape Memory Alloy Actuators

Shape Memory Alloys use the so called *Shape Memory* effect. After a mechanical deformation, the Shape Memory materials are able to return to an un-deformed state, previously memorized, as a consequence of a specific stimulus. Usually the stimulus is a heating flow; but there also other kind of shape memory based on different effects, like the PH variation. The shape memory effect is generated by the transition between two phases of the material (martensite and austenite) as a consequence of the stimulus.

The most popular Shape Memory alloy based on temperature is NiTi due to its properties of reduced cost and non-toxicity. Shape Memory actuators have already considered for some robotic application because they show a very high power to mass ratio, bigger than the classic actuators. However some problems limited the use of this technology. Shape Memory actuators can contract much faster than they can relax. The contraction time it is related by the amplitude of the current pulse flowing into the actuator, and so, increasing the width of the current pulse, the contraction time can be reduced a lot. On the contrary the relaxation time depends on the cooling rate of the wire, that results hard to be improved. The design of an active cooling system would be a good solution allowing to partially solve the main problems related to this technology; this solution will strongly reduce the main goodness of the actuator: the extremely high power to weight ratio.

Other problems related to this technology are the very low efficiency and the interaction between multiple Shape Memory alloys, both caused by the concept of generating power as a consequence of a heating flow. Waste heat will raise the temperature of surrounding elements and inhabit the cooling of others near actuators.

Polymeric Actuators

Some synthetic polymers are known to be able to convert electrochemical energy into mechanical energy similarly to the human muscles. Polyelectrolyte gels, synthetic and natural rubbers and hybrid multiple-layers electrode-electrolytes are only few examples of this actuators; they are able to shrink, bend or contract as a consequence of variation of external conditions such as PH, electric field, temperature, light and so on.

Although the mechanisms of some polymers are different from muscles, they are one of the most muscle-like technology. The Polymeric Actuators have serious fatigue problem and are slow but all those properties could be improved a lot in future by means of miniaturization. Even if strength and speed could be improved, the control of this technology results to be very complex because based on chemical reactions. In robotics polymeric actuators are mainly speculative today, they require a complex chemical setup with fluid circulation and they still lack the time response needed by robotic devices.

CHAPTER 3:

"The five separate fingers are five independent units. Close them and the fist multiplies strength. This is organization."

James Cash Penney

THE HUMAN HAND

The complexity of the human hand, due to its large number of degree of freedom, the significantly reduced working space and the enormous amount of configurations, postures and movements it can reproduces requires an exhaustive preliminary analysis of all the characteristics of this limb.
The aim of this chapter is to provide a comprehensive study on the human hand as a preliminary step towards the development of any application or device to be interfaced with the human being, which needs to emulate and imitate the human hand shape and functionality, such as the exoskeleton. This chapter starts with an anatomical study of the human hand. The most important biometric parameters have been gathered from literature in order to define fundamental constraints for the device. Anthropometric length, range of forces, torques and velocities, maximum displacement, intra and inter constraints are some examples of the amount of information collected during this activity. Then, an overview on the human hand grasp taxonomy is reported: this part aims to classify all the possible human grips and pinches into groups based on similarity. Each group has its specific rank and can be aggregated in a higher rank group thus creating a hierarchical classification. Finally, in the last part of the chapter the kinematic analysis of the human hand will be investigated in detail. However, being the goal the realization of a finger-like structure it has been considered mandatory to study the dynamic analysis of a single human finger.
This deep study aims to completely understand the complex structure represented by the human hand, in order to design and realize a suitable device as much compliant as possible.

Human Hand Anatomy

The human hand is constituted by five digits: four fingers (index, middle, ring and little) and the thumb. As shown in Figure 32, the human finger is composed of three articulations, distal-interphalangeal (DIP),

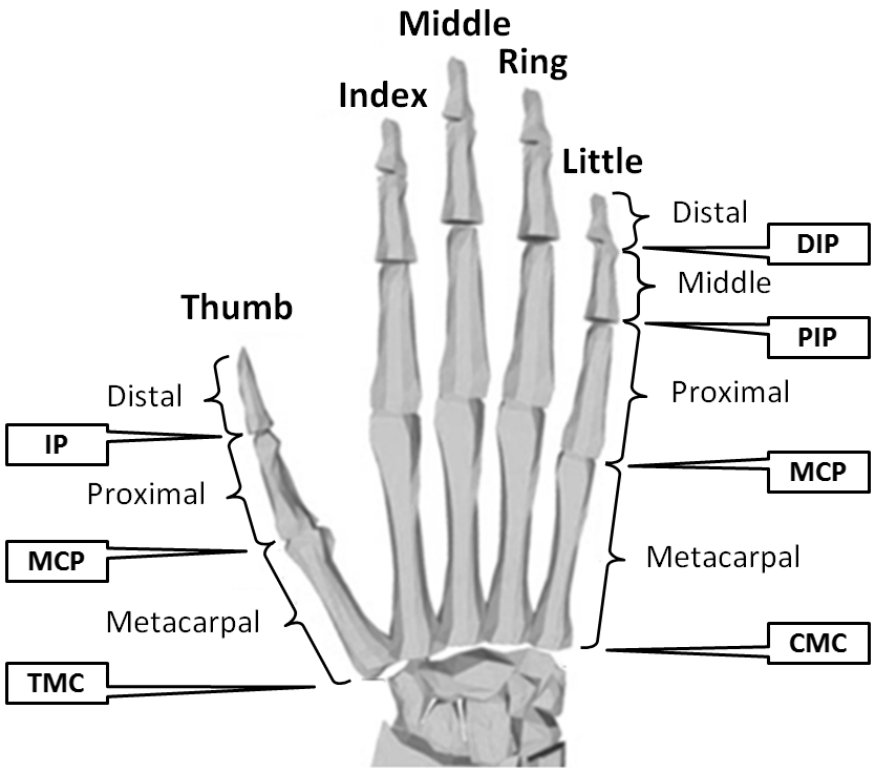

Figure 32: Anatomical details of the human hand.

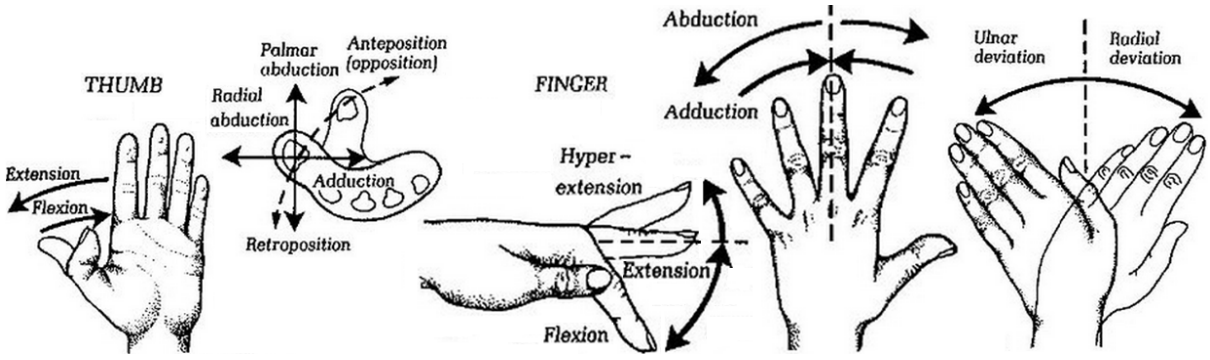

Figure 33: Hand motion terminology.

proximal-interphalangeal (PIP), metacarpophalangeal (MCP) and four phalanges, distal, middle, proximal and metacarpal phalanx. On the contrary, the human thumb is composed by three articulations, interphalangeal (IP), metacarpophalangeal (MCP), trapeziometacarpal (TMC), and only three phalanges, distal, proximal and metacarpal phalanx. The TMC joint of the thumb similarly to the finger's MCP joint hosts two different degrees of freedom: flexion/extension and adduction/abduction. All the other articulations, the MCP and IP joints for the thumb as well as the PIP and DIP joints for the fingers, are characterized by only one degree of freedom, related to the flexion/extension movement. Moreover the eight bones of the carpus articulate finely with each other producing small deformations. In this specific case their representation in a single rigid body is considered a consistent approximation [94]. Additionally the wrist introduces two functional DoF. Figure 33 illustrates the terminology related to the finger movements [95]. With the main goal of analyzing the kinematics and the dynamics of the hand,

the knowledge of the anthropometric dimensions of the fingers and the palm, their respective range of motion (RoM) and internal constraints were considered fundamental information to define the main geometrical limit of the future device.

Anthropometric Dimensions

The knowledge of the length of each phalanx of the fingers, the size of the hand and the position of each articulation is essential for the design of the future device. This information not only allows the main geometrical structural dimensions to be defined, but also results to be very important in the future study of the kinematic behaviour of the exoskeleton. Several studies and reports present a data collection related to the anthropometric data. The main informations gathered during the study have been reported as follows. Table 3, Table 4 and Table 5 show the analysis of the Garrett's studies [96, 97] related to finger and hand dimensions; the measurements are referred to the right hand of 148 men and 211 women. Mean value, standard deviation and values related to the 5 and 95 percentiles were provided for each dimension. Table 3 reports the main dimensions of the whole hand. There are some other measurements in literature considered important in relation to a specific grip, posture or gesture; those information are neglected for simplicity in this thesis, but are available in the cited works and reports. Table 4 shows the two main dimensions which describe the whole fingers: Crotch to tip and Wrist crease to tip. The dimension called Crotch to tip is the length along the hypothetical axis of the finger from the midpoint of its tip to the corresponding webbed crotch between the two fingers; similarly the dimension called Wrist crease to tip is the length along the hypothetical axis of the finger from the midpoint of its tip to the wrist crease baseline. Finally, Table 5 describes the dimensions of the articulation of each finger, excluding the TMG or TMC knuckles. In addition, all these data are related to U.S. Air Force people which could be quite representative of possible EVA users, both in terms of age and physical presence.

		Length [cm] Hand Dimensions			
		mean	**st.d.**	**5%**	**95%**
Male	**Length**	19.72	0.93	18.32	21.15
	Breadth	8.96	0.40	8.32	9.71
	Metacarpal Circ.	21.59	0.90	20.02	23.08
	Fist Circ.	29.61	1.35	27.34	31.86
	Wrist Circ.	17.50	0.94	15.99	19.09
	Wrist Breadth	6.78	0.37	6.26	7.33
	Thickness	3.29	0.20	2.98	3.61
	Depth	6.19	0.45	5.50	7.02
Female	**Length**	17.93	0.86	16.53	19.27
	Breadth	7.71	0.38	7.06	8.32
	Metacarpal Circ.	18.71	0.83	17.45	20.15
	Fist Circ.	24.83	1.31	22.86	27.18
	Wrist Circ.	14.98	0.98	13.85	16.21
	Wrist Breadth	5.83	0.33	5.36	6.44
	Thickness	2.76	0.18	2.46	3.05
	Depth	5.17	0.39	4.53	5.82

Table 3: Main dimension of the human hand measured on a sample of male and female U.S. Air Force members.

		Length [cm]							
		Finger crotch to tip				Finger wrist crease to tip			
		mean	st.d.	5%	95%	mean	st.d.	5%	95%
Male	Thumb	5.87	0.45	5.07	6.57	12.70	1.13	11.05	14.68
	Index	7.53	0.46	6.83	8.19	18.52	0.88	17.33	20.06
	Middle	8.57	0.51	7.82	9.74	19.52	0.92	18.10	21.04
	Ring	8.0	0.47	7.44	8.93	18.72	0.91	17.52	20.28
	Little	6.14	0.47	5.44	6.99	16.61	0.91	15.11	18.10
Female	Thumb	5.37	0.44	4.68	6.12	11.05	1.00	9.51	12.83
	Index	6.90	0.52	6.10	7.80	16.67	0.89	15.21	18.14
	Middle	7.79	0.51	7.01	8.68	17.65	0.87	16.22	19.05
	Ring	7.31	0.52	6.52	8.22	16.76	8.94	15.28	18.20
	Little	5.46	0.44	4.80	6.24	14.64	0.92	13.11	16.12

Table 4: Mean length of the human hand measured on a sample of male and female U.S. Air Force members.

			Length [cm]											
			Breadth				Depth				Circumference			
			mean	st.d.	5%	95%	mean	st.d.	5%	95%	Mean	st.d.	5%	95%
M.	Thumb	IP	2.29	0.13	2.07	0.51	2.02	0.15	1.78	2.25	6.79	0.38	6.12	7.41
	Index	PIP	2.15	0.13	1.96	2.37	1.94	0.12	1.75	2.16	6.43	0.36	5.84	7.10
		DIP	1.84	0.12	1.65	2.04	1.55	0.13	1.36	1.75	5.34	0.33	4.85	5.81
	Middle	PIP	2.18	0.14	1.97	2.41	2.01	0.14	1.79	2.26	6.60	0.39	6.02	7.20
		DIP	1.84	0.12	1.65	2.04	1.60	0.13	1.38	1.81	5.41	0.34	4.87	5.98
	Ring	PIP	2.02	0.13	1.80	2.23	1.89	0.13	1.67	2.12	6.14	0.37	5.54	6.79
		DIP	1.72	0.11	1.55	1.92	1.51	0.13	1.30	1.73	5.08	0.31	4.59	5.67
	Little	PIP	1.77	0.14	1.55	2.01	1.67	0.12	1.47	1.89	5.40	0.36	4.88	6.00
		DIP	1.57	0.12	1.37	1.76	1.37	0.13	1.17	1.55	4.64	0.32	4.11	5.20
F.	Thumb	IP	1.90	0.12	1.71	2.11	1.66	0.12	1.49	1.87	5.61	0.33	5.07	6.18
	Index	PIP	1.82	0.10	1.65	2.00	1.62	0.10	1.45	1.79	5.40	0.29	4.96	5.88
		DIP	1.54	0.10	1.38	1.71	1.28	0.09	1.15	1.45	4.46	0.26	4.08	4.94
	Middle	PIP	1.83	0.10	1.68	2.01	1.67	0.11	1.49	1.86	5.50	0.28	5.05	6.00
		DIP	1.53	0.09	1.38	1.70	1.31	0.09	1.16	1.48	4.48	0.26	4.10	4.93
	Ring	PIP	1.69	0.10	1.51	1.85	1.57	0.11	1.39	1.76	5.12	0.27	4.69	5.59
		DIP	1.43	0.09	1.30	1.60	1.25	0.09	1.10	1.40	4.22	0.24	3.86	4.64
	Little	PIP	1.46	0.09	1.32	1.64	1.39	0.09	1.27	1.56	4.48	0.25	4.13	4.94
		DIP	1.31	0.09	1.17	1.47	1.13	0.09	0.99	1.29	3.86	0.24	3.51	4.24

Table 5: Main dimensions of each articulation on a sample of male and female U.S. Air Force members.

			Mean length [cm]											
		Hand	Index			Middle			Ring			Little		
			Di[a]	Mi	Pr	Di	Mi	Pr	Dil	Mi	Pr	Di	Mi	Pr
Male	Right	19.29	2.32	2.37	2.65	2.60	2.78	2.80	2.29	2.56	2.76	1.96	1.92	2.51
	Left	19.36	2.32	2.39	2.61	2.60	2.82	2.75	2.30	2.59	2.78	1.95	1.98	2.49
Female	Right	17.60	2.23	2.24	2.45	2.44	2.55	2.56	2.12	2.34	2.52	1.79	1.74	2.26
	Left	17.62	2.20	2.24	2.35	2.24	2.43	2.53	2.13	2.36	2.49	1.77	1.77	2.26

[a] Di = distal ; Mi = Middle; Pr = Proximal

Table 6: Mean length of the human hand and phalanges of index, middle, ring and little.

Literature includes some reports of researchers who decided to measure the length of each phalanx separately. Sahar Refaat [98] performed a study with a great variety of candidates; Table 6 shows the results of her study divided by each phalanx of each finger. A similar survey was also performed by Jasuja [99] in his study based upon various measurements of stature, hand length and individual phalange length of each finger related to subjects including 30 males and 30 females aged between 18 and 60 years old. As previously mentioned, all this data collection has been performed in order to provide an idea of the mean length of each element which composes the human hand. With proper modifications, these data could also be used to create a model and simulate its movements.

Finger Constraints

During everyday activities it is easy to notice that the movements of the phalanges of the human hand are not perfectly decoupled between each other. On the contrary, even executing a very simple movement it is easy to notice that other, not planned, actions are performed. Everyone can easily verify this effect bending his index finger and observing its middle finger which involuntary moves by a certain degree. Another example occurs when the PIP joint of any finger is bent: during this movement the corresponding DIP joint is also bent involuntarily of a certain degree, in relation with the PIP angular displacement through a kinematic ratio. All these effects are caused by hand internal elements like tendons, ligaments and skin that generate accidentally coupled movements between the articulations. Hand and digit movements are limited by several constraints, which reduce the theoretical natural movement capability of the human hand. Some studies related to the hand internal constraints were performed in the past. The hand constraints can be roughly divided into two categories: static and dynamic constraints. Static constraints limit the movement of a specific articulation independently from the others; on the contrary, dynamic constraints impose limits which change in time as a function of the other articulations position. Dynamic constraints can be further divided into two sub categories: intra-finger and inter-finger constraints. The former includes constraints between different joints of the same finger, while the latter is referred to constraints between joints belonging different fingers. It is important to underline that the range of motion is something ambiguous when referred to the human being because it depends on various elements, involving the human biomechanics and specific personal characteristics; they are therefore extremely difficult to be expressed in closed form, this typology of model still need further specialized investigations. The role the finger constraints could acquire in the project may be very relevant. This constraint modifies the number of effective degree of freedom of the human hand during movements, reducing it; this effect could be used in order to simplify and relax specific constraints of the future device.

Static constraints

Static constraints generate limitations of the movement of the specific joint, independently from the position of the other articulation of the hand. The collection of all the static constraints defines the Range of Motion (RoM) of the human hand, defining all the maximum and minimum values of the bending angles for each articulation. The main static constraints were collected by Cobos et al. [100] and are reported in Table 7. The knowledge of this type of constraint of the human hand allows realistic limits on the maximum angular displacement to be imposed on the future device.

Dynamic Intra-Finger constraints

Dynamic intra-finger constraints are limitations which couple joints that belong to the same finger. The movement of one of the constrained joints generates an involuntary movement of the others articulations involved in the coupling. Several constraints for fingers and thumb are presented in the study by Cobos et al. [100].

Maximum Angular Displacement [°]				
Finger	**Joint**	**Flexion**	**Extension**	**Abd/Add**
Thumb	**TMC**	50 - 90	15	45 – 60
	MCP	75 - 80	0	5
	IP	75 - 80	5 - 10	5
Index	**CMC**	5	0	0
	MCP	90	30 – 40	60
	PIP	110	0	0
	DIP	80 – 90	5	0
Middle	**CMC**	5	0	0
	MCP	90	30 – 40	45
	PIP	110	0	0
	DIP	80 – 90	5	0
Ring	**CMC**	10	0	0
	MCP	90	30 – 40	45
	PIP	120	0	0
	DIP	80 – 90	5	0
Little	**CMC**	15	0	0
	MCP	90	30 - 40	50
	PIP	135	0	0
	DIP	90	5	0

Table 7: Main static constraints of the human hand.

Equation 1 shows an example of this type of constraint, where θ_{DIP}, θ_{PIP}, θ_{MCP} are the three bending angles related to the DIP, PIP and MCP joint respectively and the subscript f/e means that the flexion extension movement is considered. When the PIP joint is bent, the DIP joint follows the movement with a displacement of approximately 2/3 of the PIP one. The same result was first proposed by Rijpkema [101]. Equation 1 shows that a similar relationship also exists between the MCP joint and the PIP joint with a ratio of approximately 3/4.

$$\theta_{DIP} \approx \frac{2}{3}\theta_{PIP} \quad ; \quad \theta_{PIP} \approx \frac{3}{4}\theta_{MCP_{f/e}} \qquad 1$$

Another example is provided by Equation 2, which shows the joints of the thumb during the flexion or the extension.

$$\theta_{IP} \approx \frac{1}{2}\theta_{MCP_{f/e}} \quad ; \quad \theta_{MCP_{f/e}} \approx \frac{5}{4}\theta_{TMC_{f/e}} \qquad 2$$

It is important to underline that these constraints are not strictly kinematic constraints similar to the mechanical ones. Some individuals are better than others at controlling the movements of their articulations, forcing different behaviours with respect to the “standard” one defined by the equations. However, in normal conditions and without any external influence, these constraints are respected quite faithfully. As previously mentioned, the constraints analyzed in this chapter are caused by the physiologic structure of each element that compounds the human hand.

Dynamic Inter-Finger constraints

Dynamic inter-finger constraints are limitations which couple joints belonging to different fingers. The movement of one of the constrained articulations of the finger A generates an involuntary movement of one or more articulations of the finger B. For example, with the hand open in rest position and placed on its back on a surface, when the MCP joint of whatever finger is bent also the MCP joints of the others fingers move as a consequence of the internal constraint. It is important to underline that, in this case as well, different individuals could show important differences as a consequence of their physiologic structure and personal abilities and the constraint could be forcefully overcome. The complexity of the hand structure causes some constraints not to be explicitly represented through equations. Some other articulations, on the contrary, seem to be naturally coupled with a quite proportional behaviour; in these cases the respective angles move with a specific relationship, unless a voluntary external force is applied imposing a modification in the behaviour. Anyway, trying to move an articulation in an unnatural way often results in an excessively strenuous, and sometimes painful, movement.

Providing a complete list of all the inter-finger constraints would not be useful and interesting. Only some examples of coupled movements are explained below. In the following examples the angular displacement is described through the parameter θ followed by three nested subscripts that specify the finger involved, the articulation and if the movement is a flexion extension (f/e) or abduction adduction (a/a).

Equation 3 describes a direct coupled movement between the articulation of middle and ring finger, when index and little finger are at rest.

$$\theta_{M_{MCP_{f/e}}} \approx \theta_{R_{MCP_{f/e}}} \qquad 3$$

Equation 4 shows an indirect coupled movement generated when the ring finger is bent. As a consequence of this movement the middle and little fingers slightly move with the same angular displacement.

$$\theta_{M_{MCP_{f/e}}} \approx \theta_{L_{MCP_{f/e}}} \qquad 4$$

Equation 5 reports an example of coupled movement related to the abduction adduction movement between the ring and the little finger.

$$\theta_{R_{MCP_{a/a}}} \approx \theta_{L_{MCP_{a/a}}} \qquad 5$$

The previously described relationships are very simple, while some more complex relationship exist binding the articulation in a more intricate way. They can be divided into two types. The first typology occurs when there is a flexion of the MCP articulation, as in the case of the previously cited index finger, generating movements also in the others fingers with a specific kinematic ratio. Equation 6 expresses this relation between the middle and the index fingers.

$$\theta_{M_{MCP_{f/e}}} \approx \frac{1}{5}\theta_{I_{MCP_{f/e}}} \qquad 6$$

This relationship occurs only when there is a single flexion of the first finger MCP joint (in this case the index finger): when it takes place, the MCP joint of the second one will bent naturally and passively with the specific kinematic ratio.

The second type occurs when a single articulation generates multiple effects on different joints. Equations 7 show the effects of the bending of the MCP joint of the little finger on the other articulations.

$$\theta_{R_{MCP_{f/e}}} \approx \frac{7}{12}\theta_{L_{MCP_{f/e}}} \quad ; \quad \theta_{M_{MCP_{f/e}}} \approx \frac{2}{3}\,\theta_{R_{MCP_{f/e}}}$$
$$\theta_{R_{MCP_{f/e}}} - \theta_{M_{MCP_{f/e}}} < 60° \quad ; \quad \theta_{L_{MCP_{f/e}}} - \theta_{R_{MCP_{f/e}}} < 50° \qquad 7$$

All these constraints end up being very important because they express natural physical relationships between the various articulations of the human hand. The design of devices planned to emulate and reproduce the movements of the hand have to comply as much as possible these constraints.
One last aspect must be underlined: in addition to what explained, other constraints could rise as a consequence of the interaction with a specific shape object. These "ergonomic constraints" are strictly related to a specific task, such as grasping an object with a specific geometry. Table 8 and Table 9 show the typical dynamic (both intra- and inter-finger) ergonomic constraints generated during a circular grasp and a prismatic grasp. According to the information provided by Table 8 it could be assert that, as a consequence of the internal relationship between the articulations, the number of degrees of freedom is reduced as follows: the thumb and the index finger are defined by 2 DoF, the middle finger and the ring finger by only 1 DoF and the little finger by 3 DoF. The middle and the ring fingers are also influenced by the two adjoining fingers (index and ring for the middle and middle and little for the ring). It can therefore be affirmed that the thumb, the index and the little finger are the most important digits

	CMC (TMC)	MCP		PIP (IP)
Thumb	$\theta_{T_{TMC}} = \frac{11}{10}\theta_{T_{MCP}}$	$\theta_{T_{MCP}} = \frac{4}{5}\theta_{T_{IP}}$		x
Index	$\theta_{I_{CMC}} = \theta_{\mathrm{M_{CMC}}}$	x	$\theta_{\mathrm{I_{MCP_{f/e}}}} = \frac{4}{3}\theta_{I_{PIP}}$	$\theta_{I_{PIP}} = \frac{3}{2}\theta_{\mathrm{I_{DIP}}}$
Middle	$\theta_{\mathrm{M}_{CMC}} = \frac{1}{2}\theta_{R_{CMC}}$	$\theta_{M_{MCP_{a/a}}} = \frac{1}{5}\theta_{I_{MCP_{a/a}}}$	$\theta_{M_{MCP_{f/e}}} = \frac{4}{3}\theta_{\mathrm{M_{PIP}}}$	$\theta_{\mathrm{M_{PIP}}} = \frac{3}{2}\theta_{\mathrm{M_{DIP}}}$
Ring	$\theta_{R_{CMC}} = \frac{2}{3}\theta_{L_{CMC}}$	$\theta_{R_{MCP_{a/a}}} = \frac{1}{2}\theta_{L_{MCP_{a/a}}}$	$\theta_{R_{MCP_{f/e}}} = \frac{4}{3}\theta_{\mathrm{R_{PIP}}}$	$\theta_{\mathrm{R_{PIP}}} = \frac{3}{2}\theta_{\mathrm{R_{DIP}}}$
Little	x	x	$\theta_{R_{MCP_{f/e}}} = \frac{4}{3}\theta_{\mathrm{L_{PIP}}}$	$\theta_{\mathrm{L_{PIP}}} = \frac{3}{2}\theta_{\mathrm{P_{DIP}}}$

Table 8: Dynamic constraints of the human hand during a circular grasp.

	CMC (TMC)	MCP		PIP (IP)
Thumb	$\theta_{T_{TMC}} = \frac{11}{10}\theta_{T_{MCP}}$	$\theta_{T_{MCP}} = \frac{6}{5}\theta_{T_{IP}}$		**x**
Index	$\theta_{I_{CMC}} = \theta_{\mathrm{M_{CMC}}}$	**x**	$\theta_{\mathrm{I_{MCP_{f/e}}}} = \frac{3}{2}\theta_{I_{PIP}}$	$\theta_{I_{PIP}} = 2\theta_{\mathrm{I_{DIP}}}$
Middle	$\theta_{\mathrm{M}_{CMC}} = \frac{1}{2}\theta_{R_{CMC}}$	$\theta_{M_{MCP_{a/a}}} = \frac{1}{2}\theta_{I_{MCP_{a/a}}}$	$\theta_{M_{MCP_{f/e}}} = \frac{3}{2}\theta_{\mathrm{M_{PIP}}}$	$\theta_{\mathrm{M_{PIP}}} = 2\theta_{\mathrm{M_{DIP}}}$
Ring	$\theta_{R_{CMC}} = \frac{2}{3}\theta_{L_{CMC}}$	$\theta_{R_{MCP_{a/a}}} = \frac{1}{2}\theta_{L_{MCP_{a/a}}}$	$\theta_{R_{MCP_{f/e}}} = \frac{3}{2}\theta_{\mathrm{R_{PIP}}}$	$\theta_{\mathrm{R_{PIP}}} = 2\theta_{\mathrm{R_{DIP}}}$
Little	**x**	**x**	$\theta_{R_{MCP_{f/e}}} = \frac{3}{2}\theta_{\mathrm{L_{PIP}}}$	$\theta_{\mathrm{L_{PIP}}} = 2\theta_{\mathrm{P_{DIP}}}$

Table 9: Dynamic constraints of the human hand during a prismatic grasp.

during the circular grasp [100]. A similar analysis also can be performed with the data coming from a prismatic grasp task, shown in Table 9.

Hand Grasp Taxonomy

Taxonomy is the branch of biology concerned with the classification of organisms into groups based on similarity; each group has its rank and can be aggregated in a higher rank group thus creating a hierarchical classification. The hand grasp taxonomy aims at classifying and understanding what types of grasps human beings can perform and commonly use in everyday tasks. These researches are useful not only from a biological and medical point of view, but also from a robotic point of view because they can be an inspiration for the designing of prosthesis, exoskeleton and robotic hands.
Since grasping results to be a wide area and is not completely standardized, it is necessary to find a definition to fit with the specific needs of what grasp is in the specific project. A suitable definition could be: *"a grasp is every static hand posture with which an object can be held securely with at least one hand"*. The large number of muscles and joints of the hand obviously provides the equipment for

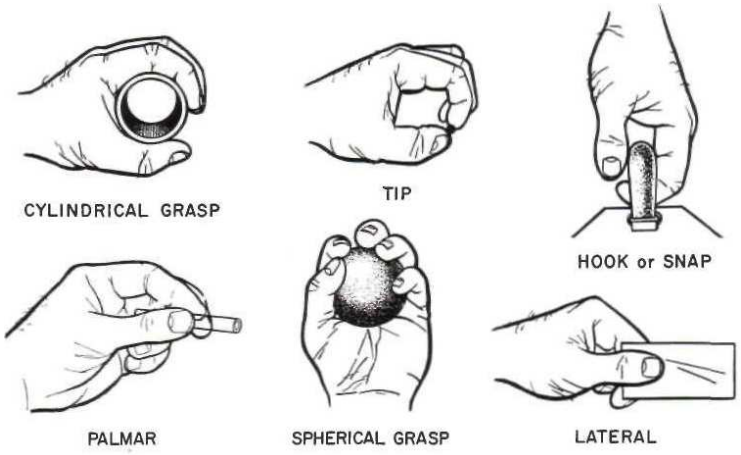

Figure 34: Six hand groups based on the grasped object shape

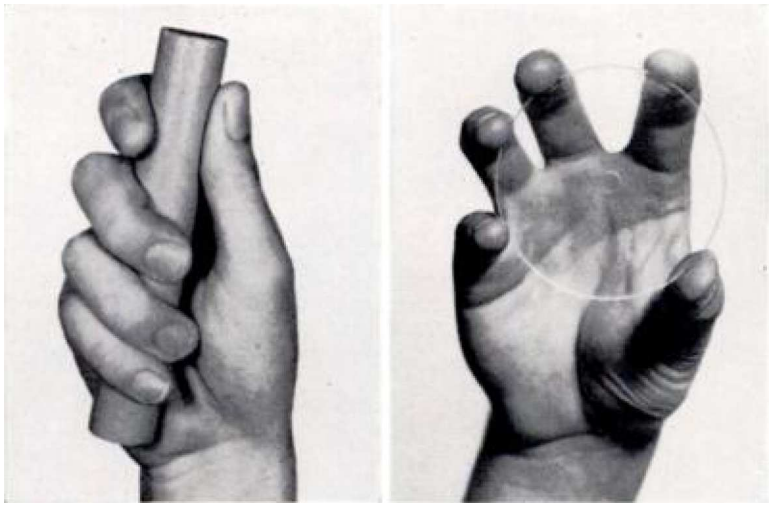

Figure 35: Two hand groups based on the purpose of the task: power grip (left) and precision grip (right)

Power						Intermediate			Precision				
Palm		Pad				Side			Pad				Side
3-5	2-5	2	2-3	2-4	2-5	2	3	3-4	2	2-3	2-4	2-5	3
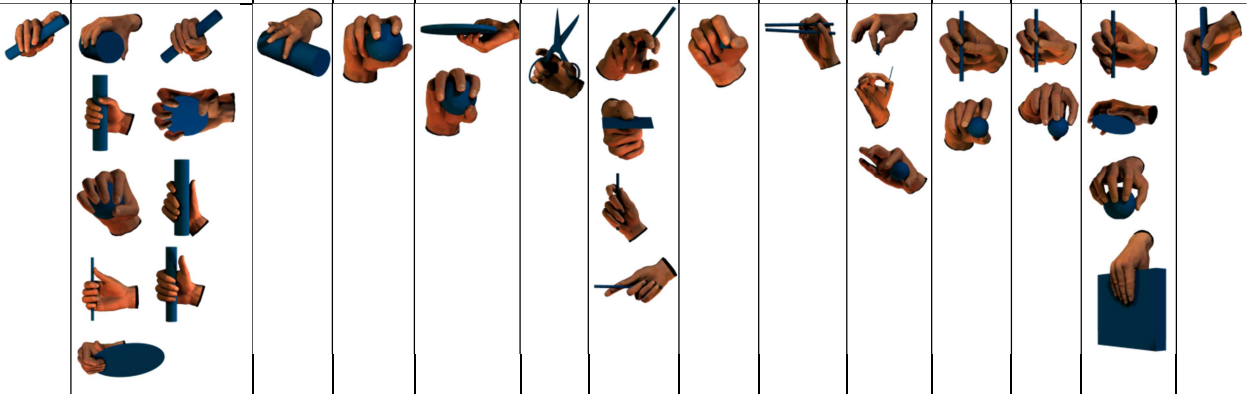													

Table 10: Exhaustive grasp taxonomy

numerous and varied patterns of movements. There are several studies on grasping capabilities, both from the anatomical and functional point of view coming from the medical community. Taylor and Schwartz [102] developed their characterization of the human grasp defining six groups and associating each of them to a different object shape: cylindrical, fingertip, hook, palmar, spherical and lateral Figure 34.

A completely different philosophy of interpretation came from Napier [103], who divided the grasps only into two groups based on the purpose of the task: power grasp and precision grasp. The classification into power and precision grasp is today the most widely accepted and utilized in the medical, biomechanical and robotic community. A power grasp usually involves a large contact area and is characterized by a higher stability and security at expense of a reduced maneuverability. On the contrary, a precision grasp requires a small contact area between hand and manipulated object, which guarantees a high possibility of movements (Figure 35). 147 grasp examples can be found in literature; it has been decided to consider a simplified subset, which excluded a series of grips which were considered useless in the current project like the bi-manual grasps, the gravity dependent grasps and so on [104]. Table 10 shows a possible grasp taxonomy considered exhaustive in that specific case: the classification on the columns is based on the type of grips (power or precision), the opposition kind (palm, pad or side) and finally on the virtual finger involved in the opposition. The virtual finger is a way of describing the mechanics of grips; each human finger is associated to a number, starting from 2 (the index finger) to 5 (the little finger). The virtual finger is the representation of all the fingers involved in the opposition to the thumb [105].

Hand Tasks and the Number of Fingers

Considering all the possible hand tasks and grips, Mishkin and Jau claim in their study [106] that, varying the number of fingers involved in a specific task, the number of performable tasks changes as follows: two fingers can perform 40% of the possible hand tasks, three fingers can accomplish up to 90% and four fingers can complete the 99%. This suggests that the passage from two to three fingers will give the maximum benefit considering only the percentage of performable tasks. Passing from two to three fingers the number possible tasks more than doubled; adding the forth finger only increases the capability by an additional 10%. On support of this affirmation Salisbury [107] demonstrated, starting from kinematic considerations, that three fingers are mandatory for manipulation tasks, obviously if a

specific task belongs to the one tenth of the unfeasible one, then the forth finger acquires a fundamental importance. For example Salisbury asserts that four fingers are necessary in order to re-grasping objects in the hand. Moreover, the number of tasks which can really be performed with two fingers manipulators, but not by a parallel-jaw gripper, is very small; this makes the two fingers configuration a really poor choice.
Jacobsen et al. [108] analysed in their study a wide range of tasks, from delicate precision tasks, such as threading nuts onto bolts, to high power tasks, such as wielding a hammer. For each type of action the number of digits and the number of degrees of freedom were determined in order to guarantee a minimum level of dexterity. For all the tasks the thumb and two fingers were declared necessary. The thumb required all his four degrees of freedom, three related to flexion-extension and one related to abduction-adduction, in order to guarantee the passage of the digit from a position on the side of the hand to the one in opposition with the fingers. Regarding the two fingers, each of them requires only two over three degrees of freedom related to flexion-extension. Finally, regarding the abduction-adduction degrees of freedom of the two fingers, only one of the two was considered sufficient in order to be able to spread the fingers. Burdea [109] confirmed Jacobsen's study asserting that three digits are optimal both for the human hand and for robotic manipulators.
It could seem that three fingers are the overall optimal solution, but the reality is a bit more complicated. The everyday work usually requires a lot of complex manipulation tasks and the use of tools appositely designed for a five finger hand, all of them belonging to one tenth of the actions performable only with at least four fingers. The experiments performed by Mishkin and Jau after their article confirmed this sentence. The four fingers configuration allows to use three fingers to hold an object or a tool, using the forth for the re-grasping itself or acting on specific elements, like triggers or buttons. A big drawback of the three fingers solution is that it narrows the contact area of the power grasps, reducing stability. It is easy to understand that a hammer could be used using only three fingers, but a better grasp, and consequently a better work, is guaranteed using the whole hand.
These considerations are fundamental in order to consider all the advantages and disadvantages related to the number of independent fingers and degrees of freedom of the future device.

Hand Capabilities

The last type of information gathered from literature related to the human hand concerns capabilities in terms of forces, torques, velocities and power. All this information is fundamental for the development of a device that aims to emulate the human hand; in particular information on velocity and torque will become a basic constraint on whatever actuators are planned to be used. In the following part the main studies on the human hand capabilities are analyzed, gathering the main interested information for each phalanx of each finger. It is important to underline that the following information has to be used in a clever way. Human capabilities, such as velocity and force, result to be strongly influenced by the physical presence and the training of the subject and therefore this data collection has the aim of obtaining an idea of the order of magnitude of the variables more than an exac set of numeric values.

Finger Joint's Force and Torque

Several studies aim to record the maximum forces exchanged by the hand with grasped objects. The work done by An et al. [110] measured all the normal forces applied on each phalanx of each finger during a cylindrical maximum strength power grasp upon data collected from an unknown number of subjects.

The measurement system was composed by a series of strain gauge placed in correspondence of the mid-point of each phalanx. Table 11 reports the maximum values measured by the device during the experiment; this, even though limited to the specific task, provides good information regarding the range of forces during this specific activity.
Considering emblematic and relatively representative the phalangeal length and the joint angles assumed by the human hand during a cylinder grasp, the joint torques related to the measured applied forces were calculated by An et al. as follows. It is necessary to choose a certain set of phalanx length and joint angles assumed as representative sample in order to calculate the joint torques. Table 12 shows the assumed values of the phalanges lengths and joint angles used by the author in the study. The joint angles are obtained in a differential way with respect to the fully extended position and thus equal to zero in the straight configuration. Figure 36 shows the vector diagram for the torque computation [111].

	Force [N]		
	Proximal	**Middle**	**Distal**
Index	42	22	62
Middle	24	40	68
Ring	15	28	44
Little	7	20	31

Table 11: Maximum forces exerted by the human phalanges during cylindrical power grasp (An).

	Lengths [cm]			Angles [°]		
	Proximal	**Middle**	**Distal**	**Proximal**	**Middle**	**Distal**
Index	5	3	2.5	53	61	51
Middle	5.5	3.25	2.5	53	61	51
Ring	5	3	2.5	53	61	51
Little	3.75	2.75	2.5	53	61	51

Table 12: Assumed values of phalanges lengths and joints angles used to calculate the joint torque (An).

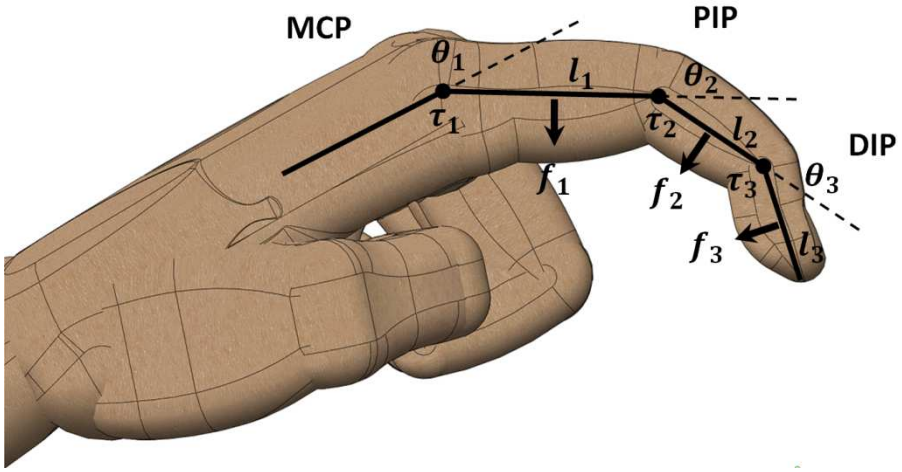

Figure 36: Vector diagram for the torque computation.

The cross product between the force vector and the vector that describes the application point of the force gives the contribution of each force to the joint torque τ_i. The two vectors could be calculated as follows:

$$\begin{cases} \overrightarrow{\boldsymbol{l_i}} = l_i \cos\left(\sum_{j=1}^{i} \theta_i\right)\vec{\boldsymbol{\imath}} + l_i \sin\left(\sum_{j=1}^{i} \theta_i\right)\vec{\boldsymbol{\jmath}} \\ \overrightarrow{\boldsymbol{f_i}} = f_i \cos\left(\frac{\pi}{2} + \sum_{j=1}^{i} \theta_i\right)\vec{\boldsymbol{\imath}} + l_i \sin\left(\frac{\pi}{2} + \sum_{j=1}^{i} \theta_i\right)\vec{\boldsymbol{\jmath}} \end{cases} \quad 8$$

The joint torques can then be calculated as follow:

$$\begin{cases} \boldsymbol{\tau_1} = \frac{\boldsymbol{l_1}}{2} \wedge \boldsymbol{f_1} + \left(\boldsymbol{l_1} + \frac{\boldsymbol{l_2}}{2}\right) \wedge \boldsymbol{f_2} + \left(\boldsymbol{l_1} + \boldsymbol{l_2} + \frac{\boldsymbol{l_3}}{2}\right) \wedge \boldsymbol{f_3} \\ \boldsymbol{\tau_2} = \frac{\boldsymbol{l_2}}{2} \wedge \boldsymbol{f_2} + \left(\boldsymbol{l_2} + \frac{\boldsymbol{l_3}}{2}\right) \wedge \boldsymbol{f_3} \\ \boldsymbol{\tau_3} = \frac{\boldsymbol{l_3}}{2} \wedge \boldsymbol{f_3} \end{cases} \quad 9$$

The joint torques related to a cylindrical power grasp are calculated in this way and shown in Table 13. Another study related to the measurement of forces during a cylinder power grasp was performed by Lowe et al. [112]. The measurement setup utilized in this experiment was composed by 20 force sensors attached on a thin leather glove. The force sensors used in this case were resistance based conductive polymers with a circular sensitive area of around 9.5 mm of diameter and placed in correspondence of the mid-point of each phalanx. Table 14 shows the distribution of the forces measured over the 16 sensing elements mounted on the four finger fingers. This information is provided through the mean value of the forces and their percentage with respect to the entire force exchanged during the circular grasp. This analysis allows to know forces and their distribution among specific points

	Joint Torque [N*cm]		
	MCP	**PIP**	**DIP**
Index	270	228	77.5
Middle	322	289	85
Ring	203	180	55
Little	126	120	39.8

Table 13: Joint torques exerted by human fingers in cylindrical grasp (An).

	Mean Force [N]							
	Proximal		**Middle**		**Distal**		**Meta-head**	
Index	21	4.7%	26.1	5.9%	45.9	10.4%	17.3	3.9%
Middle	29.3	6.6%	36.5	8.2%	64.1	14.5%	24.2	5.5%
Ring	22.3	5%	27.8	6.3%	48.8	11%	18.4	4.2%
Little	11.6	2.6%	14.5	3.3%	25.4	5.7%	9.6	2.2%

Table 14: Average distribution of forces during a circular power grip (Lowe).

	Force [N]
	At the tip
Index	49
Middle	49
Ring	37
Little	n/a

	Joint Torque [N*cm]		
	MCP	PIP	DIP
Index	463	213	62.5
Middle	500	225	62.5
Ring	370	170	50
Little	n/a	n/a	n/a

Table 15: Maximum forces measured at the fingertip (left) and the corresponding maximum torques (right) (Sutter).

of the hand. Comparing An's and Lowe's studies it can be noticed that the results are quite similar, taking into account the preliminary observation based on the difference between the human beings. The two measurements are in range between the 0.7% and the 25.9% for each single phalanx; it must be noticed that the proximal phalanges cannot be compared as a consequence of the different sensor placement.

Analysing these results, it can be noticed that the index and the middle fingers result to be the strongest and generate the biggest part of the force during the grip. These observations result very important because they allow different strategies for the future device to be considered; in particular this one assert that, a device concept which implies only thumb, index and middle, could be a reasonable simplification with respect to one composed by all the five digits without big losses of force.

An additional study was performed by Sutter et al. [113], aiming at measuring the maximum force exerted by the human fingers at the tip, while in this case no data was acquired for the little finger. The results are reported in the left part of Table 15. The data is referred to 10 subjects of different ages and gender. The same approach previously explained to calculate the torques starting from the forces measured by An et al. has also been used with Sutter study's data. In this case the fingertip force was measured with the fully extended finger, so all the angles are equal to zero, with a simplification of the calculus. The torques obtained from Sutter's study are shown in the right part of Table 15.

The two sets of obtained torques describe the articulation torques in two different joint positions, the cylindrical grasping and the fully extended, allowing to perform some comparisons. Sutter observed that the maximum joint torque is quite independent from the MCP joint angle. Although the two presented tests provided sets of data obtained under different conditions and circumstances, a careful comparison could be useful in order to understand hand capabilities and determine constraints for the final device. Comparing results, it could be noticed that the MCP measured by Sutter is bigger than An's one, while the opposite behaviour occurs for PIP and DIP torques. Hasser [111] claimed in his study that the torques obtained by Sutter represent the effective maximum human torque only in relation to the MCP joint, while results coming from An's data are a better representation of the PIP and DIP joints. Hasser justifies his thesis analysing the two different test protocols. Since An's measurement setup was able to measure only the normal component of forces, the tangential one, generated during the cylindrical grasp, was completely neglected, underestimating therefore the activity of the MCP joint, but granting a

	Joint Torque [N*cm]		
	MCP	PIP	DIP
Index	463	228	77.5
Middle	500	289	85.0
Ring	370	180	55.0
Little	N/A	120	39.8

Table 16: Maximum torque capabilities of human finger joints considering both An and Sutter works.

	Lateral Finger Strength [N]						
	Pinch			Radial deviation		Ulnar deviation	
	Tip	Palmar	Key	Thumb	Index	Thumb	Index
Male	65	61	109	43	43	75	42
Female	45	43	76	25	31	43	28

	Force [N]
	Index-middle
Abduction	40
Adduction	30

Table 17: Measurement of the abduction adduction forces in different conditions (An).

challenging test for PIP and DIP joints. On the contrary, Hasser claimed that the study performed by Sutter was more challenging for the MCP joint than PIP and DIP. Since the fingertip torque measured by Sutter results from three joints placed in series, the maximum contributor will be limited by the weakest one. The composite result of the two studies is shown in Table 16.

Some studies which aim to investigate the finger abduction-adduction force capabilities are analysed as follows. An et al. [110] measured the maximum abduction force and adduction force between index and middle finger measured at the fingertip. Abduction-adduction forces between the other fingers were comparable or smaller than the index-middle one. In the same work An also measured the lateral force of the index finger and the thumb during different pinches and in two different wrist position. Table 17 shows the data related to all these measurements. As easily predictable, the thumb is the most powerful of the digits.

It could be appreciated looking at the value of the key pinch reported in Table 17: the key pinch requires the thumb to press against the lateral size of the index finger. This value could be interpreted like the thumb fingertip maximum force (109N) and it results more than double Sutter's maximum index fingertip (50N). Analysing another study by Kroemer and Gienapp [114], it can be noticed that the results confirm An's work. Kroemer and Gienapp performed the same study made by An on a sample of 31 male Air Force pilots. The average thumb fingertip force ranges from 84N for the measurement performed in the straight position up to 99N for the key pinch position.

Mathiowetz [115], Imrhan and Astin [116] studied the average strength during key pinch, palmar pinch and power grip for male and female subjects; Table 18 shows a comparison between results obtained in these works. They confirmed the order of magnitude already obtained in the previously reported studies. Finally, Bretz et al. [117] performed a similar experiment to measure the fingers forces; the results are shown in Table 19.

	Mean Strenght [N]								
	Lateral pinch			Palmar pinch			Cylindrical grasp		
	Astin	Mathiowetz	Imrhan	Astin	Mathiowetz	Imrhan	Astin	Mathiowetz	Imrhan
Male	97	110	92	63	76	72	452	466	487
Female	65	73	64	45	51	46	289	280	308

Table 18: Comparison between results from Astin, Mathiowetz and Imrhan studies.

	Average Force Measurement [N]					
	Hand	Little	Ring	Middle	Index	Thumb
Right hand	551	31	38	55	57	108
Left hand	505	28	37	54	60	109

Table 19: Results of the Bratz study.

Finger Joint's Velocity

Few information is available in relation to the maximum speed of finger joints during hand activities. Similarly to forces and torques, the knowledge of the maximum velocities would be useful to define constraints related to the upper speed limit achievable during typical hand tasks. The maximum speed can also be used in order to estimate the human articulation power capability in absence of instantaneous measurements of synchronized forces and velocities.
Darling et al. [118, 119] measured the joints velocities (with the exception of the DIP ones) during their analysis of the finger dynamics of four subjects. During this study a maximum speed profile of one of the subject shows a MCP peak speed of 18 rad/s and a PIP peak of 12 rad/s. The author claimed that the "natural velocity" of the human finger is around 10 rad/s, while the "slow motion velocity" is around 3-6 rad/s. These experimental results are supported by Marcus' et al. [120] work, which confirms a maximum average MCP joint velocity between the four male and two female subjects of 17 rad /s; the PIP joint velocity was not measured directly but it was estimated at 18 rad/s.

Finger Joint's Power

The data collection performed since here allows to estimate the power of the finger articulations. The results coming from An et al. and Sutter contribute to obtain information related to torque, while Darling et al. and Marcus et al. furnish a measurement of velocity. Considering the middle finger, the maximum MCP stall force is equal to 5Nm, while the MCP no load speed is equal to 17 rad/s. Performing a linear interpolation between these data provide the suitable dimensions for power calculation (assuming one half of the maximum angular speed and maximum toque): 2.5Nm and 8.5 rad/s. Performing the same procedure with the PIP joint, the middle finger joint power is equal to:

$$\begin{cases} P_{M_{MCP}} = (8.5\ rad/s)(2.5\ Nm) = 21W \\ P_{M_{PIP}} = (9\ rad/s)(1.44\ Nm) = 13W \end{cases} \quad 10$$

The above calculation assumes a linear interpolation. Hollerbach et al. [121] shows that muscles do not have a linear strain stress curve, therefore the author claim that the maximum power occurs at one third of maximum velocity and maximum speed instead of one half. The power estimation of the middle finger on the basis of the Hollerback study is equal to:

$$\begin{cases} P_{M_{MCP}} = (5.67\ rad/s)(1.67\ Nm) = 9.4W \\ P_{M_{PIP}} = (6\ rad/s)(0.96\ Nm) = 5.8W \end{cases} \quad 11$$

Stated in a simpler way, the maximum power of a human muscle is equal to:

$$P_{MAX} = 0.11 \cdot \dot{\theta}_{MAX} \cdot \tau_{MAX} \quad 12$$

Human Hand Model

The previous sections explanation describes the characteristics of the human hand during the interaction with objects and/or performing everyday activities. Robotic devices planned to work together with the human being, interacting for example with the human hand, have to improve specific statistics, often to the detriment of some others. Typical examples of devices interacting in a symbiotic

way with the human hand are haptic gauntlets and rehabilitation exoskeleton; each of them is focused on a specific performance of the human hand (e.g. agility and range of motion for the former and forces and velocities for the latter) but limiting some other characteristics (e.g. the former's are generally bulky while the latter's are composed by few degrees of freedom). In any case, independently from the specific task, the common characteristic of all these devices is the ergonomics with respect to the human hand. The future device will have to fit with the human being, granting as perfect as possible a human-machine interaction, avoiding to reproduce unnatural or uncomfortable movements.

Human Hand Kinematics

As widely previously analysed, the human hand is very complex, being composed by many elements of different nature. This complexity raises the necessity and the desire to obtain a very accurate kinematic model of the hand, based on the physiology of the limb and using the characteristics obtained in advance. The complete model is very useful in order to realize hand structures such as prosthetics, exoskeletons and humanoid end-effectors in general. All the fingers have similar kinematic chains so they can be studied together in the same way; on the contrary, the thumb, due to its ability to oppose each single finger to perform grasping tasks, requires its own separate analysis.
The kinematic model proposed here is composed by 19 links, corresponding to the human bones, and 24 degrees of freedom, corresponding to the articulations; for simplicity the degrees of freedom are

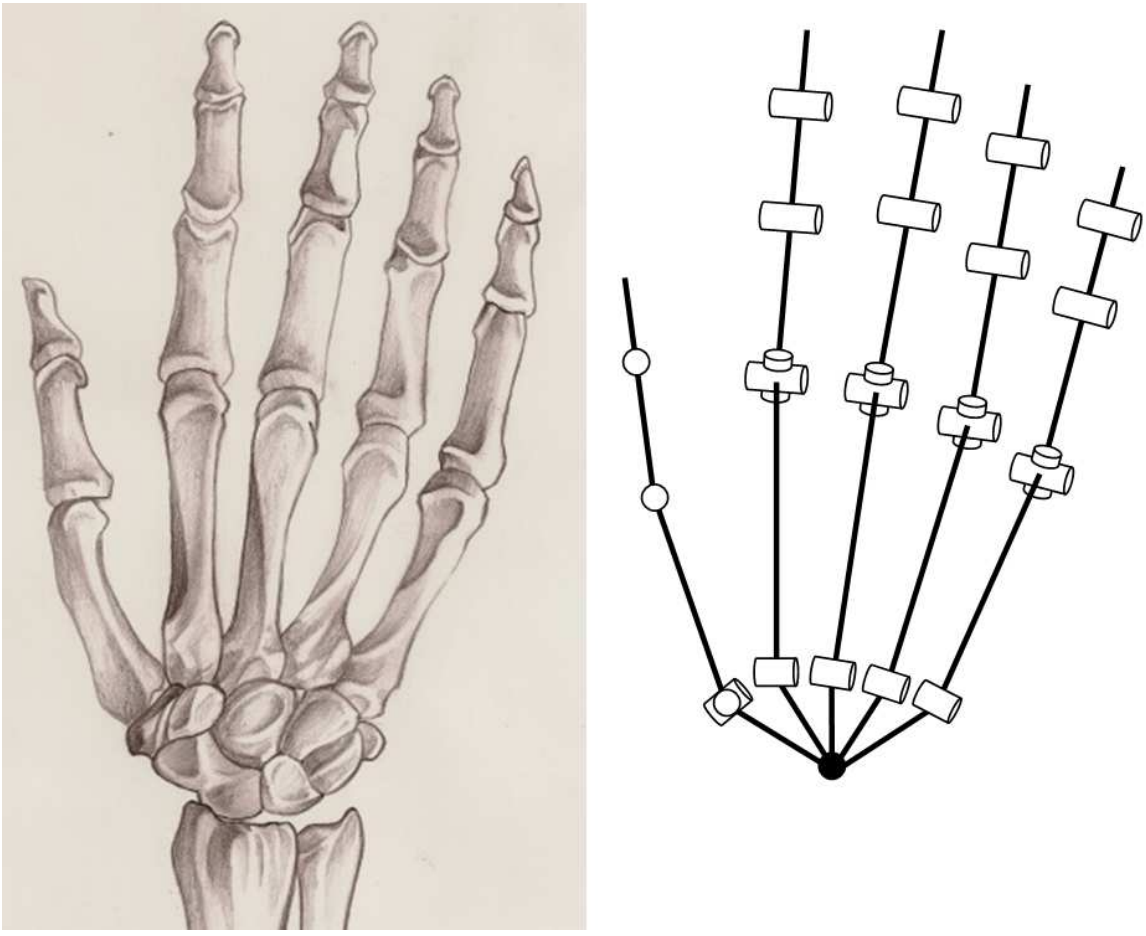

Figure 37: Kinematic chain of the human hand.

modeled by pure rotational joints. As previously mentioned, two different kinematic analysis are needed for the digits; one for the four fingers (each of them modeled with four links and five joints) and one for the thumb (modeled with three links and four joints) Figure 37. It is important to notice that the CMC joint represents the deformation of the hand palm during grasping tasks. Moreover, MCP and TMC joints were decoupled into two joints, each related to one degree of freedom (flexion/extension and abduction/adduction). In this specific kinematic analysis the MCP abduction/adduction joint is considered upstream with respect to the MCP flexion/extension one.

The Kinematics studies the motion of bodies without considering external forces or moments. There are two main ways to model a system in robotics: the Cartesian and the Quaternion space. Only the Cartesian space was considered in this analysis. Each transformation between two Cartesian coordinate systems can be decomposed into a rotation and a translation. There are several ways to represent this rotation, including the following: Euler angles, Gibbs vector, Cayley-Klein parameters, Pauli spin matrices, axis and angle, Hamilton's quaternions and orthonormal matrices [122]. Among all these representations the orthonormal matrices have been used more often in robotics. The orthonormal matrices are four by four matrices that describe homogenous transformations. Denavit and Hartemberg demonstrated in 1955 that with this representation a generic transformation between two different joints can be fully described with a minimum number of parameters equal to four. These parameters, known as Denavit Hartemberg parameters, became the standard way to describe the robot kinematics.

The kinematics model, based on the geometrical parameters of a system, allows set of coordinates to be transformed according to the needs. During a standard robotic arm analysis, the device is able to measure directly its inner kinematic parameters, called joints coordinates, and describe the position of each joint; at the same time the most important information usually required by the user is the position and the attitude of the end effector. These two sets of coordinates describe both the position of the robot in two different ways, each useful in specific cases. Direct kinematics is defined as the mapping from the joint coordinate space to the end effector coordinate space, allowing to immediately obtain the position of the robotic tip starting from the position of all the individual joints, which are usually easily measurable. On the contrary, inverse kinematics is the mapping from the end effector coordinate space to the joint coordinate space. Inverse kinematic is needed in control because the actuation system usually acts directly or indirectly on the joint coordinate space and so, once a target position of the end effector is known, the path planning starts from the joint. Figure 38 summarizes the direct and inverse kinematics.

The computation of direct kinematics is straightforward and there isn’t great complexity coming from the equations except the computation itself; moreover, an analytical solution is always guaranteed. On the contrary, inverse kinematics is a much more difficult problem; usually the solution of the inverse kinematics problem is computationally expensive and could take a very long time as a consequence of

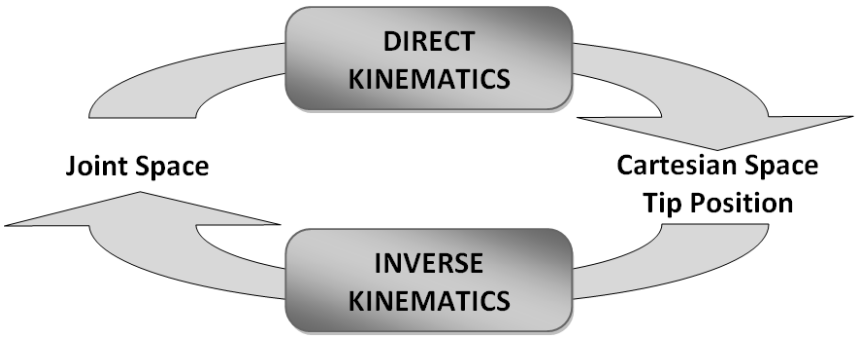

Figure 38: Direct and Inverse Kinematics.

the presence of singularities and nonlinearities. An analytical solution can rarely be achieved and in this case it is necessary to solve the problem through numerical methods.

Direct Kinematics

Direct kinematics is applied in this specific case to describe the posture of the finger and the position of the fingertip as a function of the joint angles. The model equations are calculated by means of the Modified Denavit Hartenberg (MDH) parameters, introduced by Craig [123]. In order to avoid an useless increase in complexity of the model, the articulations were considered as ideal revolute joints and the bones were considered as perfectly rigid bodies. Compliance in the joints, links, or base frames, as well as non-ideal rotational joint behaviours cannot be directly modeled using the MDH convention and are completely neglected. The kinematic chain is therefore composed by links connected with ideal revolute joints from the base, in this case the palm, to the end-effector, in this case the fingertip. A reference frame $\mathcal{R}_i$ is attached to each joint and its position and attitude is univocally defined starting from the previous one and following the MDH convention. The generic transformation matrix ${}^{i+1}_{i}T$ allows to map vectors defined with the $\mathcal{R}_i$ reference frame in the $\mathcal{R}_{i+1}$.

The MDH convention univocally defines the passage from one reference frame to the following one through a set of four elementary roto translation transformations, each defined by one of the four MDH parameters Figure 39.

The four MDH parameters are defined as follows:

- a_{i-1} is the linear displacement measured along $\hat{x}_{i-1}$ from $\hat{z}_{i-1}$ to $\hat{z}_i$
- α_{i-1} is the angular displacement measured about $\hat{x}_{i-1}$ from $\hat{z}_{i-1}$ to $\hat{z}_i$
- d_i is the linear displacement measured along $\hat{z}_i$ from $\hat{x}_{i-1}$ to $\hat{x}_i$
- θ_i is the angular displacement measured about $\hat{z}_i$ from $\hat{x}_{i-1}$ to $\hat{x}_i$

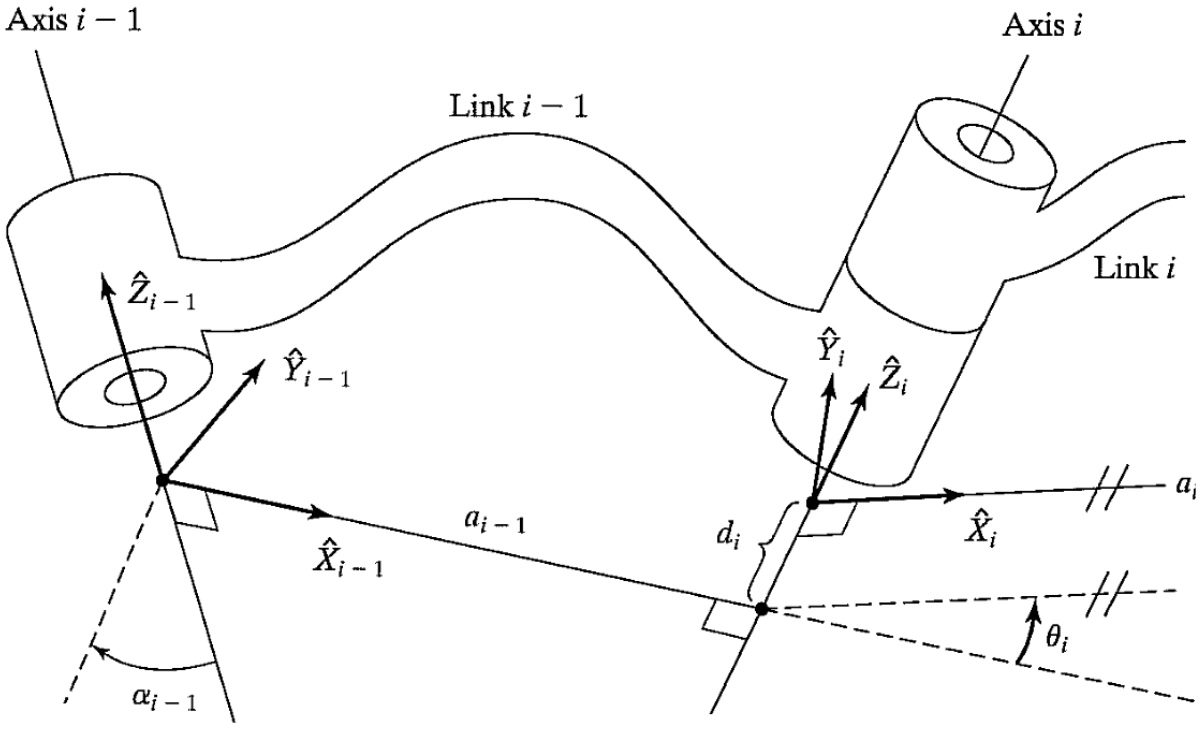

Figure 39: Visual representation of the modified Denavit Hartemberg parameters.

The transformation matrix ${}^{i-1}_{i}T$ is then the result of two pure rotations: $R(\hat{x}_{i-1}, \alpha_{i-1})$, $R(\hat{z}_i, \theta_i)$ and two pure translations: $t(\hat{x}_{i-1}, a_{i-1})$, $t(\hat{z}_i, d_i)$ and it is equal to:

$$ {}^{i-1}_{i}T = R(\hat{x}_{i-1}, \alpha_{i-1}) t(\hat{x}_{i-1}, a_{i-1}) R(\hat{z}_i, \theta_i) t(\hat{z}_i, d_i) \quad (13) $$

The difference between normal and modified Denavit Hartenberg conventions is related to the orientation of the $\hat{z}_i$ axis.
Using normal DH convention the $\hat{z}_i$ axis if the $\mathcal{R}_i$ reference frame is coincident with the rotation axis of the joint $i+1$, while with the modified DH convention the $\hat{z}_i$ axis if the $\mathcal{R}_i$ reference frame is coincident with the rotation axis of the joint i. The modified convention presents some advantages when dealing with end effectors and in particular it facilitates the dynamic analysis because the positions, velocities, acceleration and torques are given in the reference frame of the relative joint, in this case the articulation.

Direct Kinematics of the Four Fingers

Figure 37 shows the kinematic chain of all the digits. The kinematic chain of the four fingers is composed by four links, represented by the four bones (metacarpal, proximal, middle and distal from the palm to the tip) and modeled like rigid bodies, and five joints, represented by the four articulations (CMC, MCP, PIP, and DIP) and modeled like ideal rotates joints. The MCP joint is split into two different DoFs, decoupling the adduction/abduction and flexion/extension movements, while all the other joints only allow flexion/extension movements.
It has been decided to number from 0 to 4 the five digits, where digit 0 is the thumb and digits 1 to 4 are the four fingers, ranging from the index to the little. Table 20 shows the MDH parameters related to the four fingers, where i is the index representing the finger.
The following equation shows the direct kinematics of each finger, from the index (i=1) to the little (i=4):

$$ Q_i = {}^{0}_{0}T \cdot {}^{0}_{5}T \cdot {}^{5}_{6}T = {}^{0}_{0}T \cdot \prod_{j=1}^{5} {}^{j-1}_{j}T_i(\theta_j) \cdot {}^{5}_{6}T $$
$$ Q_i = {}^{0}_{0}T_i \cdot {}^{0}_{1}T_i(\theta_{CMC}) \cdot {}^{1}_{2}T_i(\theta_{MCP_{a/a}}) \cdot {}^{2}_{3}T_i(\theta_{MCP_{f/e}}) \cdot {}^{3}_{4}T_i(\theta_{PIP}) \cdot {}^{4}_{5}T_i(\theta_{DIP}) \cdot {}^{5}_{6}T_i \quad (14) $$

Where the Q_i matrix expresses the position and the attitude of the i-th fingertip as a function of the angles if the various joints θ_i.
Moreover ${}^{(j-1)}_{j}\mathrm{T}_i(\theta_j)$ is the generic transformation matrix between the (j-1)-th and the j-th reference frame, containing all the geometrical information of this specific part of the structure; its generic form is

MDH parameters of the i-th finger

	Joint	$\boldsymbol{\alpha_{j-1}}$	$\boldsymbol{a_{j-1}}$	$\boldsymbol{d_j}$	$\boldsymbol{\theta_j}$
j_{1i}	**CMC**	$\pi/2$	0	0	θ_{CMC}
j_{2i}	**MCP a/a**	$-\pi/2$	L_{0i} (metacarpal)	0	$\theta_{MCP_{a/a}}$
j_{3i}	**MCP f/e**	$\pi/2$	0	0	$\theta_{MCP_{f/e}}$
j_{4i}	**PIP**	0	L_{1i} (proximal)	0	θ_{PIP}
j_{5i}	**DIP**	0	L_{2i} (middle)	0	θ_{DIP}

Table 20: Modified Denavit Hartemberg parameters for the four fingers.

MDH parameters of the thumb i=0

	Joint	α_{j-1}	a_{j-1}	d_j	θ_j
j_{10}	**TMC a/a**	0	0	0	$\theta_{TMC_{a/a}}$
j_{20}	**TMC f/e**	$\pi/2$	0	0	$\theta_{TMC_{f/e}}$
j_{30}	**MCP**	0	L_{00} (metacarpal)	0	θ_{MCP}
j_{40}	**IP**	0	L_{10} (proximal)	0	θ_{IP}

Table 21: Modified Denavit Hartemberg parameters for the Thumb.

the following:

$$ {}^{(j-1)}_{j}\mathrm{T}_i(\theta_j) = \begin{bmatrix} cos(\theta_j) & -sin(\theta_j) & 0 & a_{j-1} \\ sin(\theta_j)cos(\alpha_{j-1}) & sin(\theta_j)cos(\alpha_{j-1}) & -sin(\alpha_{j-1}) & -d_j sin(\alpha_{j-1}) \\ sin(\theta_j)sin(\alpha_{j-1}) & sin(\theta_j)sin(\alpha_{j-1}) & cos(\alpha_{j-1}) & d_j cos(\alpha_{j-1}) \\ 0 & 0 & 0 & 1 \end{bmatrix} \quad 15 $$

The matrix ${}^{0}_{5}T_i(\theta_j)$ is the composition of all the transformation matrices ${}^{(j-1)}_{j}\mathrm{T}_i(\theta_j)$ coming from each joint; it contains the geometrical transformation related to the i-th finger between the wrist reference frame and the one attached to the last joint.
The matrix ${}^{0}_{0}T_i$ describes a transformation that aim at taking into account the fact that the fingers are not parallel between each other but slightly fanned out, causing a different initial orientation which inevitably reverberates on the position of the fingertip. Finally, the matrix ${}^{5}_{6}\mathrm{T}_\mathrm{i}$ describes the position of the fingertip with respect to the distal reference frame, containing for example the length of the last phalanx of each finger. The coefficients of the matrix Q_i obtained by the equation 14 are provided in the appendix.

Direct Kinematics of the Thumb

Similarly to the four fingers, the kinematic chain of the thumb is composed by three links, represented by three bones (metacarpal, proximal and distal) and four joints, represented by the three articulations (TMC, MCP and IP) and modeled like ideal rotate joints. The TMC joint, similarly to the MCP of the fingers, is split into two different DoFs, decoupling the adduction/abduction and flexion/extension movements. Table 21 shows the MDH parameters related to the thumb.
Similarly to equation 14, the following equation shows the direct kinematics of the thumb (i=0):

$$ Q_0 = {}^{0}_{0}T \cdot {}^{0}_{4}T \cdot {}^{4}_{5}T = {}^{0}_{0}T \cdot \prod_{j=1}^{4} {}^{j-1}_{j}T_0(\theta_j) \cdot {}^{4}_{5}T $$
$$ Q_i = {}^{0}_{0}T_0 \cdot {}^{0}_{1}T_0(\theta_{TMC_{a/a}}) \cdot {}^{1}_{2}T_0(\theta_{TMC_{f/e}}) \cdot {}^{2}_{3}T_0(\theta_{MCP}) \cdot {}^{3}_{4}T_0(\theta_{IP}) \cdot {}^{4}_{5}T_0 \quad 16 $$

Regarding all the matrices present into the equation, similar considerations to the ones provided for equation 14 can be done.

Inverse Kinematics

Inverse kinematics is used to obtain the joint angles according to the fingertip position and attitude. Usually, the computation of the inverse kinematic is computationally very expensive and takes a lot of

time. However, as already said, the actuators usually work in the joint space, while the tasks to be performed by the end-effector are planned in the Cartesian space.
The solution of the inverse kinematic problem is strictly linked to and depending on the robotic structure. Two approaches for the computation of the inverse kinematics are possible: the analytical and the numeric solution. The first one is based on the decoupling of the spatial geometry of the robotic structure into several geometric elementary equations. In case of manipulators with a high number of degrees of freedom or with three dimensional movements, the analytical solution usually results to be very complicated and tedious. Moreover, non linearity or singularities could impede the inversion of the equation system; in these cases the numerical solution is chosen.
As for direct kinematics, inverse kinematics has been solved separately for the fingers and for the thumb. It is important to notice that, due to the structure of the kinematic chain, the model of the human finger is redundant. The joint with parallel axes generates multiple solutions in relation with the inverse kinematic problem. It is necessary to take into account the constraints relating to the finger movements shown in the previous section in order to obtain a unique solution.

Inverse Kinematics of the four Fingers

As explained before, the goal is to obtain the values of the joint angles. Starting from equation 14, the five interested angles values (θ_{CMC}, $\theta_{MCP_{a/a}}$, $\theta_{MCP_{f/e}}$, θ_{PIP} and θ_{DIP}) can be obtained manipulating the matrix Q_i of each finger. The procedure shown here solves the inverse kinematic of any of the four fingers, from the index (i=1) to the little finger (i=4). For sake of brevity and clarity the index *i* will be omitted in the following part. Observing the structure of the matrix Q (placed in the appendix), it can be noticed that some joint angles are easily obtainable from the elements of the matrix itself, while some others result hardly achievable or require too complex computation. As a result, it has been decided to algebraically obtain the equations related to θ_{CMC}, $\theta_{MCP_{a/a}}$ and θ_{DIP} while $\theta_{MCP_{f/e}}$ and θ_{PIP} joints were solved through a geometric method. The duplication of solutions, obtained when solving the trigonometric equations, is managed applying the physiological constraints related to the maximum angular displacement achievable by the human finger. Defining Q_{rc} the element of the matrix Q placed on the *r*-th row and on the *c*-th column, the three angles are obtainable as follows:

$$\theta_{CMC} = atan\frac{Q_{33}}{Q_{13}} \quad ; \quad \theta_{MCP_{a/a}} = atan\frac{Q_{13}}{-Q_{23}\cos(\theta_{CMC})} \quad ; \quad \theta_{DIP} = atan\frac{a}{b} \qquad 17$$

Where the parameters *a* and *b* are the following:

$$a = -\frac{mQ_{22} + nQ_{21}}{m^2 + n^2} \quad ; \quad b = \frac{Q_{21}(m^2 + n^2) - n(mQ_{22} + nQ_{21})}{m(m^2 + n^2)} \qquad 18$$

And

$$\begin{aligned} m &= \sin(\theta_{MCP_{a/a}})\cos(\theta_{MCP_{f/e}} + \theta_{PIP}) \\ m &= \sin(\theta_{MCP_{a/a}})\sin(\theta_{PIP} - \theta_{MCP_{f/e}}) \end{aligned} \qquad 19$$

At this point the three previous joint angles are solved. The $\theta_{MCP_{f/e}}$ and θ_{PIP} joints are then solved through geometric considerations referred to Figure 40.

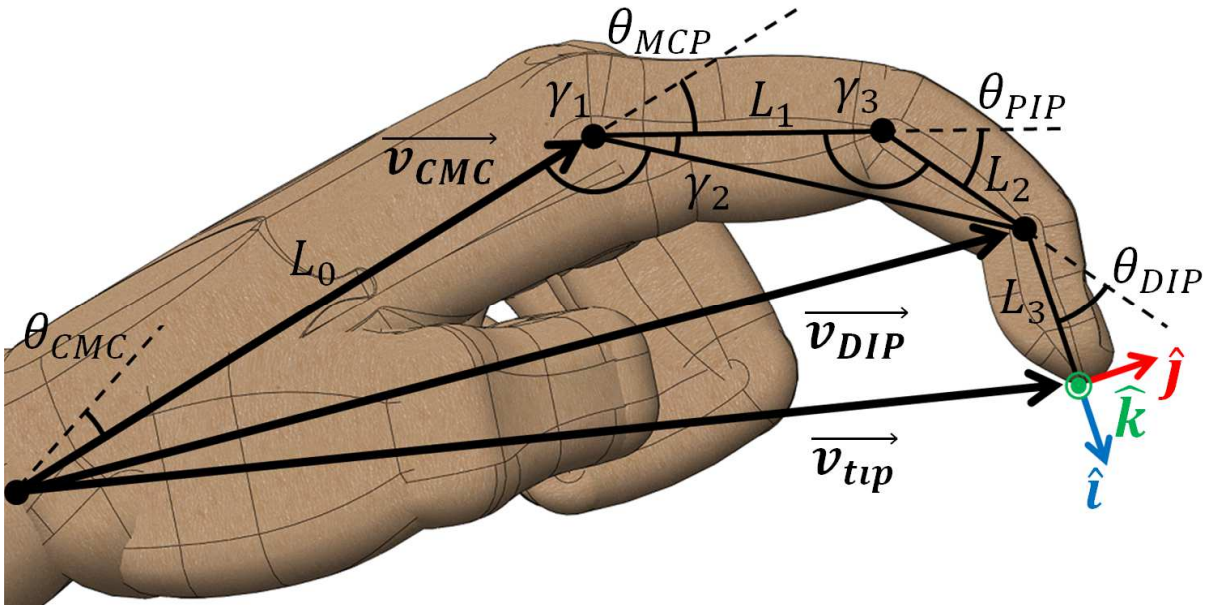

Figure 40: Inverse Kinematics of the four Fingers.

Starting from the vector $\overrightarrow{\boldsymbol{v_{tip}}}$, which contains the information related to the position of the fingertip, it is possible to obtain the vector $\overrightarrow{\boldsymbol{v_{DIP}}}$, which describe the position of the distal joint, with the following equation:

$$\overrightarrow{\boldsymbol{v_{DIP}}} = \overrightarrow{\boldsymbol{v_{tip}}} - L_3 * \hat{\boldsymbol{\imath}} \qquad 20$$

Where L_3 is the length of the distal phalanx and $\hat{\boldsymbol{\imath}}$ is the versor of the reference system attached to the fingertip.
Then the components of vector $\overrightarrow{\boldsymbol{v_{MCP}}}$, which describes the position of the metacarpal joint, can be easily obtained as follows:

$$\overrightarrow{\boldsymbol{v_{MCP}}} = \begin{bmatrix} L_0 \cos(\theta_{CMC}) \\ L_0 \sin(\theta_{CMC}) \\ 0 \end{bmatrix} \qquad 21$$

Where L_0 is the length of the metacarpal link. The angles γ_1 , γ_2 and γ_3 shown in Figure 40 can be obtained as follows:

$$\begin{aligned} \gamma_1 &= \operatorname{acos}\frac{{L_0}^2 + \|\overrightarrow{\boldsymbol{v_{DIP}}} - \overrightarrow{\boldsymbol{v_{MCP}}}\|^2 - \|\overrightarrow{\boldsymbol{v_{DIP}}}\|^2}{2L_0\|\overrightarrow{\boldsymbol{v_{DIP}}} - \overrightarrow{\boldsymbol{v_{MCP}}}\|} \\ \gamma_2 &= \operatorname{acos}\frac{{L_1}^2 + \|\overrightarrow{\boldsymbol{v_{DIP}}} - \overrightarrow{\boldsymbol{v_{MCP}}}\|^2 - {L_2}^2}{2L_1\|\overrightarrow{\boldsymbol{v_{DIP}}} - \overrightarrow{\boldsymbol{v_{MCP}}}\|} \\ \gamma_3 &= \operatorname{acos}\frac{{L_1}^2 + {L_2}^2 - \|\overrightarrow{\boldsymbol{v_{DIP}}} - \overrightarrow{\boldsymbol{v_{MCP}}}\|^2}{2L_1L_2} \end{aligned} \qquad 22$$

Where L_1 and L_2 are respectively the lengths of the distal and middle phalanges. The two interested joint angles can then be obtained as:

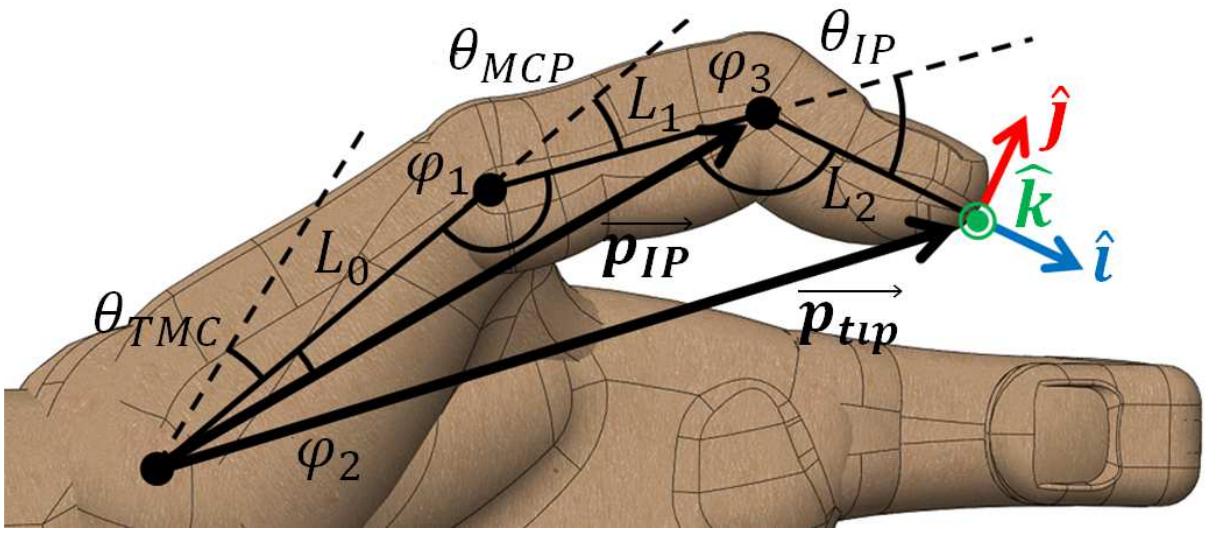

Figure 41: Inverse Kinematics of the Thumb.

$$\theta_{MCP_{f/e}} = \pi - (\gamma_1 + \gamma_2) \quad ; \quad \theta_{PIP} = \pi - \gamma_3 \tag{23}$$

Inverse Kinematics of the Thumb

A similar procedure to the previous one could be also applied to the thumb in order to obtain its inverse kinematics. In this case it is necessary to manipulate the matrix Q_0 coming from the equation 16 in order to obtain the values of the joint angles ($\theta_{TMC_{a/a}}$, $\theta_{TMC_{f/e}}$, θ_{MCP}, θ_{IP}). It was decided to algebraically obtain the equations related to $\theta_{TMC_{a/a}}$ and $\theta_{TMC_{f/e}}$, while θ_{MCP} and θ_{IP} were solved through a geometric method. Defining Q_{rc} the element of the matrix Q placed on the r-th row and on the c-th column, the two angles related to the TMC joint are obtainable as follows:

$$\theta_{TMC_{a/a}} = atan\left(-\frac{Q_{13}}{Q_{23}}\right) \quad ; \quad \theta_{TMC_{f/e}} = atan\frac{c}{d} \tag{24}$$

Where the parameters c and d are the following:

$$c = \frac{Q_{31} - (Q_{32} + Q_{31})\cos(\theta_{MCP} + \theta_{IP})\sin(\theta_{MCP} + \theta_{IP})}{\cos(\theta_{MCP} + \theta_{IP})}$$
$$d = (Q_{32} + Q_{31})\cos(\theta_{MCP} + \theta_{IP}) \tag{25}$$

The other three joint angles are then solved through geometric considerations referred to Figure 41.
Also in this case, starting from the vector $\overrightarrow{\boldsymbol{p_{tip}}}$, which contains the information related to the position of the fingertip of the thumb, it is possible to obtain the vector $\overrightarrow{\boldsymbol{p_{IP}}}$, which describes the position of the distal joint of the thumb, with the following equation:

$$\overrightarrow{\boldsymbol{p_{IP}}} = \overrightarrow{\boldsymbol{p_{tip}}} - L_2 * \hat{\boldsymbol{\imath}} \tag{26}$$

Where L_2 is the length of the distal phalanx of the thumb and $\hat{\boldsymbol{\imath}}$ is the versor of the reference system attached to the fingertip. The angles φ_1 , φ_2 and φ_3 shown in Figure 41 can be obtained as follows:

$$\varphi_2 = \operatorname{acos}\frac{{L_0}^2 + {L_1}^2 - \|\overrightarrow{\boldsymbol{p_{IP}}}\|^2}{2L_0L_1}$$
$$\varphi_1 = \operatorname{acos}\frac{{L_2}^2 + \|\overrightarrow{\boldsymbol{p_{IP}}}\|^2 - \left\|\overrightarrow{\boldsymbol{p_{tip}}}\right\|^2}{2L_2\|\overrightarrow{\boldsymbol{p_{IP}}}\|} \qquad 27$$
$$\varphi_3 = \operatorname{acos}\frac{{L_1}^2 + \|\overrightarrow{\boldsymbol{p_{DIP}}}\|^2 - {L_0}^2}{2L_1\|\overrightarrow{\boldsymbol{p_{IP}}}\|}$$

Where L_0 and L_1 are the lengths respectively of the metacarpal link and the proximal phalange. The two interested joint angles can then be obtained as:

$$\theta_{MCP} = \pi - \varphi_1 \quad ; \quad \theta_{IP} = \pi - (\varphi_2 + \varphi_3) \qquad 28$$

Human Hand Dynamics

Dynamics is a physics-based modeling approach in which forces and torques are analysed in relation with their effect on the motion of an articulated object with mass, performed in order to obtain the spatial parameters of each body. This aspect distinguishes dynamics from kinematics, which studies motion without taking into account the specific causes that generates the motion. In robotics, due to its multidisciplinary characteristics, the most general and used method is the Euler-Lagrange method, which studies the energy, kinetic or potential, of each element that compound the structure.
As a consequence of the remarkable impact of the Newton's Principia, classical mechanical was re-proposed in the 18th century by Euler and Lagrange in a different way. According to their work, particles do not follow specific trajectories as a consequence of the action of external forces, as Newton proposed. Instead, among all the possible trajectories that connect two points, the particles choose the one that minimizes a particular integral of kinetic and potential energy.
Lagrange called this new approach to classical mechanics Analytical Mechanics to differentiate it from Newton's mechanics, based on vectors and on the concept of forces.

Dynamics of the Four Fingers

This part provides a brief explanation of the steps performed in order to obtain the dynamic equations system of the generic single digit *i*. With respect to the kinematic chain previously studied, a couple of

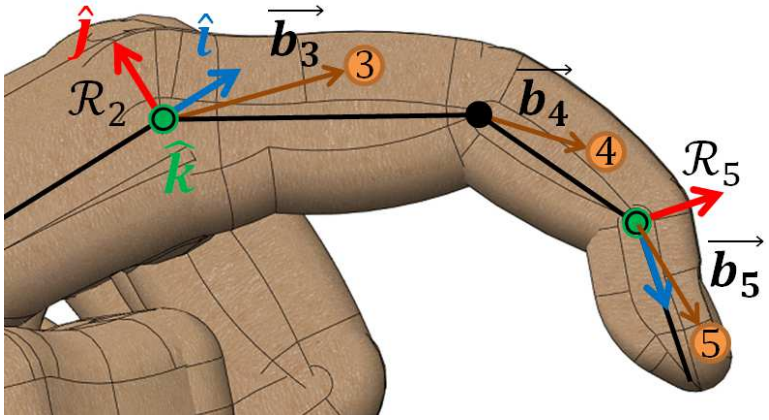

Figure 42: Dynamic of the finger: reference frames and centre of masses.

simplifications were adopted for the dynamic system: first, the metacarpus articulation was considered fixed, then the abduction-adduction degree of freedom of the MCP joint was neglected. In conclusion, the finger system is composed by only three joints, corresponding to the MCP flexion-extension, PIP and DIP and the only moving parts are the three finger phalanges Figure 42. Again the index *i* will be omitted during the treatment for sake of brevity.
Based on the convention shown in Figure 42, the dynamic model is obtained; therefore the reference frame, placed in the MCP joint, is called $\mathcal{R}_2$ and all the equations are written with respect to it, in order to keep the nomenclature as similar as possible with the kinematics. It is important to underline that the following equations are applicable to any 3R (i.e. with three rotative joints) serial robot, after making the necessary variable adaptations.
As previously explained, the Euler Lagrange equations require the estimation of the energies of the elements that compound the structure. In the following part kinematic and potential energies were obtained.
Kinetic energy is calculated starting from the position vector of the centre of mass of each phalanx with respect to the base reference frame $\mathcal{R}_2$. The coordinates of the *j*-th centre of mass with respect to the *j*-th reference frame $\mathcal{R}_j$ are:

$$\overrightarrow{\boldsymbol{b_j}} = [b_{jx} \quad b_{jy} \quad 0]^T \quad ; \quad j = 3{,}4{,}5 \tag{29}$$

The mass of the *j*-th phalanx is defined as m_j and the respective moment of inertia with respect to the axis z of the reference frame $\mathcal{R}_j$ is called I_j.
The following change of coordinates has been introduced in order to simplify the treatment:

$$\psi_3 = \theta_{MCP_{f/e}} \quad ; \quad \psi_4 = \theta_{MCP_{f/e}} + \theta_{PIP} \quad ; \quad \psi_5 = \theta_{MCP_{f/e}} + \theta_{PIP} + \theta_{DIP} \tag{30}$$

The generic position vector of the generic *j*-th centre of mass with respect to the reference frame $\mathcal{R}_2$ is:

$$\overrightarrow{\boldsymbol{c_j}} = \begin{bmatrix} b_{jx}\,cos(\psi_j) - b_{jy}\,sin(\psi_j) \\ b_{jx}\,sin(\psi_j) + b_{jy}\,cos(\psi_j) \\ 0 \end{bmatrix} + \sum_{k=3}^{j-1} L_{k-2} \begin{bmatrix} cos(\psi_k) \\ sin(\psi_k) \\ 0 \end{bmatrix} \tag{31}$$

The velocity of the generic *j*-th centre of mass can be obtained by differentiating the position vector coming from equation 31:

$$\overrightarrow{\boldsymbol{v_{c_j}}} = \dot{\psi}_j \begin{bmatrix} -b_{jx}\,sin(\psi_j) - b_{jy}\,cos(\psi_j) \\ b_{jx}\,cos(\psi_j) - b_{jy}\,sin(\psi_j) \\ 0 \end{bmatrix} + \sum_{k=3}^{j-1} L_{k-2}\dot{\psi}_k \begin{bmatrix} -sin(\psi_k) \\ cos(\psi_k) \\ 0 \end{bmatrix} \tag{32}$$

The total kinetic energy of the system can then be calculated and expressed as:

$$T = \frac{1}{2}\sum_{j=3}^{5}\left(m_j \left\|\overrightarrow{\boldsymbol{v_{c_j}}}\right\|^2 + I_j \dot{\psi}_k{}^2\right) \tag{33}$$

In a fully mechanical system there are two forms main of potential energy: the gravitational potential energy and the elastic potential energy, both considered in this case. The gravitational potential energy is easily obtained by the standard equation, knowing the masses of each phalanx. Regarding the elastic

potential energy it is necessary to obtain the values of stiffness of each joint. Milner and Franklin [124] proposed in their work a detailed model of multi joint finger stiffness as a function of the position and the forces applied. In this case it was decided to consider an average value of stiffness, keeping the value k_j constant, as a close approximation of the non-linear and anisotropic stiffness. Therefore k_3, k_4 and k_5 are the stiffness values for the MCP, DIP and PIP joints respectively. At this point, defining g as the acceleration of gravity, the potential energy can be expressed as:

$$U = \sum_{j=3}^{5} \left[m_j c_{jy} g + \frac{1}{2} k_j \left(\psi_j - \psi_{j-1} \right)^2 \right] \quad 34$$

Moreover, it is necessary to introduce the function usually referred as the Rayleigh dissipation function *F*, that models the damping forces as a function of the velocities. This function is expressed as:

$$F = \sum_{j=3}^{5} \left[\frac{1}{2} \beta_j \left(\dot{\psi}_j - \dot{\psi}_{j-1} \right)^2 \right] \quad 35$$

Where the damping constant β_j considers the non-conservative contribution caused by the muscles during the actuation of the finger. The viscosity of the human muscles acts like a dissipative and non-conservative element, resulting in a force field with non-zero curl. Non-conservative forces contribute less than 15% to the total force response to static displacement [124]. Therefore β_3, β_4 and β_5 are the damping values for the MCP, DIP and PIP joints respectively.
Considering the three generalized coordinates ψ_j, the Euler Lagrange equation can be written as follows:

$$\frac{d}{dt}\left(\frac{\partial (T-U)}{\partial \dot{\psi}_j} \right) - \frac{\partial (T-U)}{\partial \psi_j} + \frac{\partial F}{\partial \dot{\psi}_j} = \tau_j \quad ; \quad j = 3,4,5 \quad 36$$

Where τ_j are the generalized external forces that contain the action applied by the muscles in order to actuate the phalanges and the contact forces that perform work on ψ_j. According to the virtual work principle, the equation to calculate the generalized force τ_j can be expressed as:

$$\tau_j = \frac{\sum_{k=3}^{5} \delta W_k}{\delta \psi_j} \quad ; \quad j = 3,4,5 \quad 37$$

Where δW_k is the virtual work performed by the *k*-th force applied on the system. In conclusion, the generalized forces result to be equal to:

$$\tau_j = \left(F_{jy} e_{jx} - F_{jx} e_{jy} \right) + C_{mj} - C_{m(j+1)} \sum_{k=j+1}^{5} l_{j-2} \begin{bmatrix} \sin\theta_j \\ \cos\theta_j \\ 0 \end{bmatrix} \begin{bmatrix} F_{kx}\, cos(\psi_k) - F_{ky}\, sin(\psi_k) \\ F_{kx}\, sin(\psi_k) + F_{ky}\, cos(\psi_k) \\ 0 \end{bmatrix} \quad 38$$

Where the term C_{mj} represents the torque produced by the muscles on the *j*-th joints, $\overrightarrow{\boldsymbol{F_j}}$ is the contact force applied on the *j*-th phalanx in correspondence to the point defined by the vector $\overrightarrow{\boldsymbol{e_j}}$, as shown in Figure 43.

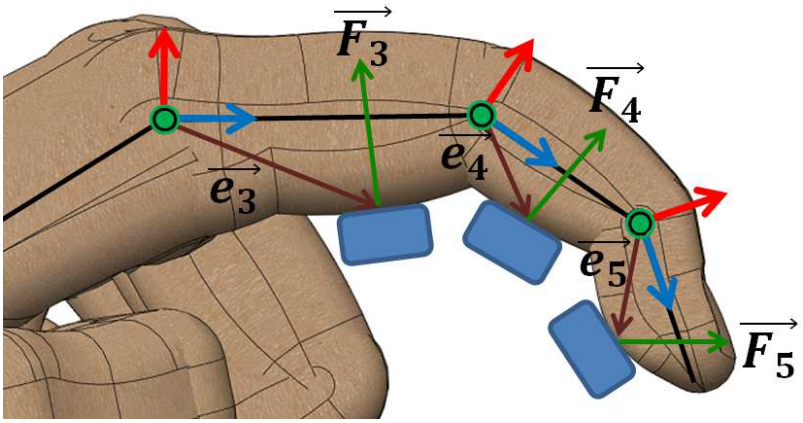

Figure 43: Dynamic of the finger: external forces.

Calculating each element of the Euler Lagrange equation, the system described by equation 36 could be rewritten in matrix form as follows:

$$\begin{cases} A_{11}\ddot{\psi}_3 + A_{12}\ddot{\psi}_4 + A_{13}\ddot{\psi}_5 = B_1 \\ A_{21}\ddot{\psi}_3 + A_{22}\ddot{\psi}_4 + A_{23}\ddot{\psi}_5 = B_2 \\ A_{31}\ddot{\psi}_3 + A_{32}\ddot{\psi}_4 + A_{33}\ddot{\psi}_5 = B_3 \end{cases} \quad ; \quad [\boldsymbol{A}][\ddot{\psi}] = [\boldsymbol{b}] \qquad 39$$

Where each element of the 3x3 matrix [$\boldsymbol{A}$] contains the coefficient of the accelerations and the 3x1 vector [$\boldsymbol{b}$] contains the remaining terms.
Equation 37 allows the direct dynamics of the human finger, with which the movement of the finger can be calculated given the torques generated by the muscles on each phalanx, to be solved. On the other hand, if an inverse dynamic problem is imposed, equation 37 could be easily rearranged in order to obtain the trend of the muscle torque, starting from the phalanges motion law. A detailed expansion of the coefficients of matrix [$\boldsymbol{A}$] and vector [$\boldsymbol{b}$] are reported in the appendix.

Dynamics Model Validation

Starting from the dynamic equation calculated in the previous section, it has been decided to implement a numerical example, related to an index finger, in order to validate the model, comparing the results coming from the simulation with the ones found in literature. In order to perform as realistic as possible

	j	m_j [g]	I_j [gmm^2]	k_j [N/m]	β_j [sN/m]	L_j [mm]	b_j [mm]	e_j [mm]
Proximal	3	7.05	1000	0	0	$\begin{bmatrix}50\\0\\0\end{bmatrix}$	$\begin{bmatrix}25\\0\\0\end{bmatrix}$	$\begin{bmatrix}25\\-8\\0\end{bmatrix}$
Middle	4	C	240	0	0	$\begin{bmatrix}20\\0\\0\end{bmatrix}$	$\begin{bmatrix}10\\0\\0\end{bmatrix}$	$\begin{bmatrix}12.5\\0\\0\end{bmatrix}$
Distal	5	2.70	120	0	0	$\begin{bmatrix}25\\0\\0\end{bmatrix}$	$\begin{bmatrix}10\\-7\\0\end{bmatrix}$	$\begin{bmatrix}12\\-6\\0\end{bmatrix}$

Table 22: Anthropometric data and numerical constants used in the simulation.

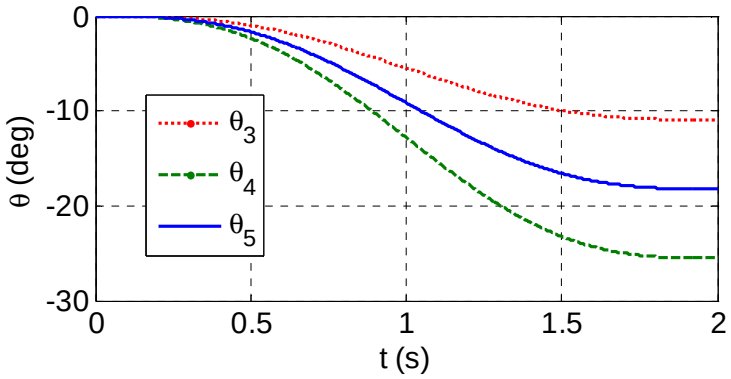

Figure 44: Behavior of the joint angles during the simulation.

an example, the anthropometric data and numerical constant, found in literature [98, 99] and previously presented in the relative section, have been imposed and are shown in Table 22. It has been decided to emulate the movement of the human hand during a circular grasp. In particular, the proposed simulation deals with an inverse dynamic study in which, given the motion law of the system (i.e. behaviour of the angular displacement of the articulation and their time derivative), the torques exerted by the muscles on each phalanx are calculated.

Figure 44 shows the behaviour of each angle imposed during the simulation, starting from the straight position with all angles equal to zero degree and performing the flexion movement. In order to emulate the circular grasp, the relation between the angles is imposed on the basis of the data coming from the physiological constraints [101, 100], already reported in Table 8 and relative to the intra-finger constraints. It is important to underline that, due to the reference frame orientation established, the angles of any grasping operation are negative values.

Figure 45 shows the behaviours of the three joints torques obtained by the simulation and required to perform the selected grasping operation described by Figure 44. $\mathrm{C_{m3}}$, $\mathrm{C_{m4}}$ and $\mathrm{C_{m5}}$ are respectively the MCP, PIP and DIP joint torques.

The maximum values of contact forces imposed during the simulation were obtained by the previously described study of An et al. [110], which reports the maximum mid-phalangeal joint normal forces exerted by the human finger during a cylindrical power grasp; on the basis of this study, these maximum forces for the index finger are equal to:

	$\boldsymbol{F_{j_{max}}}$ [N]
Proximal j=3	42
Middle j=4	22
Distal j=5	62

It has been decided to perform three different simulation cases applying each time a different percentage of the $\boldsymbol{F_{max}}$ on the three phalanges and in particular:

- Case *a*: $\boldsymbol{F} = \boldsymbol{F_{max}}$
- Case *b*: $\boldsymbol{F} = 0.5 \cdot \boldsymbol{F_{max}}$
- Case *c*: $\boldsymbol{F} = 0.25 \cdot \boldsymbol{F_{max}}$

The results relative to the case *a* allow a comparison between the maximum torque values obtained by the simulation and the ones calculated by Hasser [111]. Hasser claimed that the maximum torque capabilities of the human hand for each phalanx are equal to:

	$C_{j_{max}}$ [Nmm]
Proximal j=3	4630
Middle j=4	2280
Distal j=5	775

The maximum obtained values of torque relative to the middle and distal phalanges are very similar to

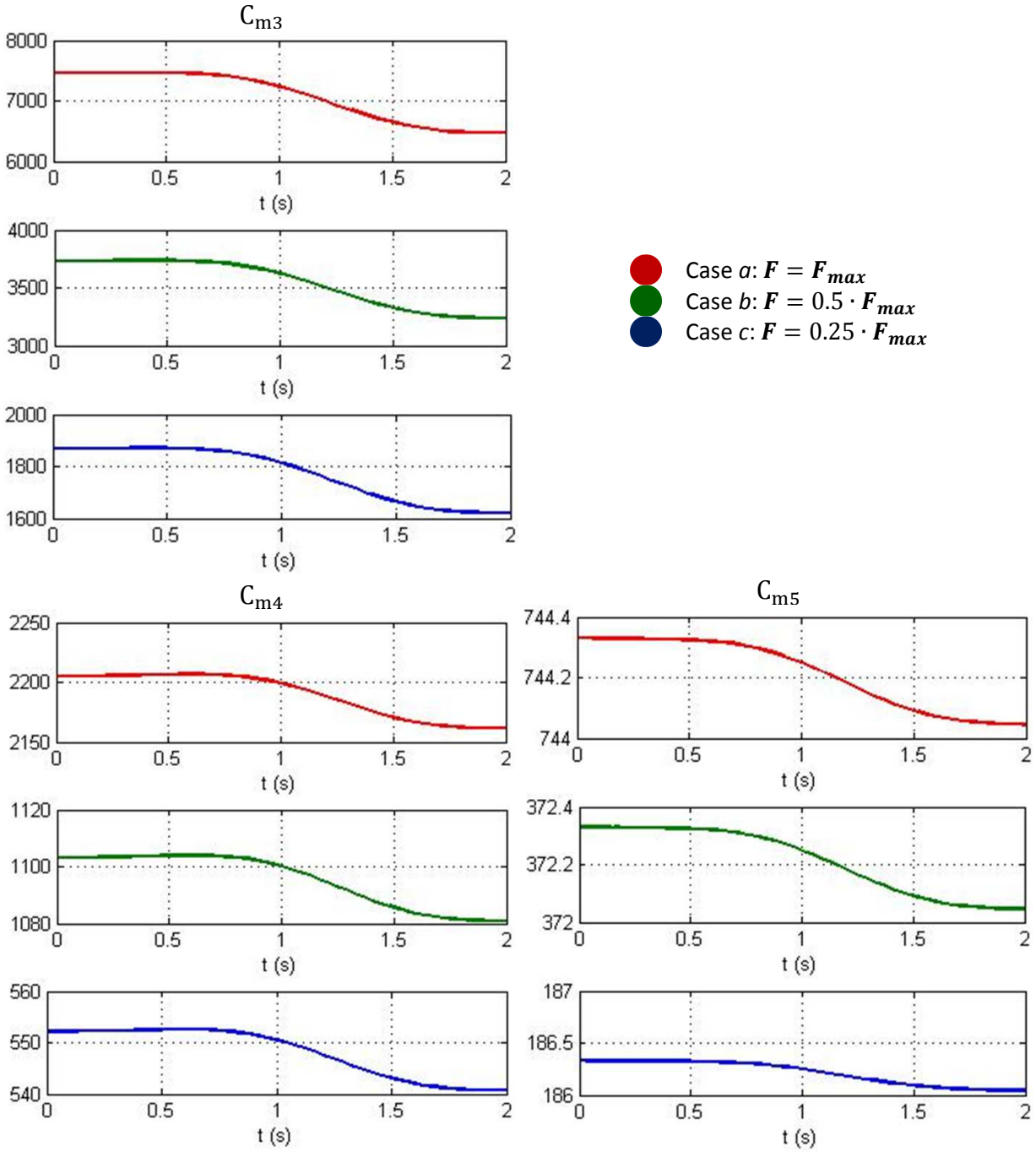

Figure 45: Behaviour of the joint torques during the simulation.

the ones found in literature with a difference of 3.2% for C_{m4} and 4% for C_{m5}. On the contrary, the result related to the proximal phalanx is very different if compared to Hasser's study. This effect may be caused by an error either in An's analysis or in its interpretation made by Hasser. Finally one last aspect, not explicitly mentioned in the two mentioned works, could be taken into account: it is not taken for granted that the three articulations can contemporarily exert their maximum torque. In this case, both results could be interpreted as equally correct.